GEORG-AUGUST-UNIVERSITÄT
GÖTTINGEN IN PUBLICA COMMODA SEIT 1737

Multiple Extended Target Tracking in Maritime Environment Using Marine Radar Data

Dissertation
for the award of the degree
"Doctor rerum naturalium" (Dr.rer.nat)
at the Georg-August Universität Göttingen

within the doctoral program Ph.D. Programme in Computer Science (PCS)
of the Georg-August University School of Science (GAUSS)

submitted by
Jaya Shradha Fowdur
from Mauritius

Göttingen, 2022

Thesis Advisory Committee

Prof. Dr.-Ing. Marcus Baum
Institute of Computer Science, Georg-August Universität Göttingen, Germany

Dr. rer. nat. Frank Heymann
Institute of Solar-Terrestrial Physics, German Aerospace Center, Neustrelitz, Germany

Members of the Examination Board

Reviewer: Prof. Dr.-Ing. Marcus Baum
Institute of Computer Science, Georg-August Universität Göttingen, Germany

Second Reviewer: Dr. rer. nat. Frank Heymann
Institute of Solar-Terrestrial Physics, German Aerospace Center, Neustrelitz, Germany

Additional Reviewer: Prof. Dr. Jesús García Herrero
Computer Science and Engineering Department, Universidad Carlos III de Madrid, Madrid, Spain

Further Members of the Examination Board

Prof. Dr. Alexander Ecker
Institute of Computer Science, Georg-August Universität Göttingen, Germany

Prof. Dr. Ramin Yahyapour
Gesellschaft für Wissenschaftliche Datenverarbeitung mbH, Göttingen, Germany

Prof. Dr. Maciej Gucma
Department of Marine Navigation, Maritime University of Szczecin, Szczecin, Poland

Date of Oral Examination
13.07.2022

Georg-August-Universität Göttingen
Institute of Computer Science

Goldschmidtstraße 7
37077 Göttingen
Germany

☎ +49 (551) 39-172000
FAX +49 (551) 39-14403
✉ office@informatik.uni-goettingen.de
🌍 www.informatik.uni-goettingen.de

A Sankskrit prayer for the well-being of everyone given the turbulent times lately:

Sarveshaam Svastir-Bhavatu
Sarveshaam Shaantir-Bhavatu
Sarveshaam Purnnam-Bhavatu
Sarveshaam Mangalam-Bhavatu
Om Shaantih Shaantih Shaantih
$\sim$ *Brihadaaranyak Upanishad*

Translation:

"May we all be healthy, at peace, and have fulfilling pleasant experiences.
And may none be, even a little, in suffering. Peace."

Acknowledgements

Looking back at the past four years, I cannot help but be grateful to be at the point of completion, during which I have learnt and grown a lot through my experiences. Fortunately, I have been surrounded by the support of many.

I would begin by expressing my deepest gratitude to my supervisors, Prof. Marcus Baum and Dr. Frank Heymann, who have done their best in guiding me and who have been extremely considerate regarding organisational matters. Marcus, thank you for your constant encouragement, patience, and making me strive for better quality of work. Frank, you have always been there, from our three hours-long *small* discussions to giving me the freedom to explore a few concepts on my own. You stuck around and made sure I am done with my studies despite not being in the same institute anymore. *Merci*!

My colleagues –Lars, Pawel, Daniel, Sandeep, Kateryna, Christoph, Filipo, Arthur, Daniela, JuanMa, Axel, Torsten, Aman, Uwe, Maria and Astrid –at the DLR have, almost everyone, contributed directly or indirectly to my thesis be it with discussion on some formulae, our presentation-based discussions, technical help, even for our daily lunch and early morning or late afternoon motivational or all-joke coffee breaks. Thoralf, our department head, ensured my PhD journey faced as little inconvenience as possible. My PhD mates at the Data Fusion group from the University of Göttingen have also been of pivotal help. Shishan, thank you for being my inspiration and for your advices. Hauke and Kolja, I am fortunate that we shared similar experiences, and supported each other from our Masters studies until now. Laura and Kolja, thank you for your valuable and timely suggestions during the drafting stages.

Being in Neustrelitz for over four years is a huge achievement for me personally. Living here has been challenging, especially as an expat. The what-seemed-to-be-never-ending pandemic and the war did not make it any easier. My close friends from around the world –Vidhoushee, Pooja, John, Patrick, Michal, Guryash, Vanessa, and Tanusha –were just a phone call away, for which I am very grateful. The same is applicable for my relatives who keep checking up on me: *Nani* Mala and *Nana* Raj, *Mamu* Kumar and *Mami* Indira, *Mamu* Shyam, Bhavna, Chetan, and Anish.

The unconditional love and support from *la famille* go without saying. My parents, my brother

and my sister-bestie, have been my motivators along every step of the way, on whom I can always count in happy as well as in hard moments. And Friedrich, who leaves no stone unturned to ensure that I continue strong, day after day, till *la ligne d'arrivée* with the best cherry-chocolate muffins ever.

Abstract

Target tracking is today one of the main pillars supporting applications for Maritime Traffic Situation Assessment and Monitoring (MTSAM). It provides information on the targets (vessels) obtained from the sensors within an observation region of interest, allowing the users (from the on board captain to the port authorities) to get a more complete knowledge on the current traffic situation. Such knowledge could contribute significantly to detect and avert potential collisions, and could help traffic analysis by studying long-term trajectories of vessels. As sensor technologies have improved in terms of spatial resolution, measurements recorded from the Radio Detection and Ranging (radar) sensors –predominantly used for maritime navigation –occur in point clouds. This provides us with opportunities to estimate the kinematic properties of vessels as well as their extent (shape) information, a problem known as Multiple Extended Target Tracking (METT).

The METT problem can be divided into two parts: Extended Target Tracking (ETT) and Multiple Target Tracking (MTT). ETT considers extent estimation using basic shapes like the ellipse or more complex ones like the star-convex. Even for the basic shapes, the major challenge would be to find a trade-off between an accurate representation and the processing time, factoring in the measurement quality, for instance, in terms of noise level, spatial density of the point clouds and external influences such as weather conditions. MTT considers the problem of concurrently estimating the states of multiple vessels and the number of vessels itself. The approaches based on Data Association (DA) to associate a measurement to its potential source often rely on a one-to-one constraint between them, and require to now cater for the association of a point cloud to its potential source efficiently.

We propose two elliptical tracking approaches for the ETT problem, with particular focus on real-world marine radar data. The first one involves the opportunity to estimate the orientation (heading) of a vessel while keeping its dimensions fixed, targeting commonly encountered maritime-based situations where the heading is not aligned with the vessel's course. The second one is another elliptical tracker which estimates the extended state of the vessel in a batch-fashion to help achieve the aforementioned trade-off. We then propose a custom DA-based MTT algorithm to process measurements that are priorly subject to a clustering approach so as to satisfy the one-to-one association constraint to handle the point cloud-nature of the measurements. The results have been evaluated using simulations and real data, and presented with comparisons (against state-of-the-art methods) and discussions.

The final contribution is an approach for METT, which combines our batch elliptical tracker and our custom MTT tracker. The approach has been implemented on our demonstrator software that receives radar video streaming from harbours, in a multiple sensor-setting. To make the system autonomous and more robust, a track management scheme has also been integrated to maintain the tracks. We present random frame captures to illustrate the performance of our framework as a whole, for MTSAM.

x

Contents

List of Figures

List of Tables

List of Abbreviations

AIS	Automatic Identification System	2
ASTERIX	All Purpose Structured EUROCONTROL Surveillance Information Exchange	10
COG	course over ground	35
DA	Data Association	7
DAAN	Data Association with Aids to Navigation	13
DARC	Data Association with Radar Beacon	13
DBSCAN	Density-based Spatial Clustering of Applications with Noise	70
DLR	German Aerospace Centre (Deutsches Zentrum fuer Luft- und Raumfahrt)	13
DoH	Determinant of Hessians	15
EC-JPDA	Extended Centroid-based JPDA	xx
EKF	Extended Kalman Filter	23
ENU	East North Up	14
ETT	Extended Target Tracking	3
EVD	eigenvector decomposition	47
GP	Gaussian Processes	25
GPS	Global Positioning System	2
GT	Group Tracking	60
GW	Gaussian Wasserstein	51
IID	Independent and Identically Distributed	29
IMO	International Maritime Organization	2
JIPDA	Joint Integrated Probabilistic Data Association	72
JPDA	Joint Probabilistic Data Association	7
KF	Kalman Filter	7
lidar	Light Detection and Ranging	2
MANV	Manoeuvres	13
MEM	Multiplicative Error Model	34
MEM-EKF*	Multiplicative Error Model-Extended Kalman Filter*	34
METT	Multiple Extended Target Tracking	5
MHT	Multiple Hypothesis Tracker	12

MMSI	Maritime Mobile Service Identification	14
MTT	Multiple Target Tracking	6
MTSAM	Maritime Traffic Situation Assessment and Monitoring	1
MS	multi-sensor	71
MSE	Mean Squared Error	53
NCV	Nearly Constant Velocity	39
NN	Nearest Neighbour	12
OSPA	Optimal Subpattern Assignment	97
PAKF	Principal-Axes based Kalman Filter	xx
PAKF-JPDA	Principal-Axes based Kalman Filter (PAKF)-based Extended Centroid-based JPDA (EC-JPDA) Filter	59
PDA	Probabilistic Data Association	12
PDF	Probability Density Function	19
PMF	Probability Mass Function	65
PPP	Poisson Point Process	24
RACON	Radar Beacon	16
R-Mode	Ranging Mode	3
radar	Radio Detection and Ranging	2
RHM	Random Hypersurface Model	25
RFS	Random Finite Sets	12
RMM	Random Matrix Method	25
RMSE	Root Mean Squared Error	40
SOG	speed over ground	35
SOLAS	Convention for the Safety of Life at Sea	2
sonar	Sound Navigation and Ranging	2
SPD	Symmetric and Positive Definite	25
T-MEM-EKF*	Tailored MEM-EKF*	36
UAV	Unmanned Aerial Vehicles	2
VTS	Vessel Traffic Services	2
WGS84	World Geodetic System 1984	14

Nomenclature

English Letter Symbols

a	Scalar
$\mathbf{a}$	Column vector
$\hat{a}$	Estimate of a
$\dot{\mathbf{a}}$	Velocity vector
$\mathbf{a}^T$	Transpose of $\mathbf{a}$
$\mathbf{A}$	Matrix
$\lvert\mathbf{A}\rvert$	Matrix determinant
$\cos(a)$	Cosine of a
$\sin(a)$	Sine of a
$\text{atan2}(a, b)$	Inverse tangent of a/b
$\cosh(a)$	Cosine hyperbolic of a
$\sinh(a)$	Sine hyperbolic of a
$\mathbf{C^a}$	Covariance of $\mathbf{a}$
$\mathbf{I}_a$	Identity matrix of dimension a
$\mathbf{0}_a$	Square matrix with all-zero elements of dimension a
$\text{Tr}(\mathbf{A})$	Trace of $(\mathbf{A})$ (sum of its diagonal elements)
$\text{diag}(\mathbf{A})$	Diagonal elements of $\mathbf{A}$ corresponding to individual covariances
$a \sim \mathcal{N}(0, \mathbf{C^b})$	a has Gaussian distribution with zero-mean and covariance $\mathbf{C^b}$
$\mathcal{N}(\mathbf{a}; \hat{\mathbf{a}}, \mathbf{C^a})$	Multivariate Gaussian with mean $\hat{\mathbf{a}}$ and covariance $\mathbf{C^a}$
$\lvert\lvert\mathbf{a} - \mathbf{b}\rvert\rvert^2$	Euclidean distance between the two vectors
E[a]	Expected value of a
$[0, 1]$	Range between 0 and 1, including limits
$(0, 1)$	Range between 0 and 1, excluding limits
$1e^a$	1×10^a
$f(\cdot)$	Function
$f'_b(a)$	First order derivative evaluated at point $b = a$
$\min(a, b)$	Selects minimum value a if $a < b$, otherwise b

$n_{\mathbf{a}}$	Dimension of vector **a**
$p(a)$	Probability density function of a
$p(a\|b)$	Probability a given b
$1-1$	One-to-one association
$m-1$	Many-to-one association

Filter-related Symbols

k	Current observation or time step
$\hat{a}_{k-1\|k-1}$	Prior estimate of a from step $k-1$
$\hat{a}_{k\|k-1}$	Prediction of a at step k given data through step $k-1$
$\hat{a}_{k\|k}$	Posterior estimate of a at current step k
$P_D^{(s)}$	Target detection probability (for sensor s)
P_G	Gating probability
T	Time interval

Special Letter Symbols

σ_a	Standard deviation of a
σ_a^2	Variance in a
χ_a^2	Chi-square distribution with a degrees of freedom
λ	Spatial density / Poisson rate
λ_a	Eigenvalue
Θ	Association event
$\mathcal{L}_a$	Likelihood of a
$\boldsymbol{\mathcal{R}}(.)$	Rotation matrix
$\mathbb{R}$	Set of real numbers
$\mathbb{N}$	Set of natural numbers

Units

$^{\text{o}}$	Degree(s)
GT	Gross tonnage(s)
km/h	Kilometre(s) per hour
m	Metre(s)
rad	Radian(s)
s	Second(s)

Chapter 1

Introduction

Many applications nowadays are focused on having insight and awareness of the situation prevailing in some region of interest by relying on information from exteroceptive sensors. These include time-varying and desired properties such as the number of targets, each target's type or shape, its position and velocity –to name a few. To help achieve this objective, this thesis is broadly concerned with target detection and state estimation in the maritime context. The first step involved is to collect sensor data over a period of time. Appropriate methods are then applied for detecting potential targets, whose measurements are later used to estimate targets' states. We thereby propose methods for state estimation in maritime environments surveyed by radar sensors.

Contents

1.1 Motivation

Ocean shipping today accounts for above 80% of international trade, experiencing continuous and steady growth over the past three decades. This has laid great stress on maritime security and the safety of life, environment and goods at sea [Eur21, Eur20, WCM+16]. A constant Maritime Traffic Situation Assessment and Monitoring (MTSAM) over a particular region of interest (also known as the observation region) can help establish higher security and safety margins, by avoiding collisions timely and enabling the detection of unlawful and anomalous activities such as illegal fishing

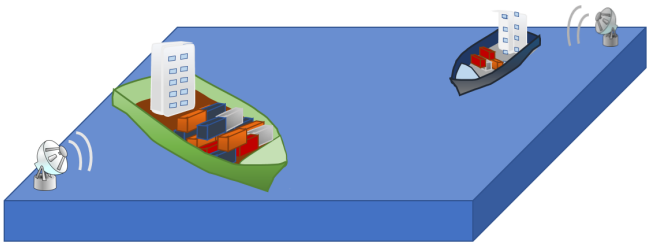

Figure 1.1: A simple observation region covered by two radar sensors.

or piracy [BWE+19, EWF+18, Gra18, FZ20, NOK+19, DBMW18, Tai05]. Like the introduction of autonomy in diverse fields, for instance, autonomous driving [MBMW17, KNW+15, KHB19, GLZZ16, ACE+16, HK20], autonomous shipping has also been given much focus over the past few years [AUT22] for supporting MTSAM. Overall, MTSAM aims to deliver insight on vessels' activities and their surroundings by processing information that has been provided by at least one sensor platform covering the observation region(s) over a certain time interval (as shown in Figure 1.1). Generally, maritime observation regions can span over hundreds of nautical miles, encompassing the air and both ocean and underwater surfaces, respectively, thus requiring the incorporation of data from a system of heterogeneous sensor platforms [HL97]. Such sensor platforms comprise (although not limited to) the Automatic Identification System (AIS), Radio Detection and Ranging (radar), infrared, Light Detection and Ranging (lidar), Sound Navigation and Ranging (sonar) and Unmanned Aerial Vehicles (UAV). The information that they all produce is basically energy that has been either reflected or emitted, from or by, targets of interest (vessels, in our case) as well as background noise clutter and internal sources of error [Bla86].

The AIS is a Global Positioning System (GPS) based system that broadcasts information at speed-dependent intervals among vessels and stations ashore, such as the Vessel Traffic Services (VTS) stations. It provides dynamic, static and voyage-related information of vessels for monitoring and locating vessels and navigational marks in their own vicinity [AIS18]. According to the International Maritime Organization (IMO)'s Convention for the Safety of Life at Sea (SOLAS), all vessels of at least 300 GT on international voyages and passenger ships are required to be equipped with the positioning system [SOL03, Mar]. Despite these benefits, AIS, as a stand-alone system, does not ensure a flawless service, having multiple well-known GPS vulnerabilities namely spoofing and jamming [The20, Mar, FZ20]. We also consider the case where not all vessels are fitted with an AIS transponder (leisure crafts, for example) and that there exist further inconsistencies within the timestamps and manifestations of unknown data due to incomplete transmission of AIS messages [BHG20, BSH16]. In contrast, the radar is an "all-weather, all-condition" sensor as coined by Prof. Alfonso Farina, one of the founding fathers of modern radar

systems. This makes the radar, either on board or at ground stations, a dominant sensor in the field and is today at the helm of a lot of applications for MTSAM and maritime surveillance systems [SRW15, ZWH+19, FBSS83, VBG+15, JBK21, WBSWB19, HKK21, BGV+12]. Information from multiple sensors has also been fused in order to overcome the limitations of individual sensors and this has been found to be advantageous in terms of precision, coverage and reliability [HBHE19, VGBW17, VGBW16, SBH16, SBHH17, Sie17, HBSH17].

When discontinuous, the basic sensor information (in the form of measurements or detections) that is acquired at an observation step (or scan) within the observed time interval lacks what is known as temporal continuity. Depending on the sensor system in use, measurements can be obtained at both regular intervals as well as irregular ones. The standard on board marine radar for instance refreshes its display at approximately every 2.5 seconds, and AIS measurements vary based on the own vessel dynamics. This makes target tracking approaches fundamental to the processing of sensor data for MTSAM. Target tracking can be defined as the estimation of a target's parameter state, that comprises properties of interest (for example, its kinematic attributes), given at least one sensor measurement in a time-varying system. Traditionally, tracking methods were developed based on the so-called single point assumption, where a target was represented by a single measurement. Lately however, with newer sensor technologies being developed, tracking methods need to account for cases whereby multiple measurements originate from a single target (see Figure 1.2a) as the latter occupies more than one sensor resolution cell. This is true in particular for the radar sensors, which are our main focus in this thesis. A benefit of having multiple measurements arising from a target is that it allows not only the kinematic attributes of the target to be estimated, but also its shape or extent which is also known as Extended Target Tracking (ETT) in literature [MCS+14, GBR17].

In the maritime context, ETT using radar systems could largely aid MTSAM for applications requiring target size estimation and categorisation [VB16, JBK21, HKK21, VBGW16, EAFBV15]. They could somewhat compensate for the limitations of the AIS as a backup system complementing the emerging terrestrial positioning system Ranging Mode (R-Mode) [GRG+21, KG20]. Newly constructed vessels, for example cargo ships, today having increased capacity as compared to their former models and spanning over lengths of over 400m, navigate on maritime sea routes and across ports for trade [Mar21a, Mar21b]. The larger the vessel, the greater is the possibility of misrepresentation of its true position, if we consider only the location of the transponder on board as illustrated in Figure 1.2a [STGS14]. It would be even worse in compromised cases due to jamming or spoofing in addition to poor environmental conditions at sea, more critically calling for collision avoidance. The same scenario could be enhanced when the radar is being considered. It not only detects the presence of the large vessel but it also provides a point cloud of measurements stemming from the vessel's surface as shown in Figure 1.2b. This incident can be exploited to estimate the extent properties of a vessel, which motivates our contributions.

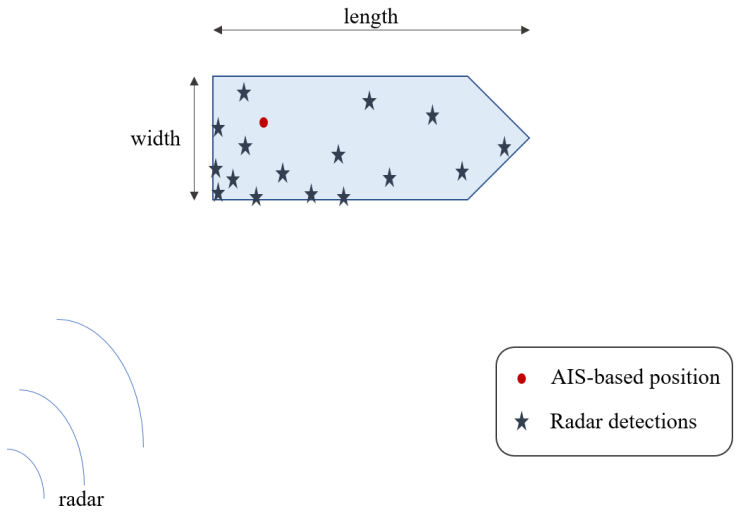

(a) The AIS-based position is illustrated as the red dot and the stars are the simplistic representation of radar detections arising from the vessel. The detections could be useful in MTSAM by estimating the true dimension of the vessel.

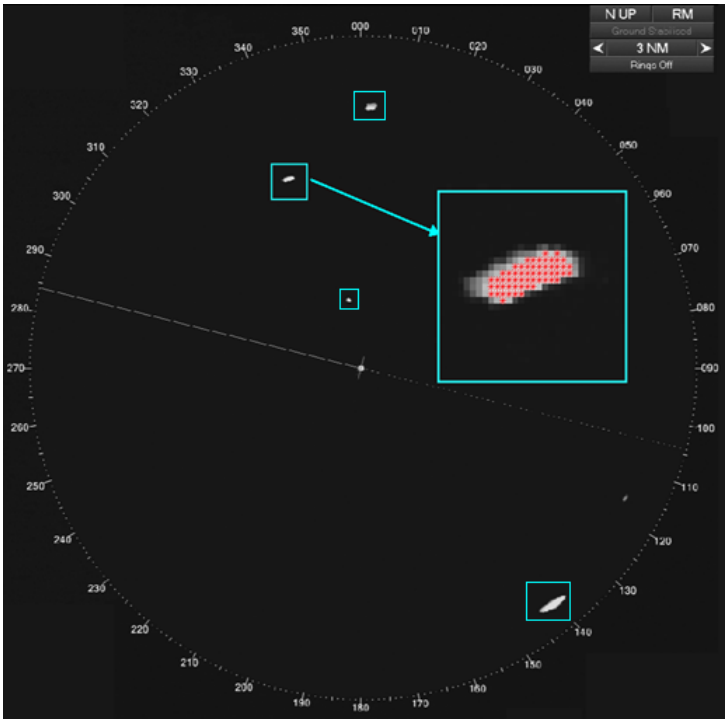

(b) A standard on board marine radar image captured during a measurement campaign. The potential targets are enclosed in cyan rectangles with a target's detections magnified. The point cloud formed by red crosses is the result of an intensity-based filter to obtain stronger detections.

Figure 1.2: Availability of multiple measurements from the radar sensor.

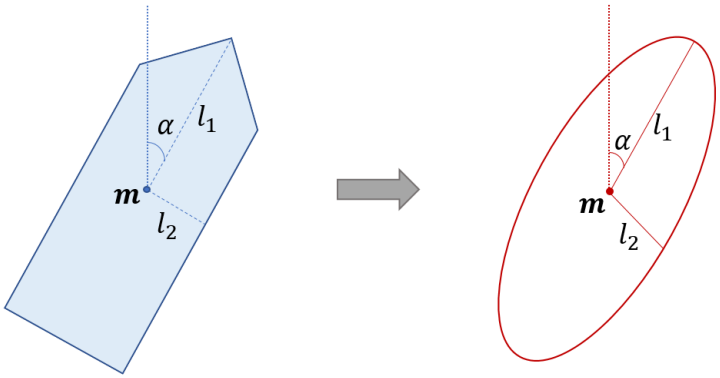

Figure 1.3: An elliptical parametrisation of a vessel with the lengths of the semi-axes l_1 and l_2 and orientation α. The centre $\boldsymbol{m}$ corresponds to the vessel's position.

A good tracking system for MTSAM would involve the ability to track the states of all potential vessels, whether or not equipped with AIS transponders, also referred to as Multiple Extended Target Tracking (METT). We focus on their extended states given radar detections, with each elliptically parametrised by their length, width and orientation as shown in Figure 1.3. The orientation corresponds to the true heading of the vessel and is measured from the North.

We now describe the challenges that have been considered in the thesis, framed by appropriate research questions in the following section.

1.2 Challenges and Research Questions

Radar systems, despite being "all-weather, all-condition" sensors, are still complex. Our research questions have been derived based on the challenges involved at distinct steps to achieve the broader perspective and work towards METT.

1.2.1 Environmental Factors

In a plethora of applications, a target's orientation is assumed to be aligned with its velocity. While it is a common and intuitive assumption for automotive applications, the same cannot be said with respect to maritime applications. The ocean as well as inland waterways are sensitive to the wind, ocean currents and tidal effects [NLR+18]. Vessels therefore require specific manoeuvrability skills to navigate through them, a result of which the vessel's heading might not necessarily coincide with its course over ground. *How can the true heading of a vessel be independently estimated, weighing in the existing elliptical approaches?* Chapter 4.1 addresses the first research question by the adaptation

and application of an elliptical tracker over real-world marine radar data.

1.2.2 Nature of Measurements

While measurement multiplicity is a factor we are exploiting for extent estimation, having to process above hundreds of measurements from multiple vessels could be tedious in computational and real-time processing capacities. Furthermore, as outlined in Chapters 2 and 4, radar measurements tend to be noisy and distorted, and not necessarily from uniformly distributed sources over the surface of the target. *Given a weak relation between the distribution of the dense distorted measurements and the true underlying target, how can the extended state of the target be estimated in a batch fashion?* It comes naturally based on application-specific requirements that uncertainty values to each extended state parameter can be separately assigned. For instance, while the estimated dimension of a vessel remains constant, orientation changes are more likely so the uncertainties should be flexible to reflect this. Therefore, we look at the next related research question: *how can a flexible and yet efficient filter be designed in addition to the previous quest, so as to allow for explicit parameterisation?* These two questions are addressed in Chapter 4.2, in which a linear and computationally efficient tracker has been proposed for elliptical ETT with explicit uncertainty representation of the ellipse's parameters.

1.2.3 Data Association

The two previous subsections considered tracking a single target whose approaches are now extended for the process of Multiple Target Tracking (MTT) and METT. Multiple target trackers need to employ strategies for partitioning the set of measurements received at an observation step and thereby associating them with existing tracks (of targets), potential tracks, or clutter otherwise. This is also known as the data association problem [Bla86, BSDH09, CMME11]. For our processing chain, where we have to deal with multiple measurements belonging to a target, *how can the above elliptical target tracker be integrated into a framework that can partition and associate measurements to their particular tracks efficiently?* Chapter 5 provides a framework based on a centroid-based data association scheme that integrates the elliptical method developed in Chapter 4.2 aimed for radar video processing.

1.3 Contributions

A summary of subsequent contributions made to the aforementioned research questions are listed as follows:

1. Proposing and curating a trio of radar-based datasets captured from measurement campaigns to the research community for evaluating target tracking methods where
    - information from AIS messages are being used as ground truth,

   - the recorded radar images are provided, and
   - extracted measurements from potential targets are included.
2. Proposing a framework for processing radar data from its acquisition to a maritime tracking application that includes vessel size categorisation.
3. Proposition and application of elliptical tracking approach tailored to estimate a vessel's true heading under rigid body conditions.
4. A novel principal-axes based elliptical tracker tailored for estimating the extended state of vessels
   - with explicit extent parametrisation, and
   - a linear batch update for the extent.
5. A centroid-based Joint Probabilistic Data Association (JPDA) tracker for MTT that takes the target's extent into account and applying the tracker to all of the proposed datasets.
6. An elliptical METT approach that integrates the principal-axes model into the centroid-based tracker.

Almost all of the proposed approaches were first developed and tested based on simulations, before being applied to processing real radar data in the proposed datasets. The final achievement is to have a tracker that sums up the contributions and that can be applied on a live radar video streaming from some harbour region on the German coast.

1.4 Thesis Structure

In Chapter 2, we describe a processing chain containing the functional blocks to show how targets' estimations are obtained, from detecting the radar measurements and filtering them using a tracker. The real-world marine radar datasets are introduced too, with relevant plots and information on the early stage (pre-filtering) processing. Those datasets are used in the next chapters to demonstrate the performance of our algorithms.

Chapter 3 explains the basics of filtering methodology based on the recursive Bayesian estimation. We look at linear and non-linear formulations of the Kalman Filter (KF), and describe the problem of and existing approaches to ETT. The basics of Data Association (DA), the process of measurement validation and calculation of association probabilities are covered.

The ETT-based contributions start from Chapter 4 onwards. The chapter is divided into two parts, where we present a tracker in each part. An explicit elliptical parameterisation and the tracker-specific modelling concepts are proposed. We have developed and implemented the algorithms both on simulated trajectories and on our datasets. The first algorithm focuses on estimating the orientation of a vessel with fixed semi-axes and the second one has been proposed with the aim

of computational efficiency. The two dedicated parts are broken down into specific subsections to have the conception, implementation, and results all compiled as a flow, as each development leads to the other based on the specific results.

Chapter 5 deals with MTT and its extension to METT. Following the same aforementioned format, the first part of the chapter describes an MTT algorithm tailored to centroids. Here, we are already considering a framework that includes additional steps, such as clustering. The second part puts together all of our findings and proposes the integration of our elliptical ETT and centroid-based MTT algorithms, with the addition of several other features to take care of track management and multi-sensor processing. The final method is applied on a real-world radar stream for our demonstrator software, and the results are illustrated.

We conclude the thesis in Chapter 6, where the findings are highlighted with appropriate discussions. The potential future endeavours connected to our work are also stated in the chapter to further improve the MTSAM process as a whole.

In addition, we provide supplementary materials in Appendix A to explain the concepts that have been used in the thesis, although they are not directly related to the final outcome of our work itself. Appendix B contains some additional results that were obtained when analysing our algorithms.

1.5 Guidance Notes

At the end of each chapter, the own research publications contributing to the concerned algorithm or concept are acknowledged. There are in-section citations as well as citations included in captions of images and tables for our own publications. When the term *adopted* is used, it refers to the original appearance in the said publication. The term *adapted* is used when the original data has been modified to fit the current parameter definition and/or the current nomenclature.

The own publications covering the scope of the thesis' research are cited in a numerical citation style and are listed first in the bibliography sections. The normal references are then listed with an alpha-numeric citation style.

Chapter 2

Processing Chain and Data Description

This chapter is bifurcated into two parts, covering a proposed processing chain and a description of the datasets proposed for evaluating maritime target tracking approaches. For the processing chain, we first look at the steps required to process raw data for potential target detection and extraction to achieve the desired framework for an exemplar MTSAM application. The desired results are to have extended state estimates of vessels with a further estimate of their size categories. Such an application could provide a strong base for maritime situational awareness systems for instance, to detect anomalous activities within some region of interest. We then provide a description of the marine radar-based data that are going to be used to test and apply the methods developed within the scope of the thesis.

Contents

2.1 Processing Chain

Our processing chain is described to provide an overall inspection of the application objectives and requirements at specific stages. As mentioned in Chapter 1.1, raw sensor data, for example an

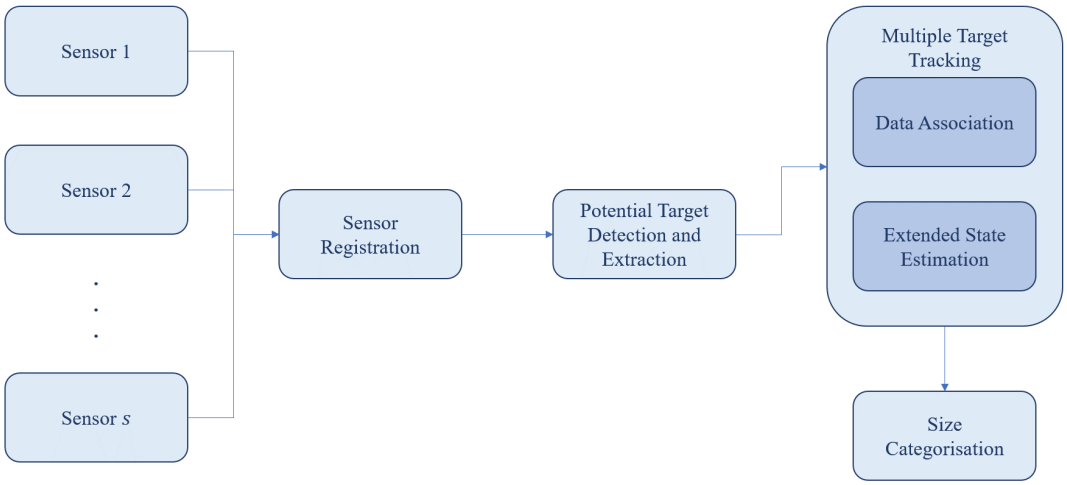

Figure 2.1: Functional blocks in our processing chain.

individual radar image, provides no representation of temporal continuity. To establish continuity, the processing chain employs target tracking and association approaches thereby connecting measurements from preceding to succeeding images and enabling the extended states of targets to be estimated. Such a chain is shown in Figure 2.1. The steps within the chain are discussed in the following text.

2.1.1 Raw Sensor Data and Preprocessing

Raw radar sensor data lies at the lowest level of the processing chain that we consider and provides us with detections that have been reflected back based on its surroundings. On the typical radar screen as shown in Figure 1.2b, the brightness of the detections denotes their equivalent intensity. We consider processing these types of detections, either from continuous recorded radar images or from live radar video streaming (for example, as defined by the All Purpose Structured EUROCONTROL Surveillance Information Exchange (ASTERIX) protocol of Category 240 [EUR]) from multiple sensor sources/platforms. The data then undergoes preprocessing so that only pixel-wise representations of the potential targets are obtained. A thorough explanation on this process is found in Chapter 2.2.

With ASTERIX streams, data is transmitted among cooperating sensors, that can be both static or dynamic. This creates an abstraction of the different sensor sources and ensures that the data is in a standard format. ASTERIX data requires to be decoded appropriately to obtain radar detections, following which the above-mentioned pixel-wise preprocessing is carried out.

2.1.2 Sensor Registration

Having data from multiple sensors brings about a number of challenges. A significant one is the need for a common-reference coordinate system to ensure each sensor is representing the same region, whose axes are defined by the same units [BP99, HL97]. This requires an appropriate coordinate transformation and positioning schemes. The two dimensional coordinates of radar detections are normally given in polar coordinates, in range and bearing (azimuth) with respect to the sensor's own position, either as a stationary ground station or as a dynamic on board system. In the case of ground stations, the transformation and registration are simpler. An arbitrary point is chosen as a common reference point for all sensors within the observation region and the detections can be rotated and translated into the required coordinate system. Under dynamic settings however, knowledge on the true sensor position is often limited [HL97, LNG06]. In this case, a specific positioning can be provided by a secondary source (for instance the AIS).

The detections, originally in polar coordinates, can either be directly processed, or converted to Cartesian coordinates through coordinate transformation schemes before further processing [FS85, LBS93, Fra07].

2.1.3 Target Detection and Extraction

Typical radar detections arise from a collection of sources in a dense environment, necessitating to distinguish those that are most likely to be targets (also known as potential targets) as well as to identify static aids to navigation. In addition, the detections are in the form of point clouds with finer sensor resolutions (we note that, the sensor resolution can be expected to be up to a metre per pixel for the video streams), making the distinction among targets, aids to navigation and background clutter imperative. Appropriate feature-based target detection and extraction methods are therefore required for fulfilling that purpose [1] [HBS15, HHBS17, VB16, SHBH18]. These methods may include a series of sub-techniques by themselves to match the form of measurements that are needed as input for the target tracking steps. In Chapter 2.2, we shall elaborate on the specific techniques that were employed on the respective dataset during the course of the thesis.

2.1.4 Multiple Target Tracking

At this stage, we will have received a set of measurement point clouds with unknown origins. They could, for instance, have originated from one of the following:

- at least one vessel in a dense target background with rapidly manoeuvring targets or static aids to navigation,
- at least one aid to navigation, and
- background clutter due to external environmental factors or internal errors.

This problem is also known as MTT, where the states and cardinality of multiple targets are to be estimated [VMBS+15]. DA and Random Finite Sets (RFS) are principal and well-known approaches to solve the problem and are continuously being improved on in the community. Variations of the established data association-based Multiple Hypothesis Tracker (MHT) and Probabilistic Data Association (PDA) approaches have been applied vastly for tracking. While MHT enumerates exhaustively over all association hypotheses having high measurement-to-track assignment probabilities [Bla04, Bla16, Mah00], the PDA approach restricts the number of hypotheses by applying a gating and combines the filtered hypotheses into a single one [BSDH09, Kir04, ME04, RCBSW10, FBSS81, SSGW11, HTT+13]. The PDA methodology, having been formulated for a single target, can be expanded to track multiple targets by the JPDA filter [BSDH09]. The relatively lower computational requirements required by JPDA at a single scan often makes it one of the favoured alternatives to MHT's multiple-scans hypotheses enumeration or schemes involving searches for the best hypothesis. The Nearest Neighbour (NN) approach is another simple association technique based on feature-based metrics that have demonstrated practicability in several applications [Bla04, SL06, JBK21]. The RFS approach models targets of interest and their cardinality as a set of random variables whose moments are temporally propagated as a joint distribution. Implementations of the RFS include the probability hypothesis density filter [MZ01, Mah07, GO12, GLO12], and the multi-Bernoulli based filters [VVP14, VVH17, BRG+16, Mah19, GFS16, GFS19, XGS+21].

In this thesis, we focus on the JPDA approach for state estimation. Along with the estimation of kinematic state, we have also incorporated elliptical state estimation into the framework. Furthermore, for our cooperative multi-radar sensor processing, we have chosen to use a central-level sequential update scheme [Bla04] for processing the measurements from individual sensors thus accounting for their uncertainties.

2.1.5 Size Categorisation

The size categorisation step comes as an additional feature of the framework. The estimated sizes of vessels are subject to a classification scheme that categorises the vessels as being either small, medium or large, based on predefined ranges [2]. This step is a start to further high-level applications, for instance, to be able to test the idea of eventually classifying the vessels types in a real-time scenario to verify whether the target matches the expected one (for example, as given by the AIS information), and is not being masqueraded by another one.

Note: All the major stages are carried out independently at each individual observation step.

2.2 DLR Marine Radar Repository

One of the prerequisites to implement the overall framework was to have at least one real-world marine radar dataset that could be used to test the algorithms that were being developed. As op-

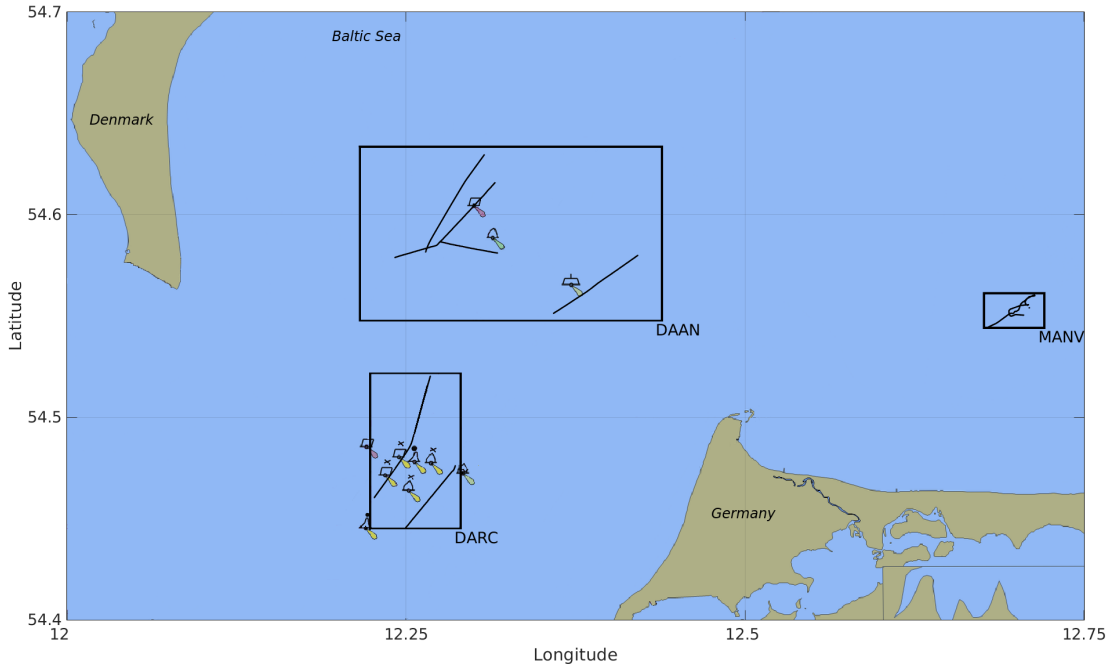

Figure 2.2: Datasets recorded from campaigns at the Baltic Sea. Their AIS-based trajectories have been plotted for illustration, as vessels navigate through aids to navigation. Image from [1] ©2021MDPI.

posed to the availability of well-established datasets such as KITTI [GLSU13], nuScenes [CBL+20] or Oxford RobotCar [BGM+20] in the automotive industry, the maritime domain has hardly any. Some of the past research have dealt with datasets [GCCG06, CGT06], although the latter have not been published. Therefore, the group at our department in German Aerospace Centre (Deutsches Zentrum fuer Luft- und Raumfahrt) (DLR) organised several measurements campaigns to record situations as close to those encountered on maritime routes in reality. The resulting datasets were then cleaned and prepared. They are now available to the research community upon request from the company's maintained repository [Ger] and are subject to approval by the company's export control principles. In this section, we provide information about the processing of the datasets and some details on the trajectories from each.

2.2.1 Data Recording

The measurement campaigns were carried out in the region of the Baltic sea, as illustrated in Figure 2.2. The three datasets from our repository are labelled as Manoeuvres (MANV), Data Association with Aids to Navigation (DAAN) and Data Association with Radar Beacon (DARC) and are framed by a rectangular bounding box wherein the trajectories of AIS-equipped vessels are included while they navigate in the vicinity of multiple aids to navigation.

Table 2.1: Dataset Outline

Dataset	Number of Targets	On board Sensor(s)
DAAN	4	Dynamic (Own)
DARC	2	Dynamic (Own)
MANV	6	Dynamic (Own) + Static (Observer)

DAAN and DARC were recorded from the own vessel in a dynamic state, by grabbing successive visuals from the on board radar screen. For the MANV dataset, data was recorded from both the own vessel (dynamic) and an observer vessel that was anchored. Table 2.1 summarises the number of targets (including the own) and the state of the sensor (based on its motion) involved in each dataset. The AIS reports covering the campaigns were also gathered for further processing.

2.2.2 AIS Data Processing

To support evaluation, the repository also provides AIS data as a ground truth. AIS messages have been decoded based on the date and time of the campaigns. In case multiple messages were received at a particular time, the most recent one was kept. Furthermore, the trajectories involved were filtered using the Maritime Mobile Service Identification (MMSI) numbers of the vessels. The information considered are dynamic data such as position, course over ground, speed over ground and true heading. Other information of interest were the vessel's reported length and width. The data, in general, is arranged chronologically in a reset time variable to wipe out the true identity of the vessels from the campaigns.

The position vectors, initially in geographical coordinate frame, are expressed based on the World Geodetic System 1984 (WGS84) in terms of longitude λ, latitude φ and altitude or height h. These are converted to a three-dimensional Cartesian coordinates based on the Earth-Centred Earth-Fixed system, in terms of the sensor's own position. They are then converted to an East North Up (ENU)-equivalent as shown in Figure 2.3 to maintain a common local frame with the radar sensor and a simplified filter modelling. The ENU is a tangential plane to the Earth's surface fixed at an arbitrary point [SJHP13, p. 43-49] in the observation region of interest. Our targets are recorded as they navigate on the Earth's surface, so we assume the Up-coordinate to be negligible.

2.2.3 Radar Image Processing

The radar images are first processed to extract potential targets based on their pixel intensities using appropriate user-defined threshold values. In this step, the weaker detections are eliminated, already reducing some of the clutter present. At this point, we emphasise on the difference in the sensor resolutions of the datasets. DAAN and DARC, have a relatively coarse resolution, whereby

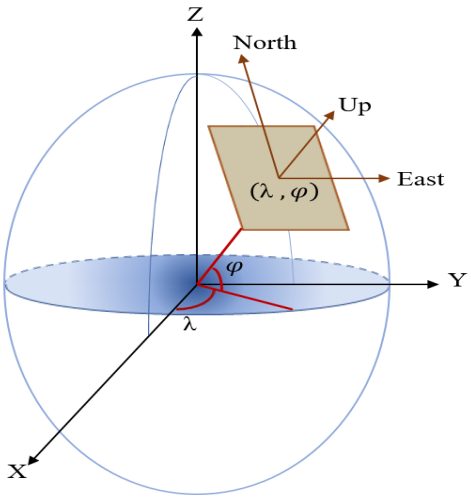

Figure 2.3: Geographic and ENU coordinate systems [SJHP13].

1 pixel of the image corresponds to 11m as compared to MANV, which has a finer resolution where a pixel covers 6m.

As the datasets were being prepared for both our own use as well as for our repository, we aimed at the provision of both images and a measurement file, respectively, for each dataset. The measurement file contains the position of all potential targets in polar as well as Cartesian coordinates, extracted by an appropriate detection method described next.

Blob Detection

The filtered image is input to a blob detection algorithm called the Determinant of Hessians (DoH), which was selected due to its scale and rotation invariance capabilities [BETV08, Pyt]. The algorithm outputs the blob's centre and its radius. The measurements extracted are all the pixels falling within the corresponding circumference and were stored on the basis of their range and bearing to the own vessel's AIS-position (the radar screen's centre point (See Figure 1.2b)). The equivalent Cartesian coordinates conversion is obtained from the standard formulae in Appendix A.2. These coordinates are the input to our target tracking approach(es).

Clustering

Clustering is a common way of partitioning measurements in multiple maritime applications [HBHE19, VB16]. The clustering step here is mainly an additional one demonstrating how to potentially process the data from our measurement file directly. Hence, an elementary approach, the k-means clustering method [Mac67, Boc08] was applied. A cluster evaluation method, complementing the k-means, based on the Calinski-Harabasz Indicator was employed to mitigate the

limitation that the number of clusters existing should be known beforehand [XT15, Sch18]. The centroids obtained are taken as the measurements of interest for our tracker(s) in Chapter 5.1. In that chapter and in Appendix B.3, we shall also see how the clustering method would be an important factor affecting the tracking results using appropriate plots.

It is to be noted that clustering could also be immediately carried out instead of the blob detection, as long as the chosen approach is not sensitive to outliers.

2.2.4 Overall Trajectories

The trajectory visuals over the duration of each dataset are depicted in Figure 2.4. The highlighted situations in each dataset [1, 3] are briefly described.

In the radar plot of DAAN, one can find the presence of aids to navigation and a trail caused by radar reflections. Target 4 is out of range of the radar sensor, hence it is not entirely visible over the course of the trajectory. Similar to DAAN, some aids to navigation are found in the radar plots for DARC, together with detections from the Radar Beacon (RACON). In MANV, there is persistent clutter and the detection of a craft/boat which was not equipped with any AIS transponder.

2.3 Chapter Summary

The first half of the chapter has covered the steps encompassed in the processing chain that has been designed to have a working demonstrator capable of performing target tracking in the maritime perspective. At the lowest level, data from live radar video streams are processed and fed to a tracker that allows for MTSAM in near real-time, at the highest level.

The second half is about the creation of three datasets-repository showing common situations occurring in the day-to-day maritime environment that has been used as a basis to evaluate the performance of our algorithms developed in the upcoming part of the thesis.

The contributions presented in this chapter were partially published in journal article [1] and conference proceedings [3] and [2].

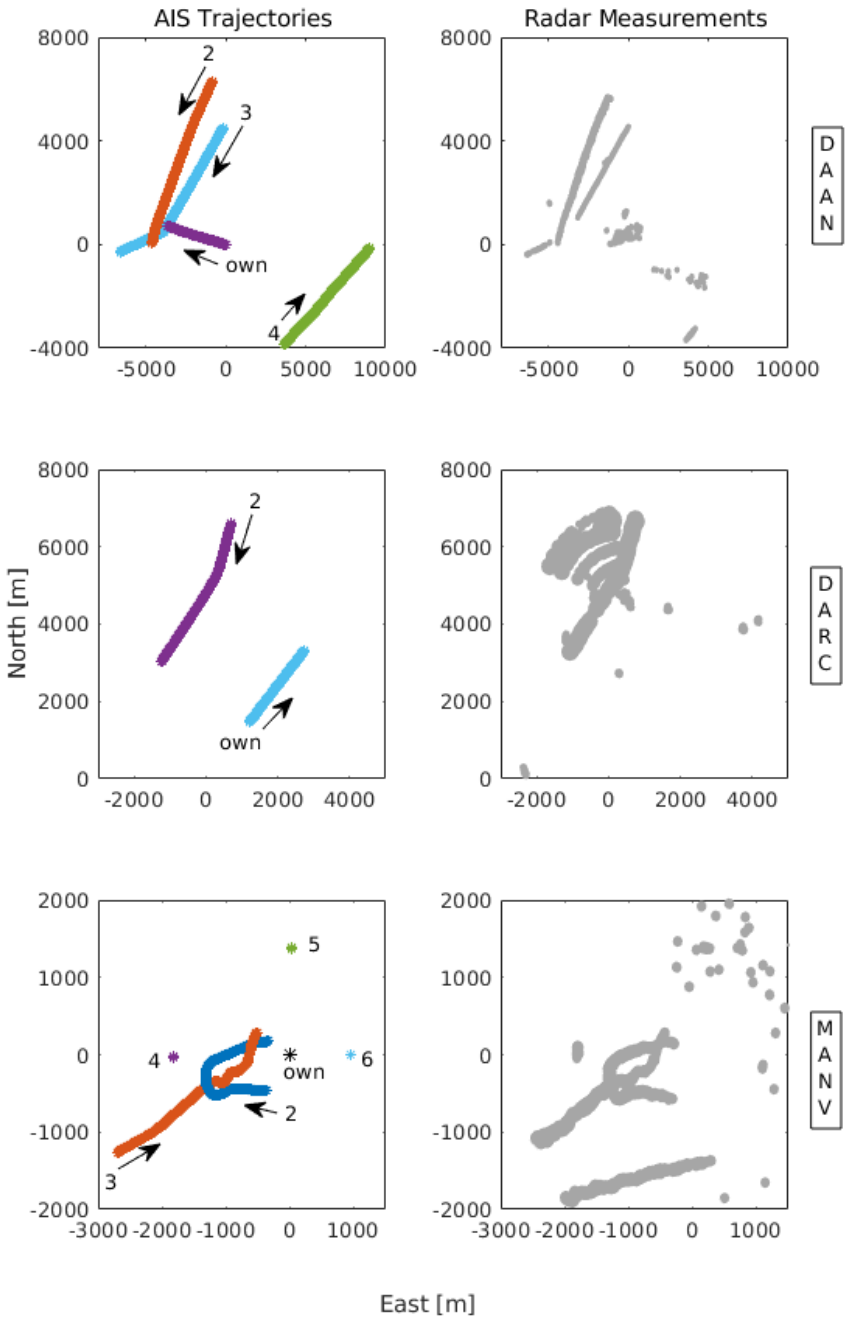

Figure 2.4: The AIS- and radar-based trajectories of the datasets. The AIS measurements are colour-coded and labelled target-wise. The radar measurements are unassociated and in the form of point clouds. Image from [1] ©2021MDPI.

Chapter 3

Fundamentals

This chapter covers the basics of the filtering methodology that is employed for the estimation of the time-varying state of a target of interest from a set of measurements as well as its propagation in time. The problem is described at first, moving towards the formulation of a linear filter and then its non-linear version. The problem of ETT is also presented followed by the foundations of DA for the measurement-to-track association problem.

Contents

3.1 Bayesian State Estimation

The target state $\boldsymbol{x}_k \in \mathbb{R}^{n_{\boldsymbol{x}}}$ is a vector that contains the parameters of interest and can be modelled as a random variable having Probability Density Function (PDF) $p(\boldsymbol{x}_k)$, where subscript $k \in \mathbb{N}$ represents the observation step and $n_{\boldsymbol{x}}$ the dimension of the state vector. Let a currently acquired measurement be denoted by $\boldsymbol{y}_k$ and all previous measurements by $\boldsymbol{y}_{0:k-1} = \{\boldsymbol{y}_0, ..., \boldsymbol{y}_{k-1}\}$. The measurement at k is assumed to be independent of the previous ones.

The purpose of Bayesian estimation is to calculate the posterior PDF of the target's state given the current measurement, $p\left(\boldsymbol{x}_k|\boldsymbol{y}_k\right)$, from a prior PDF over the state, $p\left(\boldsymbol{x}_{k-1}|\boldsymbol{y}_{0:k-1}\right)$, and the likelihood function $p\left(\boldsymbol{y}_k|\boldsymbol{x}_k\right)$. Using Bayes' formula, the posterior can be thereby expressed as follows,

$$p\left(\boldsymbol{x}_k|\boldsymbol{y}_k\right) \propto p\left(\boldsymbol{y}_k|\boldsymbol{x}_k\right) p\left(\boldsymbol{x}_{k-1}|\boldsymbol{y}_{0:k-1}\right). \tag{3.1.1}$$

Considering that targets evolve temporally, a recursive form of (3.1.1) is sought so that the state can be recursively propagated into the future to obtain a state prediction. Based on the *Chapman-Kolmogorov* equation and the prior, the state prediction PDF $p(\boldsymbol{x}_k|\boldsymbol{y}_{0:k-1})$ can be written as an integral over observation step $(k-1)$,

$$p(\boldsymbol{x}_k|\boldsymbol{y}_{0:k-1}) = \int p(\boldsymbol{x}_k|\boldsymbol{x}_{k-1}) p(\boldsymbol{x}_{k-1}|\boldsymbol{y}_{0:k-1}) d\boldsymbol{x}_{k-1}, \tag{3.1.2}$$

with state transition PDF described as $p(\boldsymbol{x}_k|\boldsymbol{x}_{k-1})$.

The prediction then incorporates measurement $\boldsymbol{y}_k$ through the likelihood function $p(\boldsymbol{y}_k|\boldsymbol{x}_k)$. Equation (3.1.1) is expressed based on the following equation [CMME11] to obtain the posterior $p(\boldsymbol{x}_k|\boldsymbol{y}_k)$,

$$p(\boldsymbol{x}_k|\boldsymbol{y}_k) = \frac{1}{p(\boldsymbol{y}_k|\boldsymbol{y}_{0:k-1})} p(\boldsymbol{y}_k|\boldsymbol{x}_k) \int p(\boldsymbol{x}_k|\boldsymbol{x}_{k-1}) p(\boldsymbol{x}_{k-1}|\boldsymbol{y}_{0:k-1}) d\boldsymbol{x}_{k-1}, \tag{3.1.3}$$

where $\frac{1}{p(\boldsymbol{y}_k|\boldsymbol{y}_{0:k-1})}$ is a normalisation factor.

To obtain a filtering solution with the KF, the initial step is to express specific system and sensor models, respectively, allowing the target's state to be estimated in a standard state-space form [BSKL02, Bar19].

3.1.1 System Model

The system model, also known as state model or motion model, can be described as a discrete time Markov process [1] which represents the target state dynamics at the current step k conditioned on all the previous measurements $\boldsymbol{y}_{0:k-1}$ at a previous observation step $(k-1)$. The state equation is given as follows,

$$\boldsymbol{x}_k = \mathbf{F}_k \boldsymbol{x}_{k-1} + \boldsymbol{\omega}_k. \tag{3.1.4}$$

$\mathbf{F}_k$ is the state transition matrix and $\boldsymbol{\omega}_k$ is random process noise with covariance $\mathbf{C}_k^{\boldsymbol{\omega}}$, that accounts for uncertainties in the evolution. The state equation is the basis to obtain the state prediction PDF $p(\boldsymbol{x}_k|\boldsymbol{y}_{0:k-1})$, corresponding to (3.1.2).

[1] Based on the Markovian property, the current state is dependent only on the previous state. In addition, measurements obtained at k are independent of the previous state(s).

3.1.2 Sensor Model

At the observation step k, a measurement $\boldsymbol{y}_k \in \mathbb{R}^{n_{\boldsymbol{y}}}$ is obtained. A sensor model, also known as observation model, maps the state vector onto the measurement vector. The sensor model can be expressed based on the measurement equation as follows,

$$\boldsymbol{y}_k = \underbrace{\mathbf{H}_k \boldsymbol{x}_k}_{:=\boldsymbol{z}_k} + \boldsymbol{\upsilon}_k. \tag{3.1.5}$$

$\mathbf{H}_k$ is the measurement matrix and $\boldsymbol{\upsilon}_k$ random measurement noise with covariance $\mathbf{C}_k^{\boldsymbol{\upsilon}}$ that describes measurement uncertainties. $\boldsymbol{z}_k$ represents the measurement source. The likelihood function $p(\boldsymbol{y}_k|\boldsymbol{x}_k)$ can be determined from Equation (3.1.5).

3.1.3 The Kalman Filter

KF functions on the basis of a few assumptions that we highlight as follows. It is assumed that the PDF of the state can be described as a Gaussian,

$$p(\boldsymbol{x}_k|\boldsymbol{y}_k) \approx \mathcal{N}(\boldsymbol{x}_k; \hat{\boldsymbol{x}}_k, \mathbf{C}_k^{\boldsymbol{x}}) \tag{3.1.6}$$

with mean $\hat{\boldsymbol{x}}_k$ and covariance $\mathbf{C}_k^{\boldsymbol{x}}$. The additive noises for the system and sensor models defined in (3.1.4) and (3.1.5) are assumed to be uncorrelated, zero-mean Gaussian PDFs as,

$$\boldsymbol{\omega}_k \sim \mathcal{N}(0, \mathbf{C}_k^{\boldsymbol{\omega}}), \tag{3.1.7}$$

$$\boldsymbol{\upsilon}_k \sim \mathcal{N}(0, \mathbf{C}_k^{\boldsymbol{\upsilon}}). \tag{3.1.8}$$

The KF applies a recursive two-stage methodology for the estimation of the posterior state of the target as the conditional mean based on the cumulative sequence of measurements [BSKL02, Kal60, Bar19],

$$\hat{\boldsymbol{x}}_k := E\left\{\boldsymbol{x}_k|\boldsymbol{y}_{0:k}\right\}, \tag{3.1.9}$$

with corresponding conditional error covariance matrix given by

$$\mathbf{C}_k^{\boldsymbol{x}} := E\left\{\left(\boldsymbol{x}_k - \hat{\boldsymbol{x}}_k\right)\left(\boldsymbol{x}_k - \hat{\boldsymbol{x}}_k\right)^T |\boldsymbol{y}_{0:k}\right\}. \tag{3.1.10}$$

The filtering process is visualised in Figure 3.1 as well as visualisation of changes in the state PDF to particularly reflect the uncertainties during the prediction and update. We consider the simple estimation of a vessel's state.

From here on, we denote the prediction and update phases of the same vector as well as matrix using subscripts $(k|k-1)$ and $(k|k)$, respectively.

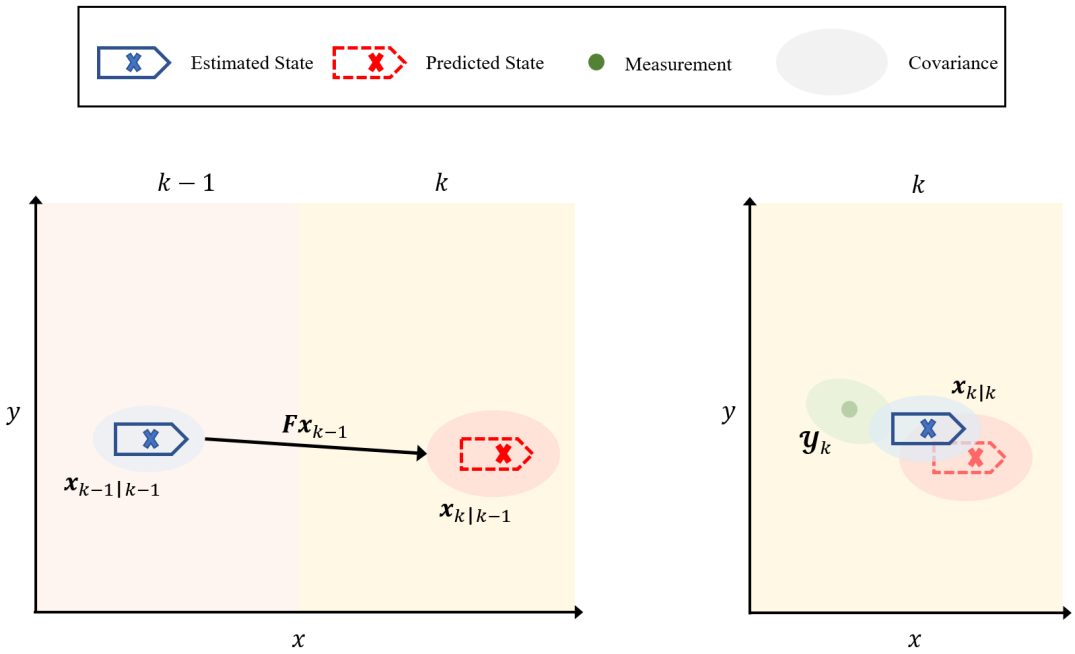

Figure 3.1: (Left) In the prediction step, the target state is propagated from $(k-1)$ to the next step k through a transition function, and grows in uncertainty. (Right) Upon the acquisition of a measurement, the prediction is then updated to give the k^{th} estimate and reinforces the certainty in the update step.

Prediction

The state prediction $\hat{\boldsymbol{x}}_{k|k-1}$ and its covariance $\mathbf{C}^{\boldsymbol{x}}_{k|k-1}$ are estimated based on the following equations:

$$\hat{\boldsymbol{x}}_{k|k-1} = \mathbf{F}_k \hat{\boldsymbol{x}}_{k-1|k-1}, \tag{3.1.11}$$

$$\mathbf{C}^{\boldsymbol{x}}_{k|k-1} = \mathbf{F}_k \mathbf{C}^{\boldsymbol{x}}_{k-1|k-1} \mathbf{F}_k^T + \mathbf{C}^{\boldsymbol{\omega}}_k, \tag{3.1.12}$$

where $(\cdot)^T$ denotes the transpose operation and $\mathbf{F}_k$ and $\mathbf{C}^{\boldsymbol{\omega}}_k$ are defined similarly as in 3.1.1.

Update

When a measurement $\boldsymbol{y}_k$ is available at observation step k, an updated estimate $\hat{\boldsymbol{x}}_{k|k}$ of state $\boldsymbol{x}_k$ is computed along with its covariance $\mathbf{C}^{\boldsymbol{x}}_{k|k}$,

$$\hat{\boldsymbol{x}}_{k|k} = \hat{\boldsymbol{x}}_{k|k-1} + \mathbf{K}_k(\boldsymbol{y}_k - \mathbf{H}_k \hat{\boldsymbol{x}}_{k|k-1}), \tag{3.1.13}$$

$$\mathbf{C}^{\boldsymbol{x}}_{k|k} = \mathbf{C}^{\boldsymbol{x}}_{k|k-1} - \mathbf{K}_k \mathbf{C}^{\boldsymbol{y}}_k \mathbf{K}_k^T, \tag{3.1.14}$$

where the gain matrix $\mathbf{K}_k$ and the innovation covariance $\mathbf{C}_k^{\boldsymbol{y}}$ are,

$$\mathbf{K}_k = \mathbf{C}_{k|k-1}^{\boldsymbol{x}} \mathbf{H}_k^T (\mathbf{C}_k^{\boldsymbol{y}})^{-1}, \tag{3.1.15}$$

$$\mathbf{C}_k^{\boldsymbol{y}} = \mathbf{H}_k \mathbf{C}_{k|k-1}^{\boldsymbol{x}} \mathbf{H}_k^T + \mathbf{C}_k^{\boldsymbol{\upsilon}}. \tag{3.1.16}$$

As the KF is recursive, it starts with an estimate (prior), generates a prediction and updates the prediction to a new estimate (posterior) given an observation. The filter predicts by explicitly employing the system model and the sensor model for generating the update. Besides the state propagation, the filter also accounts for modelling errors by propagating the covariance of the prediction and estimate.

3.1.4 The Extended Kalman Filter

In Section 3.1.3, both the system and sensor models are linear, thus limiting the applicability of the KF for more complex non-linear systems. The Extended Kalman Filter (EKF) is a version of KF that could be employed instead. In this section, we briefly go over the EKF equations [Bar19, BSKL02].

The system model can be described by a non-linear model in state-space notation with additive noise of the form

$$\boldsymbol{x}_k = f(\boldsymbol{x}_{k-1}) + \boldsymbol{\omega}_k, \tag{3.1.17}$$

where $f(\cdot)$ is a function describing the target motion. Similarly, the sensor model can be described as follows,

$$\boldsymbol{y}_k = h(\boldsymbol{x}_k) + \boldsymbol{\upsilon}_k, \tag{3.1.18}$$

where $h(\cdot)$ defines a non-linear function mapping of the state to the measurements.

Using a first-order Taylor series expansion, the EKF linearises the models by seeking an approximation around the current state estimate and prediction, respectively. Following the same steps as for the KF, the EKF prediction and update equations are stated next [Bar19].

Prediction

A prediction $\hat{\boldsymbol{x}}_{k|k-1}$ and its covariance $\mathbf{C}_{k|k-1}^{\boldsymbol{x}}$ are estimated based on the following equations:

$$\hat{\boldsymbol{x}}_{k|k-1} = f(\hat{\boldsymbol{x}}_{k-1|k-1}), \tag{3.1.19}$$

$$\mathbf{C}_{k|k-1}^{\boldsymbol{x}} = \bar{\mathbf{F}}_k \mathbf{C}_{k-1|k-1}^{\boldsymbol{x}} \bar{\mathbf{F}}_k^T + \mathbf{C}_k^{\boldsymbol{\omega}}, \tag{3.1.20}$$

where $\bar{\mathbf{F}}_k = f'_{\boldsymbol{x}}(\hat{\boldsymbol{x}}_{k-1|k-1})$ is the Jacobian matrix based on the state equation that was evaluated at $\hat{\boldsymbol{x}}_{k-1|k-1}$.

Update

When a measurement $\boldsymbol{y}_k$ is available at observation step k, an updated estimate $\hat{\boldsymbol{x}}_{k|k}$ can be computed with its covariance $\mathbf{C}^{\boldsymbol{x}}_{k|k}$ using,

$$\hat{\boldsymbol{x}}_{k|k} = \hat{\boldsymbol{x}}_{k|k-1} + \mathbf{K}_k \left(\boldsymbol{y}_k - h(\hat{\boldsymbol{x}}_{k|k-1}) \right), \tag{3.1.21}$$

$$\mathbf{C}^{\boldsymbol{x}}_{k|k} = \mathbf{C}^{\boldsymbol{x}}_{k|k-1} - \mathbf{K}_k \mathbf{C}^{\boldsymbol{y}}_k \mathbf{K}_k^T, \tag{3.1.22}$$

where the gain matrix $\mathbf{K}_k$ and the innovation covariance $\mathbf{C}^{\boldsymbol{y}}_k$ are given by,

$$\mathbf{K}_k = \mathbf{C}^{\boldsymbol{x}}_{k|k-1} \bar{\mathbf{H}}_k^T (\mathbf{C}^{\boldsymbol{y}}_k)^{-1}, \tag{3.1.23}$$

$$\mathbf{C}^{\boldsymbol{y}}_k = \bar{\mathbf{H}}_k \mathbf{C}^{\boldsymbol{x}}_{k|k-1} \bar{\mathbf{H}}_k + \mathbf{C}^{\boldsymbol{v}}_k. \tag{3.1.24}$$

Similar to the linearisation for obtaining the prediction, $\bar{\mathbf{H}}_k = h'_{\boldsymbol{x}}(\tilde{\boldsymbol{x}}_{k|k-1})$ is the Jacobian matrix based on the measurement equation evaluated at $\hat{\boldsymbol{x}}_{k|k-1}$.

3.2 Extended Target Tracking

Most of the tracking algorithms were initially developed to estimate the kinematic parameters (for instance position, velocity, or acceleration) - assuming that one target would give rise to a single detection point. However, as reflections from targets have the tendency to consume multiple sensor resolution cells nowadays, more information about the target's extent could be deduced. This means that the point-target assumption would be nullified since the detections that spring from the target's body, as mentioned in the first chapter, are in the form of point clouds (See Figure 3.2). The newer algorithms have been taking the extent into consideration in the recent past.

Let $\boldsymbol{\mathcal{Y}}_k = \left\{ \boldsymbol{y}_k^j \right\}_{j=1}^{m}$ be the set of m measurements (detections) that originated from a target of interest. An extended target can be basically modelled by likelihood $p(\boldsymbol{\mathcal{Y}}_k | \boldsymbol{x}_k)$ to capture how the measurements are distributed around its surface. A spatial model was formulated to model the measurements based on a Poisson Point Process (PPP) [GS05, GGMS05], which enables the representation of every $\boldsymbol{y}^j \in \boldsymbol{\mathcal{Y}}_k$ as some source $\boldsymbol{z}^j$ perturbed by noise, and is given as follows (omitting k for notational convenience),

$$p(\boldsymbol{y}^j | \boldsymbol{x}) = \int p(\boldsymbol{y}^j | \boldsymbol{z}^j) p(\boldsymbol{z}^j | \boldsymbol{x}) \quad d\boldsymbol{z}^j. \tag{3.2.1}$$

$p(\boldsymbol{y}^j | \boldsymbol{z}^j)$ defines the sensor noise and $p(\boldsymbol{z}^j | \boldsymbol{x})$ represents the PDF of the measurement sources over the target's extent. The spatial model was fundamental to the development of several approaches to estimate a target's spatial extent.

In the following parts, we will go briefly over some of the different types of models adopted over the years. A full review is found in [MCS+14, GBR17].

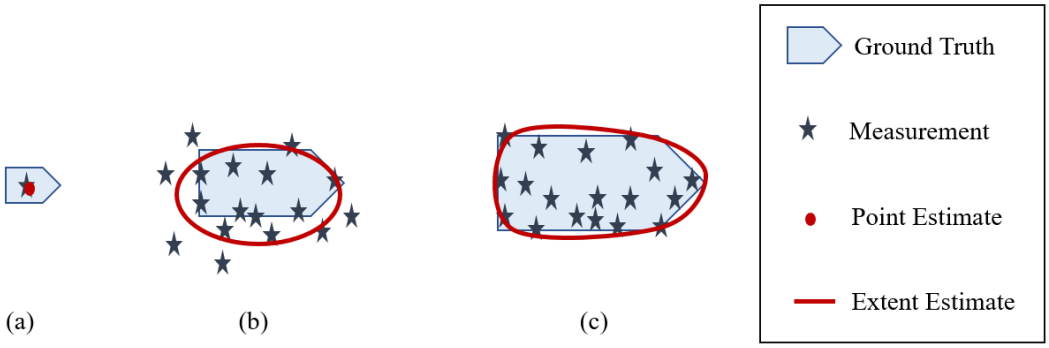

Figure 3.2: Exemplar extent modelling of a target based on the measurements' distribution. (a) A simple point-target state estimation, as replicated for a potential far-range sensor. State parameters are restricted to kinematic properties mostly. (b) An elliptical extent approximation in the case of a noisy set of measurements given the ground truth. State includes extent parameters (orientation and lengths of semi-axes). (c) An arbitrary extent approximation for shorter range sensors and their more accurate measurements. Extent parameters are based on complex descriptors.

3.2.1 Basic Geometric Shapes

Targets can be modelled by circular, elliptical and rectangular basic shapes. Circular models have been integrated within Bayesian estimators for representing a target's position as the circle's centre and the target's extent defined by a radius [BKH10, KBW16, PGMA12]. A more common choice for multiple tracking applications today involve estimating the elliptical approximation of a target with a Symmetric and Positive Definite (SPD) matrix [Koc08, FF08, FFK11, VBG+15, LL16, LL19, ZL20, ZL21] as well as with explicit extent parameters comprising its length, width and orientation [DWS11, BE18, YB19, Gov19, LLL20, TO21]. In a similar direction, the rectangular models have also been explored [GRMS14, GLO11, TYB21, XWB+21].

3.2.2 Star-Convex and Arbitrary Shapes

Some of the advanced models that provide highly descriptive and precise representation of the target's extent are the star-convex ones based on Random Hypersurface Model (RHM) [BH09, BNH10, BH11, BH14, SBZ+15, KBW17] and its Gaussian Processes (GP) derivatives [WO15, HSRD16, TKOA18]. The former models rely on radial functions and the latter on GP bases, whose extent-describing parameters are estimated. Individual elliptical sub-objects based on the Random Matrix Method (RMM) were combined to model complex structures as a whole [GWB15, LL12]. Extents have also been modelled using splines and convex-hemispheric shapes [KHB18, YWB+21, YAZ19].

Relation to Measurement Noise

The quality of sensors and measurements obtained dictate the complexity of the model as well as its computational efficiency. For instance, having accurate measurements (for short range sensors like the lidar) could provide a precise modelling of a target's extent from up close. Complex constructs as those mentioned for the arbitrary ones can therefore be used to approximate the extent. For far-range sensors like the radar, detections are quite noisy and are better approximated by basic shapes. Overall, determining the appropriate model to use depends heavily on the application for which it is being considered and the resources at hand.

3.3 Data Association

DA, concerns the problem of associating measurements to an existing set of tracks under observation at every step. A track can be defined as the trajectory of a target of interest, that is, the cumulative state estimations of the target. The DA schemes for point targets differs to those for extended targets. In this section, we shall cover the foundations of DA considering the aforementioned distinction by discussing two cases of association:

- A $1-1$ association of a point target to a single track, and,
- An $m-1$ association of a point cloud of m measurements to a single track.

The basis of DA lies in employing specific validation gates to mark measurements that most likely belong to a concerned track. The measurements, if validated, are used to update the specific tracks using specific association probabilities or can be even used to initiate new ones as needed.

3.3.1 Gating

The set of measurements recorded from an observation region comprises measurements originating from the targets present and clutter, that is, the detections that have been reflected from objects (aids to navigation, for example) in the environment, and acoustic anomalies or interferences due to weather conditions. A gating process is therefore applied to filter out the improbable measurement-to-track pairs using a validation gate, which is essentially governed by a threshold. The threshold validates measurements based on the difference between an observation and a track's measurement prediction, also known as innovation or residual. Two such schemes, the ellipsoidal gating and the rectangular gating shall be summarised next.

Ellipsoidal Gating

We define a set of measurements $\boldsymbol{Y}_k$ that contains at most one measurement per existing track, including clutter. Given a track's state prediction $\hat{\boldsymbol{x}}_{k|k-1}$, its measurement prediction $\boldsymbol{z}_k$ can be computed from (3.1.5). The difference between a measurement $\boldsymbol{y}_k \in \boldsymbol{Y}_k$ and the track's predicted

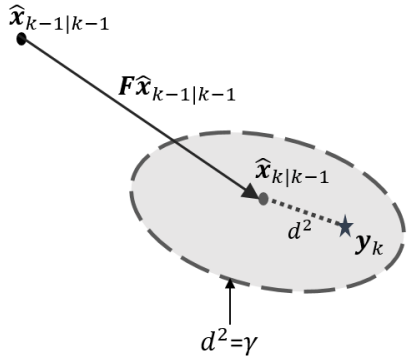

Figure 3.3: The validation gate is centred around the state prediction $\hat{x}_{k|k-1}$ of a particular track. For a fixed normalised innovation value $d^2 = \gamma$, the ellipsoidal gate can be defined by the determinant of the innovation covariance. Measurement $\boldsymbol{y}_k$ falling within the gate region would be the best association candidate to the track in question.

measurement yields the innovation vector $\mathbf{v}_k$,

$$\mathbf{v}_k = \boldsymbol{y}_k - \boldsymbol{z}_k \tag{3.3.1}$$

and its associated covariance denoted by $\mathbf{C}_k^{\boldsymbol{y}}$ in (3.1.16) and (3.1.24). A correlation is said to exist between measurement $\boldsymbol{y}_k$ and the concerned track if their normalised innovation satisfies the following gate G defined such that [Bla86, BSDH09],

$$G := \{d_k^2 = \mathbf{v}_k^T \left(\mathbf{C}_k^{\boldsymbol{y}}\right)^{-1} \mathbf{v}_k \leq \gamma\} \tag{3.3.2}$$

γ is known as the gate threshold, and is often derived from the χ^2_M distribution with M degrees of freedom, to ascertain that the gate covers a specific probability of producing a correct measurement-to-track association (also known as gating probability P_G). An ellipsoidal gating process is illustrated in Figure (3.3). Note that for convenience, the state and measurement spaces are assumed to be the same in this section's illustrative examples.

Rectangular Gating

Although the ellipsoidal gating process is effective, it can prove to be computationally expensive with a high number of measurements in complex extended multi-target systems. One can consider rectangular gating as a first gating step, so that only the measurements that have been thus validated would be subject to an ellipsoidal gating. Rectangular gating is a coarse gating scheme, which defines rectangular regions within the observation region. A measurement is validated if

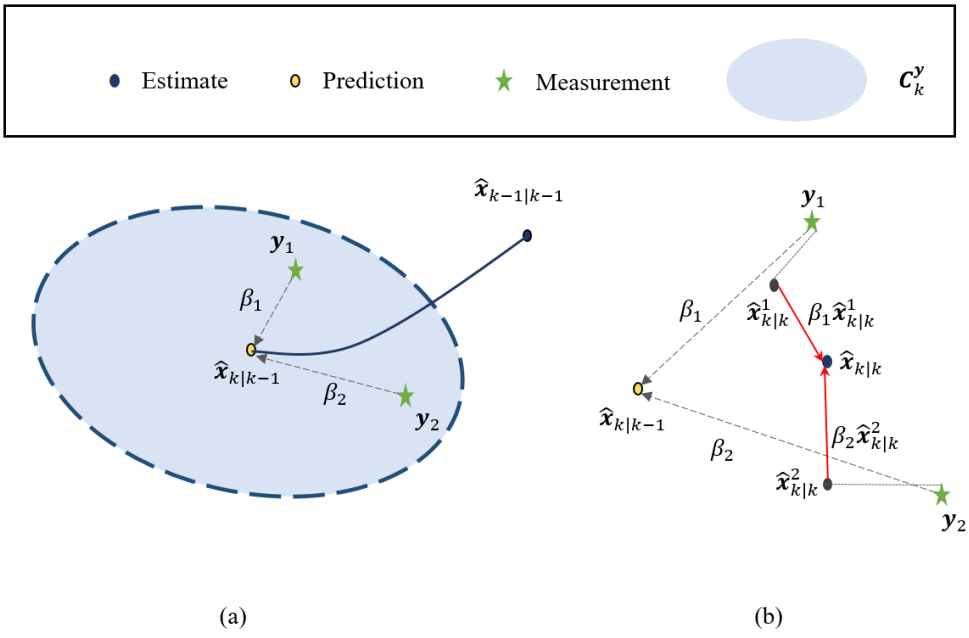

Figure 3.4: Exemplar visualisation of the PDA state update step using association probabilities given multiple validated measurements. (a) Two measurements have been validated based on the prediction. The association probabilities β_j are calculated for each measurement. (b) The combined state update can be expressed as a weighted average based on the probabilities.

the elements of $\mathbf{v}_k$ satisfy the relationship [Bla86],

$$|\mathrm{v}|_k \leq c_g \sigma_v \tag{3.3.3}$$

where $\sigma_\mathrm{v} = \sqrt{\sigma_y^2 + \sigma_x^2}$ is the innovation standard deviation calculated as the square root of the sum of the measurement variance σ_y^2, and the prediction variance σ_x^2 as obtained from the diagonal elements of $\mathbf{C}_{k|k-1}^{\boldsymbol{x}}$, the covariance of the predicted state. c_g is a gating constant based on M and corresponding gating probability P_G. Its detailed derivation can be found in the work of [Bla86]. When the rectangular and ellipsoidal methods are combined and used for a double-gating procedure as discussed earlier, it suffices to set $c_g \approx 4$.

3.3.2 Probabilistic Data Association Filter

The PDA filter is a Bayesian-based algorithm that computes a correct-association probability between an measurement and a *single* track, which is then later used to update the track's state as a weighted average [BSF88, BSWT11]. Figure 3.4 provides an illustration of the concept. In this part, the basic features of the algorithm are explained.

Let the m_k measurements falling in the ellipsoidal validation region from Chapter 3.3.1 be rep-

resented as $\bar{\boldsymbol{\mathcal{Y}}}_k \equiv \{\boldsymbol{y}\}_{j=1}^{m_k} \subseteq \mathbf{Y}_k$ with the measurement set as defined therein. We also represent all the cumulative sets of validated measurements up to k as $\bar{\boldsymbol{\mathcal{Y}}} = \left\{\bar{\boldsymbol{\mathcal{Y}}}_{l=0}^{k}\right\}$. It is assumed that measurements are produced independently with a known detection probability P_D.

The target state $\boldsymbol{x}_k$ is assumed to be a Gaussian PDF based on the latest state estimate and its covariance, given by,

$$p(\boldsymbol{x}_k|\bar{\boldsymbol{\mathcal{Y}}}_{k-1}) = \mathcal{N}(\boldsymbol{x}_k; \hat{\boldsymbol{x}}_{k|k-1}, \mathbf{C}^{\boldsymbol{x}}_{k|k-1}). \tag{3.3.4}$$

Of all the measurements that have been validated, at most one of them will have originated from the target (assuming that the latter has been detected) and the rest is treated as clutter otherwise. The clutter is modelled as Independent and Identically Distributed (IID) variables with uniform spatial distribution normally assumed as a spatial Poisson process with known spatial density λ [BSDH09].

Association Probabilities

At step k, the event that measurement $\boldsymbol{y}_j$ is target-originated is represented by θ_j. Similarly, event θ_0 denotes that none of the measurements acquired are originated from the target or that they are clutter. Taking both possibilities into account, the (association) event probabilities are denoted as follows,

$$\beta_j = p\left(\theta_j|\bar{\boldsymbol{\mathcal{Y}}}_k\right) \quad \text{for } j = 0, 1, .., m_k. \tag{3.3.5}$$

With the Poisson distributed clutter of spatial density λ, the parametric PDA version employs the following relationship to calculate the association probability that $\boldsymbol{y}_j$ is the correct measurement [BSDH09],

$$\beta_j = \begin{cases} \dfrac{\mathcal{L}_j}{1 - P_D P_G + \sum_{j=1}^{m_k} \mathcal{L}_j} & \text{for } j = 1, .., m_k \\ \dfrac{1 - P_D P_G}{1 - P_D P_G + \sum_{j=1}^{m_k} \mathcal{L}_j} & \text{for } j = 0 \end{cases} \tag{3.3.6}$$

where P_D and P_G are the detection and gating probabilities. The likelihood $\mathcal{L}_j$ is the ratio of measurement $\boldsymbol{y}_j$ being target-originated than it being clutter,

$$\mathcal{L}_j := \frac{\mathcal{N}\left(\boldsymbol{y}_j; \boldsymbol{z}_k, \mathbf{C}^{\boldsymbol{y}}_k\right) P_D P_G}{\lambda}. \tag{3.3.7}$$

Furthermore, given the assumption that the association events are mutually independent and exhaustive, their individual probabilities should sum up to 1:

$$\sum_{j=1}^{m_k} \beta_j = 1. \tag{3.3.8}$$

The posterior state estimate $\hat{\boldsymbol{x}}_{k|k}$ conditioned on the event θ_j representing that $\boldsymbol{y}_j$ has been correctly associated to the track, can be expressed as a weighted sum of PDFs,

$$\begin{aligned}\hat{\boldsymbol{x}}_{k|k} &= E\left[\boldsymbol{x}_k|\bar{\boldsymbol{\mathcal{Y}}}\right] \\ &= \sum_{j=1}^{m_k} E\left[\boldsymbol{x}_k|\theta_j, \bar{\boldsymbol{\mathcal{Y}}}_k\right] p\left(\theta_j|\bar{\boldsymbol{\mathcal{Y}}}_k\right) \\ &= \sum_{j=1}^{m_k} \hat{\boldsymbol{x}}_{k|k}^{j}\beta_j,\end{aligned} \tag{3.3.9}$$

where $\hat{\boldsymbol{x}}_{k|k}^{j}$ is the estimate corresponding to θ_j. Using the KF update equations, the latest estimate is therefore obtained from the following:

$$\hat{\boldsymbol{x}}_{k|k} = \hat{\boldsymbol{x}}_{k|k-1} + \mathbf{K}_k\mathbf{v}_k \tag{3.3.10}$$

where overall innovation $\mathbf{v}_k$, defined as

$$\mathbf{v}_k = \sum_{j=1}^{m_k} \beta_j\tilde{\mathbf{v}}_j, \tag{3.3.11}$$

is the weighted sum of the innovations $\tilde{\mathbf{v}}_j$ corresponding to every validated measurement in $\bar{\boldsymbol{\mathcal{Y}}}_k$. The individual innovations are calculated from (3.3.1). The corresponding state covariance is found as,

$$\mathbf{C}_{k|k-1}^{\boldsymbol{x}} = \beta_0\mathbf{C}_{k|k-1}^{\boldsymbol{x}} + (1-\beta_0)\left[\mathbf{C}_{k|k-1}^{\boldsymbol{x}}\mathbf{K}_k\mathbf{C}_k^{\boldsymbol{y}}\mathbf{K}_k^T\right] + \tilde{\mathbf{C}}_k \tag{3.3.12}$$

where $\tilde{\mathbf{C}}_k$ accounts for the term of the innovations spread [BSDH09]

$$\tilde{\mathbf{C}}_k = \mathbf{K}_k\left[\sum_{j=1}^{m_k}\beta_j\tilde{\mathbf{v}}_j\tilde{\mathbf{v}}_j^T - \mathbf{v}_k\mathbf{v}_k^T\right]\mathbf{K}_k^T. \tag{3.3.13}$$

The covariance $\tilde{\mathbf{C}}_k$ increases the state covariance to intuitively address the uncertainty in the measurement origin.

Joint Probabilistic Data Association Filter

The PDA filter relies on the major assumption that only one already-initialised target exists. The JPDA filter has been formulated to extend the PDA approach to multiple targets, that still require to be initialised. This means that the number of targets are to be known in advance. In addition, the JPDA comes with a $1-1$ measurement-to-track association constraint which states that a measurement could have originated from only one target and a target could have only produced at most one measurement.

Let n_k be the predefined number of targets existing at k. As an extension to its basis, the JPDA filter makes use of a joint event association [BSDH09]

$$\boldsymbol{\theta}_k = \bigcap_{j=1}^{m_k} \theta_{jt_j} \tag{3.3.14}$$

where θ_{jt_j} denotes the event whereby measurement j has originated from target t over $t = \{1, ..., n_k\}$, and t_j denotes the target to which j has been assigned. The probability of the joint events can be represented by a summation over all joint events to obtain marginal probabilities as follows [BSDH09],

$$\begin{aligned} \beta_{jt} &= p\left(\theta_{jt}|\bar{\boldsymbol{\mathcal{Y}}}_k\right) \\ &= \sum_{\theta:\theta_{jt}\in\boldsymbol{\theta}_k} p\left(\theta|\bar{\boldsymbol{\mathcal{Y}}}_k\right). \end{aligned} \tag{3.3.15}$$

The filtering equations for estimating the state are then similar to those for PDA. The JPDA will be revisited with more details in Chapter 5.

Adaptability to Extended Targets

Newly developed models for including the extent properties in the target state represent significant improvements in the filter, overriding the initial constraints. We now consider cases where targets produce multiple measurements so that the measurements-to-track require an $m:1$ association [Bau15, HTT+13] scheme instead. The works in [YTB18, YWB20, SRW15] propose applying the PPP for spatially modelling extents and update extended states using appropriate DA formulations. Of late, sampling methods based on likelihood have been applied for stochastic optimisation in [Gra18]. On the other hand, the alternative approach of partitioning the measurement set by clustering methods have been performed and involve carrying out subset-association probabilities between the clusters and tracks [VB16, GO12, BRG+16]. More on the state-of-the-art will be covered in the later chapters.

3.4 Chapter Summary

This chapter laid out a foundation for our contributions that will be followed. In its first part, the concept of Bayesian state estimation was introduced together with the KF and the EKF. In the second part, the problem description pertaining to ETT is given. The different methods to describe the extent of a target were mentioned based on two categories, basic geometric and convex/arbitrary shapes. The main factors to consider while choosing an appropriate model were stated.

Finally, the DA approach was described, which is employed by the PDA filter to track a target from multiple measurements. The initial step is to validate measurements from a gating process, and update the estimate by using association probabilities. The PDA filter is the pillar of the JPDA –targeting multiple target's state estimations using marginal association probabilities. The DA framework offers possibilities to employ $1-1$ or $m:1$ measurement-to-track association(s).

Chapter 4

Elliptical Extended Target Tracking

As explained in Chapter 3.2, having in-depth knowledge about the data in question is an essential factor to deciding which measurement model to employ. We want to consider standard marine radar data from the DLR-Repository to focus on real-world situations closely. The data vastly results from targets or from the immediate environment under observation, and occurs as noisy and dense point clouds. The latter makes ellipses convenient target extent approximators in maritime environments. Furthermore, as a radar's field of view is generally limited to the visible sides of targets, their extents could be assumed to be symmetric and they can be represented by ellipses.

Contents

This chapter therefore entails the conception of two algorithms for ETT with elliptical shape representation models. The first algorithm is a custom one used to estimate the orientation of a vessel with known spatial extent by following a sequential update approach. Such a requirement could already be useful in a couple of applications. It would be advantageous to have a proper

knowledge of the true heading of the vessel which in general does not always align with the vessel's velocity (contrary to automotive applications, where a vehicle's orientation-velocity alignment is a common [Gov19, TO21] assumption for tracking) for collision avoidance at sea as well as during tedious manoeuvres in harbours. The orientation is also beneficial for anomaly detection, for example, an unexpected turn of higher than 30^o within a considered time interval could be classified as an anomaly based on the normal patterns considered for specific routes [4]. With the aim to optimise the extent tracking process while retaining the core features of the first algorithm, the second algorithm follows a batch-based approach for estimating the elliptical approximation of a vessel.

The performances, in terms of computational efficiency and estimation accuracy, of both algorithms are also demonstrated on simulated data and on our dataset, covered in the later subsections. Where applicable, the algorithms were run on a system with MATLAB (R2018b for the first part and R2021a for the second part) and processed using a 2.60 GHz Intel Quad Core processor. It is to be noted that unless stated otherwise, the same notations utilised from the previous chapters are carried forward to the current one.

4.1 Estimating Vessel Orientation Given Known Size Parameters

A target's elliptical extent parameters are namely the lengths of its semi-axes and its orientation, as depicted in Figure 1.3 in Chapter 1. The Multiplicative Error Model-Extended Kalman Filter* (MEM-EKF*) algorithm [YB19, YB16, YB17], based on the Multiplicative Error Model (MEM) [BFH12] considers the approximation of the spatial distribution of a target using an ellipse. In the algorithm, a measurement is related to the kinematic state and extent parameter vector (that are also assumed to be decoupled) on the basis of a corrupted additive and multiplicative noise. The multiplicative noise could be thought of as a scaling factor describing the lengths of the semi-axes. The MEM-EKF* method offers a flexible parameterisation of the extent parameters (see 4.1.2) and of their uncertainties. We have exploited this feature in particular for the current problem to obtain a tailored MEM-EKF* approach. It is rather intuitive that a vessel's size would be expected to be rigid (fixed), requiring relatively less uncertainty from one step to the other and its orientation might require more, depending on its trajectory. Particularly, we consider cases where the vessel's length and width information are known, for example from the AIS reports, and its heading is then tracked.

Later, within this first half of the chapter, we shall describe the relevant state-of-the-art, problem, our contributions and their results.

4.1.1 Related Work

The RMM-based elliptical trackers [Koc08, FF08, FFK11, LL16] are one of the most common approaches adopted. They provide separate models for the kinematic state, which is modelled

as a Gaussian PDF, and the target extent is modelled as an inverse Wishart distribution that is in turn represented by an SPD matrix. An implicit elliptical representation has been derived based on the RHM in [BH14]. These approaches restrict a flexible, explicit parameterisation of the extent parameters and their uncertainty values. For instance, the uncertainties of the RMM extent parameters are based on a single scalar value.

An explicit extent parameterisation (like in 4.1.3), however, has so far been considered by only a few works, including the MEM-EKF* and its derivative [TB21b] as well as an elliptical RHM-based approach in [TYB20]. The method in [DWS11] models the extent parameters explicitly as a Gaussian PDF without assuming the spatial distribution from [GS05]. Besides our contribution, more recent methods have been published on the topic, consolidating the conduciveness of explicit parameterisation [Gov19, LLL20, TO21]. While the target orientation is computed from the velocity components in [Gov19], it is explicitly estimated in the newest RMM work from [TO21].

4.1.2 Problem Description

We are interested in tracking the kinematic state and the extent parameters of a single target based on the assumptions that measurements are independent and their sources are uniformly distributed across the target [GS05, GGMS05]. At the observation step k, the target's extended state $\boldsymbol{x}_k$ is defined as follows,

$$\boldsymbol{x}_k = \left[\mathbf{r}_k^T, \mathbf{p}_k^T\right]^T, \tag{4.1.1}$$

and its Gaussian PDF given as $\mathcal{N}(\boldsymbol{x}_k; \hat{\boldsymbol{x}}_k, \mathbf{C}_k^{\boldsymbol{x}})$. The kinematic state vector $\mathbf{r}_k$ from (4.1.1) contains the two-dimensional ENU Cartesian position $\mathbf{m}_k = [m_{e,k}, m_{n,k}]$ of the target, its course over ground (COG) ψ_k and its speed over ground (SOG) ϑ_k,

$$\mathbf{r}_k = \left[\mathbf{m}_k^T, \psi_k, \vartheta_k\right]^T \in \mathbb{R}^4 \tag{4.1.2}$$

and the extent parameter vector $\mathbf{p}_k$ contains the orientation α_k and semi-axes lengths $\ell_{1,k}$ and $\ell_{2,k}$,

$$\mathbf{p}_k = [\alpha_k, \ell_{1,k}, \ell_{2,k}]^T \in \mathbb{R}^3. \tag{4.1.3}$$

The orientation $\alpha_k \in [0, 2\pi)$ ideally corresponds to the true heading of the target at sea. The resultant elliptical approximation of the target would be centred at $\mathbf{m}_k$. We also register a set of noisy and dense radar measurements $\boldsymbol{\mathcal{Y}}_k = \left\{\boldsymbol{y}_k^j\right\}_{j=1}^{n_k}$. Each measurement $\boldsymbol{y}_k^j$ is disturbed with noise $\boldsymbol{v}_k^j$ from its origin on the target's extent at a source point $\boldsymbol{z}_k^j$, modelled as [YB19] [5],

$$\boldsymbol{y}_k^j = \underbrace{\mathbf{m}_k + \boldsymbol{\mathcal{R}}(\alpha_k) \begin{bmatrix} \ell_{1,k} & 0 \\ 0 & \ell_{2,k} \end{bmatrix} \underbrace{\begin{bmatrix} h_{1,k}^j \\ h_{2,k}^j \end{bmatrix}}_{:=\mathbf{h}_k^j}}_{:=\boldsymbol{z}_k^j} + \boldsymbol{v}_k^j. \tag{4.1.4}$$

$\boldsymbol{\mathcal{R}}(\alpha_k) = \begin{bmatrix} \cos(\alpha_k) & -\sin(\alpha_k) \\ \sin(\alpha_k) & \cos(\alpha_k) \end{bmatrix}$ is the rotation matrix. The noise terms from the measurement equation in (4.1.4) are explained as follows:

- measurement $\boldsymbol{y}_k^j$ relates to a source $\boldsymbol{z}_k^j$ on the target by an additive Gaussian (measurement) noise $\boldsymbol{\upsilon}_k^j \sim \mathcal{N}(0, \mathbf{C}_k^{\upsilon^j})$ and,
- the source $\boldsymbol{z}_k^j$ in turn relates to the extent parameter vector $\mathbf{p}_k$ by the multiplicative noise defined as $\mathbf{h}_k^j \sim \mathcal{N}(0, \mathbf{C}_k^{\mathbf{h}})$, where $\mathbf{C}_k^{\mathbf{h}} = \frac{1}{4}\mathbf{I}_2$, $\mathbf{I}_2$ is the identity matrix of dimension 2. The variance value of $\frac{1}{4}$ corresponds to a uniform elliptical distribution.

4.1.3 Tailored MEM-EKF* Approach

We propose a tailored version of the MEM-EKF* algorithm, termed Tailored MEM-EKF* (T-MEM-EKF*), for estimating the state of a target while keeping the extent parameters fixed. As the orientation is our parameter of interest, we redefine the overall state as

$$\boldsymbol{x}_k = \left[\mathbf{r}_k^T, \alpha_k\right]^T, \tag{4.1.5}$$

thereby reducing the extent state to the orientation. The definition of $\mathbf{r}_k$ remains unaltered from (4.1.1). The system model of the kinematic state is modelled following a non-linear function defined as follows,

$$\begin{aligned} \mathbf{r}_k &= f_k(\mathbf{r}_{k-1}, \boldsymbol{\omega}_k^{\mathbf{r}}) \\ &= \begin{bmatrix} m_{e,k-1} + \sin(\psi_k) \cdot \Delta k \cdot \vartheta_k \\ m_{n,k-1} + \cos(\psi_k) \cdot \Delta k \cdot \vartheta_k \\ \psi_k \\ \vartheta_k \end{bmatrix} + \boldsymbol{\omega}_k^{\mathbf{r}} \end{aligned} \tag{4.1.6}$$

where $\boldsymbol{\omega}_k^{\mathbf{r}} \sim \mathcal{N}(0, \mathbf{C}_{\mathbf{r}}^{\boldsymbol{\omega}})$ is zero-mean random Gaussian process noise having a covariance given by $\mathbf{C}_{\mathbf{r}}^{\boldsymbol{\omega}} = \operatorname{diag}\left(\sigma_{m_e}^2, \sigma_{m_n}^2, \sigma_{\psi}^2, \sigma_{\vartheta}^2\right)$. The time interval is given by Δk. For the temporal evolution of the orientation, a linear modelling is considered,

$$\alpha_k = \alpha_{k-1} + \omega_k^{\alpha} \tag{4.1.7}$$

where ω_k^{α} is assumed to be zero-mean Gaussian distributed with variance $\mathrm{C}_{\alpha}^{\omega}$. In addition, the covariance of the predicted kinematic state (as in (3.1.19)) and orientation variance are obtained as shown below,

$$\begin{aligned} \mathbf{C}_{k|k-1}^{\mathbf{r}} &= \bar{\mathbf{F}}_k \mathbf{C}_{k-1}^{\mathbf{r}} \bar{\mathbf{F}}_k^T + \mathbf{C}_{\mathbf{r}}^{\boldsymbol{\omega}} \\ \mathrm{C}_{k|k-1}^{\alpha} &= \mathrm{C}_{k-1}^{\alpha} + \mathrm{C}_{\alpha}^{\omega}. \end{aligned} \tag{4.1.8}$$

We rewrite the measurement model from (4.1.4) into a compact version and for readability, we also omit the measurement and observation step indices as follows,

$$\boldsymbol{y} = \mathbf{H}\mathbf{r} + \mathbf{S}\mathbf{h} + \boldsymbol{v} \tag{4.1.9}$$

where measurement matrix $\mathbf{H} = [\mathbf{I}_2, \mathbf{0}_2]$, and $\mathbf{S}$ now represents the shape matrix so that

$$\begin{aligned} \mathbf{S} &= \begin{bmatrix} \cos(\alpha) & -\sin(\alpha) \\ \sin(\alpha) & \cos(\alpha) \end{bmatrix} \begin{bmatrix} \ell_1 & 0 \\ 0 & \ell_2 \end{bmatrix} \\ &:= \begin{bmatrix} \mathbf{S}_1 \\ \mathbf{S}_2 \end{bmatrix} \end{aligned} \tag{4.1.10}$$

As ℓ_1 and ℓ_2 are known apriori, $\mathbf{S}$ becomes independent of them and they are instead taken as constants.

The measurement updates for the kinematic state and the orientation parameter are as given in Table 4.1, which has been adopted from [5] and was derived from [YB19]. The orientation measurement update requires a linearisation of the measurement equation (4.1.9) around the latest estimate $\hat{\alpha}$, yielding

$$\boldsymbol{y} \approx \mathbf{H}\mathbf{r} + \mathbf{S}\mathbf{h} + \begin{bmatrix} \mathbf{h}^T \boldsymbol{J_1} \\ \mathbf{h}^T \boldsymbol{J_2} \end{bmatrix} (\alpha - \hat{\alpha}) + \boldsymbol{v}. \tag{4.1.11}$$

Using the definitions in (4.1.10), the Jacobian matrices $\mathbf{J}_1$ and $\mathbf{J}_2$ are calculated from derivatives of $\mathbf{S}$ evaluated at $\hat{\alpha}$ as

$$\mathbf{J}_1 = \mathbf{S}_1'(\hat{\alpha}) = \begin{bmatrix} -\ell_1 \sin(\hat{\alpha}) \\ -\ell_2 \cos(\hat{\alpha}) \end{bmatrix} \quad \text{and,} \tag{4.1.12}$$

$$\mathbf{J}_2 = \mathbf{S}_2'(\hat{\alpha}) = \begin{bmatrix} \ell_1 \cos(\hat{\alpha}) \\ -\ell_2 \sin(\hat{\alpha}) \end{bmatrix}. \tag{4.1.13}$$

These are employed in computing a specific measurement noise (analogous to the innovation) covariance that are subsequently all used in the KF-based updates.

In essence, the algorithm updates the kinematic state based on the real measurement $\boldsymbol{y}$ and the extent state based on its uncorrelated, 3-dimensional pseudo-measurement derived by the Kronecker product of the innovation [YB19, LL15],

$$\mathbf{Y} = \mathbf{A}\Big((\boldsymbol{y} - \hat{\boldsymbol{y}}) \otimes (\boldsymbol{y} - \hat{\boldsymbol{y}})\Big), \tag{4.1.14}$$

with $\mathbf{A}$ defined in Table 4.1 for eliminating duplicated elements. The vect-operation stacks the column vectors of a 2×2 covariance matrix represented by $\begin{bmatrix} c_{11} & c_{12} \\ c_{12} & c_{22} \end{bmatrix}$ to build a column vector

Table 4.1: Tailored MEM-EKF* for Known Extent [5][YB19]

Kinematic Update

$$\hat{\boldsymbol{y}}_k^j = \mathbf{H}\hat{\boldsymbol{r}}_k^{j-1}$$
$$\mathbf{C}_k^{\mathbf{r}\boldsymbol{y}^j} = \mathbf{C}_k^{\mathbf{r}^{j-1}}\mathbf{H}^T$$
$$\mathbf{C}_k^{\boldsymbol{y}^j} = \mathbf{H}\mathbf{C}_k^{\mathbf{r}\boldsymbol{y}^j}\mathbf{H}^T + \mathbf{C}^{\mathbf{I}} + \mathbf{C}^{\mathbf{II}} + \mathbf{C}_k^{\boldsymbol{v}^j}$$
$$\hat{\boldsymbol{r}}_k^j = \hat{\boldsymbol{r}}_k^{j-1} + \mathbf{C}_k^{\mathbf{r}\boldsymbol{y}^j}\left(\mathbf{C}_k^{\boldsymbol{y}^j}\right)^{-1}\left(\boldsymbol{y}_k^j - \hat{\boldsymbol{y}}_k^j\right)$$
$$\mathbf{C}_k^{\mathbf{r}^j} = \mathbf{C}_k^{\mathbf{r}^{j-1}} - \mathbf{C}_k^{\mathbf{r}\boldsymbol{y}^j}\left(\mathbf{C}_k^{\boldsymbol{y}^j}\right)^{-1}\left(\mathbf{C}_k^{\mathbf{r}\boldsymbol{y}^j}\right)^T$$

Orientation Update

$$\mathbf{Y}_k^j = \mathbf{A}\left(\left(\boldsymbol{y}_k^j - \hat{\boldsymbol{y}}_k^j\right) \otimes \left(\boldsymbol{y}_k^j - \hat{\boldsymbol{y}}_k^j\right)\right)$$
$$\hat{\boldsymbol{Y}}_k^j = \mathbf{A}\text{vect}\left\{\mathbf{C}_k^{\boldsymbol{y}^j}\right\}$$
$$\mathbf{C}_k^{\alpha\mathbf{Y}^j} = \mathrm{C}_k^{\alpha^{j-1}}\left(\hat{\mathbf{M}}_k^{j-1}\right)$$
$$\mathbf{C}_k^{\mathbf{Y}^j} = \mathbf{A}\left(\mathbf{C}_k^{\boldsymbol{y}^j} \otimes \mathbf{C}_k^{\boldsymbol{y}^j}\right)\left(\mathbf{A} + \tilde{\boldsymbol{A}}\right)^T$$
$$\hat{\alpha}_k^j = \hat{\alpha}_k^{j-1} + \mathbf{C}_k^{\alpha\mathbf{Y}^j}\left(\mathbf{C}_k^{\mathbf{Y}^j}\right)^{-1}\left(\mathbf{Y}_k^j - \hat{\boldsymbol{Y}}_k^j\right)$$
$$\mathrm{C}_k^{\alpha^j} = \mathbf{C}_k^{\alpha^{j-1}} - \mathbf{C}_k^{\alpha\mathbf{Y}^j}\left(\mathbf{C}_k^{\mathbf{Y}^j}\right)^{-1}\left(\mathbf{C}_k^{\alpha\mathbf{Y}^j}\right)^T$$

Additional parameter definitions

- $\mathbf{S}_k = \begin{bmatrix} \mathbf{S}_{k,1} \\ \mathbf{S}_{k,2} \end{bmatrix} = \begin{bmatrix} \cos(\alpha_k) & -\sin(\alpha_k) \\ \sin(\alpha_k) & \cos(\alpha_k) \end{bmatrix} \begin{bmatrix} \ell_1 & 0 \\ 0 & \ell_2 \end{bmatrix}$ represents the shape matrix
- Jacobian matrix $\mathbf{J}_1 = \begin{bmatrix} -\ell_1 \sin(\alpha) \\ -\ell_2 \cos(\alpha) \end{bmatrix}$ of $\mathbf{S}_{k,1}$ evaluated at $\hat{\alpha}_k^{j-1}$
- Jacobian matrix $\mathbf{J}_2 = \begin{bmatrix} \ell_1 \cos(\alpha) \\ -\ell_2 \sin(\alpha) \end{bmatrix}$ of $\mathbf{S}_{k,2}$ evaluated at $\hat{\alpha}_k^{j-1}$
- Covariance of pseudo-measurement $\mathbf{M} = \begin{bmatrix} 2\mathbf{S}_{k,1}\mathbf{C}^{\mathbf{h}}\mathbf{J}_1 \\ 2\mathbf{S}_{k,2}\mathbf{C}^{\mathbf{h}}\mathbf{J}_2 \\ \mathbf{S}_{k,1}\mathbf{C}^{\mathbf{h}}\mathbf{J}_2 + \mathbf{S}_{k,2}\mathbf{C}^{\mathbf{h}}\mathbf{J}_1 \end{bmatrix}$
- $\mathbf{A} = \begin{bmatrix} 1 & 0 & 0 & 0 \\ 0 & 0 & 0 & 1 \\ 0 & 1 & 0 & 0 \end{bmatrix}$ and $\tilde{\boldsymbol{A}} = \begin{bmatrix} 1 & 0 & 0 & 0 \\ 0 & 0 & 0 & 1 \\ 0 & 0 & 1 & 0 \end{bmatrix}$
- $\mathbf{C}^{\mathbf{I}} = \hat{\boldsymbol{S}}_k^{j-1}\mathbf{C}^{\mathbf{h}}\left(\hat{\boldsymbol{S}}_k^{j-1}\right)^T$
- $\mathbf{C}^{\mathbf{II}} = \mathrm{C}_k^{\alpha^{j-1}}\left[\mathbf{J}_1 \quad \mathbf{J}_2\right]^T\mathbf{C}^{\mathbf{h}}\left[\mathbf{J}_1 \quad \mathbf{J}_2\right]$

resulting in

$$\text{vect}\left\{\mathbf{C}_k^{\boldsymbol{y}^j}\right\} = [c_{11} \quad c_{12} \quad c_{12} \quad c_{22}]\,. \tag{4.1.15}$$

For a detailed review, the full derivation can be found in [YB19]. The construction of the corresponding pseudo-measurement noise covariance $\mathbf{M}$ is included in our table.

4.1.4 Results

The algorithm was applied to the simulated trajectory of a vessel and its performance was analysed, before being applied on real data. With the real data, we compare the T-MEM-EKF* approach to the original MEM-EKF* version. These findings are presented in this section.

Simulation

A vessel of dimensions 150m by 30m is the extended target of interest which travels in a trajectory comprising three turns. For this simulation, it is assumed that the vessel is aligned with its course, so that the ground truth could be obtained. The target commences its trajectory from the origin with a constant velocity of 3.5ms^{-1}. At each observation step, the number of measurements are drawn from a Poisson PDF with mean 50.

The kinematic state vector $\mathbf{r}_k$ from (4.1.1) now contains the two-dimensional Cartesian position $\mathbf{m}_k$ of the target and its velocity $\dot{\mathbf{m}}_k$,

$$\mathbf{r}_k = \left[\mathbf{m}_k^T, \dot{\mathbf{m}}_k^T\right]^T \in \mathbb{R}^4. \tag{4.1.16}$$

The time propagation of the kinematic state is based on a Nearly Constant Velocity (NCV) model, described in Appendix A.1. The kinematic states for both our and the original approaches are modelled alike. The kinematic prior was initialised with $\mathbf{r}_0 = [2.5, 2.5, 3, 3]^T$ with covariance $\mathbf{C}_0^{\mathbf{r}} = \text{diag}\left(3^2, 3^2, 0.5^2, 0.5^2\right)$ and process noise covariance $\mathbf{C}_{\mathbf{r}}^{\boldsymbol{\omega}} = \text{diag}\left(7^2, 7^2, 1, 1\right)$. As opposed to our datasets, where the state has the possibility to be initiated based on the AIS parameters COG and SOG, our simulations use velocity components instead, offering a linear system model.

For the original MEM-EKF*, the evolution of the extent parameters are modelled differently. The method defines the parameter vector as in (4.1.3), therefore requiring the following equations for the time update,

$$\mathbf{p}_{k|k-1} = \mathbf{F}_{\mathbf{p}}\mathbf{p}_{k-1} + \boldsymbol{\omega}_k^{\mathbf{p}} \tag{4.1.17}$$

$$\mathbf{C}_{k|k-1}^{\mathbf{p}} = \mathbf{F}_{\mathbf{p}}\mathbf{C}_k^{\mathbf{p}}(\mathbf{F}_{\mathbf{p}})^T + \mathbf{C}_{\mathbf{p}}^{\boldsymbol{\omega}} \tag{4.1.18}$$

where $\boldsymbol{\omega}_k^{\mathbf{p}} \sim \mathcal{N}(\mathbf{0}, \mathbf{C}_{\mathbf{p}}^{\boldsymbol{\omega}})$ with covariance $\mathbf{C}_{\mathbf{p}}^{\boldsymbol{\omega}} = \text{diag}(\sigma_\alpha^2, \sigma_{l_1}^2, \sigma_{l_2}^2)$ and the state transition matrix $\mathbf{F}_{\mathbf{p}} = \mathbf{I}_3$.

The prior of its extent parameters were initiated as $\mathbf{p}_0 = [2, 145, 35]^T$ with covariance $\mathbf{C}_0^{\mathbf{p}} = \text{diag}\left(1, 10^2, 10^2\right)$ and its process noise covariance $\mathbf{C}_{\mathbf{p}}^{\boldsymbol{\omega}} = \text{diag}\left(0.1^2, 0.5^2, 0.5^2\right)$. For our approach,

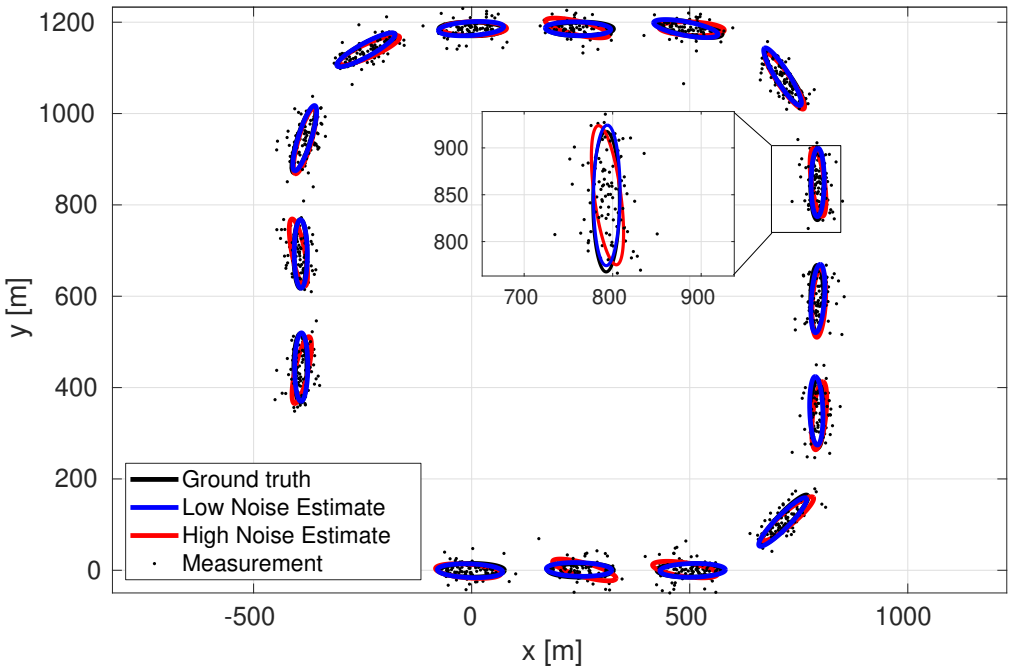

Figure 4.1: The trajectory estimation results from one run for T-MEM-EKF*. The ground truth is given in black (ellipses) and the estimates under both noise settings given in blue (low) and red (high), respectively. Image from [5]©2019IEEE

the same values were used for our adjusted state and covariance. Furthermore, we have considered two measurement noise settings for the T-MEM-EKF* version. A low noise has been chosen as $\mathbf{C}_k^{\boldsymbol{v}} = \operatorname{diag}\left(10^2, 10^2\right)$ and a higher one at $\mathbf{C}_k^{\boldsymbol{v}} = \operatorname{diag}\left(30^2, 30^2\right)$.

Both filters were executed 500 times, over which the estimated orientations were plotted comparatively against the ground truth and the filters' execution times were compared to each other. A single run results for T-MEM-EKF* is shown in Figure 4.1. The comparative orientation plot for T-MEM-EKF* resulting from the two noise settings is found in Figure 4.2, where we see that the algorithm is able to estimate the target orientation under both settings. Under the ideal simulation settings, the maximum estimation Root Mean Squared Error (RMSE)s in α when evaluated against the ground truth for low noise and for high noise over 500 runs had more or less similar performances, as given in Table 4.2. The filters also had different execution times, whereby our approach showed an improvement over the general version by 0.11s (See Table 4.2) on average.

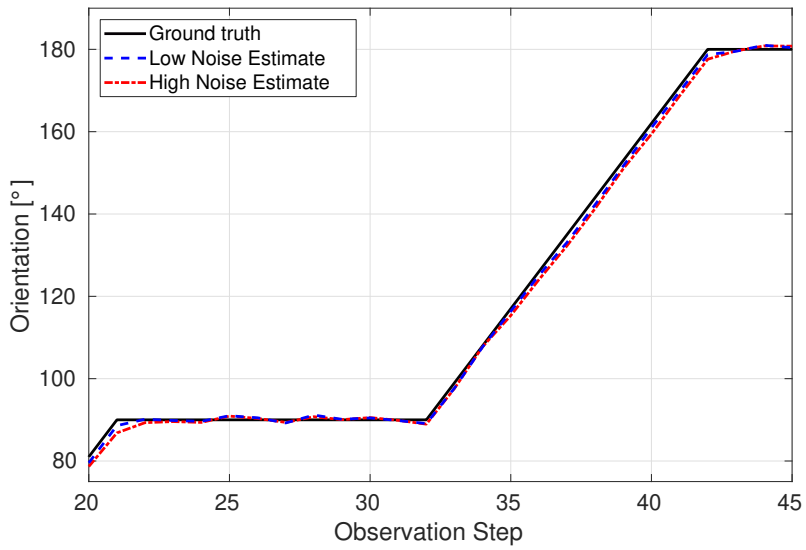

Figure 4.2: The ground truth is in black while the T-MEM-EKF* estimated orientations are plotted in broken blue and red lines over the three turns. Image from [5]©2019IEEE

Table 4.2: Filtering Execution Times and Orientation RMSEs

Evaluation	Execution Time [s]	Max Orientation RMSE Low Noise [^{o}]	Max Orientation RMSE High Noise [^{o}]
MEM-EKF*	0.45	0.44	3.10
T-MEM-EKF*	0.34	0.52	2.69

Table 4.3: Filter Initialisation Parameters

Parameter	Value
Range Std σ_r [m]	40
Bearing Std σ_φ [°]	4
Extent parameter vector $\mathbf{p}_0$ for Target 2	$[-2.10, 65, 12]$
Extent parameter vector $\mathbf{p}_0$ for Target 3	$[-1.06, 6, 2]$
Extension process noise covariance $\mathbf{C}_\mathbf{p}^\omega$ for Target 2	$\mathrm{diag}(1e^{-2}, 1e^{-4}, 1e^{-4})$
Extension process noise covariance $\mathbf{C}_\mathbf{p}^\omega$ for Target 3	$\mathrm{diag}(1e^{-4}, 1e^{-4}, 1e^{-4})$

Dataset

The T-MEM-EKF* and MEM-EKF* algorithms were both applied on the DAAN dataset captured from a dynamic own vessel, in which we find two vessels of interest, which are of dimensions 129m by 23m and 12m by 4m, respectively, observed over 781 steps (13 minutes otherwise). The two vessels shall be referred to as Target 2 and Target 3 henceforth (see dataset description in Chapter 2 for target labelling). Target 2 was within the own range only as of observation step $k = 200$. As the algorithms only track a single target, they were executed on each target individually.

The original extracted radar measurements, as formerly explained in Chapter 2, were transformed into a local ENU equivalent coordinate system from polar coordinates $[r_k, \varphi_k]$. The coordinate transformation equations are provided in Appendix A.2. The filters were initialised on the basis of the AIS information for the position as well as the extent parameters. The ground truth values that are retrieved and used from AIS are the ENU-based position, length, width, and true heading of the targets. Parameter values used for the coordinate transformation and initialisation of the extent parameter vectors of the two targets are given in Table 4.3. The table includes the prior process noise covariance for both filters, T-MEM-EKF* only estimating the α_k parameter. The noises set for the semi-axes for MEM-EKF* are small considering that the extent is known apriori.

The overall estimated trajectory using MEM-EKF* is plotted in Figure 4.3. The estimated elliptical extents are plotted at regular 20s intervals on top of the radar measurements. The measurements also show signs of occlusion, missed detections and beam spreading. Beam spreading is a term that we use to explain the phenomenon of how a target-originated point cloud has a larger volume the farther it is from the sensor. As the target is found closer to the sensor, the point cloud will be more accurately spread over the underlying target's surface.

The performances were compared against the corresponding AIS data. Each of the estimated extent parameters were plotted over time in Figure 4.4a and the positional errors are shown in Figure 4.4b. We note that while the kinematic estimates have almost full overlapping between the

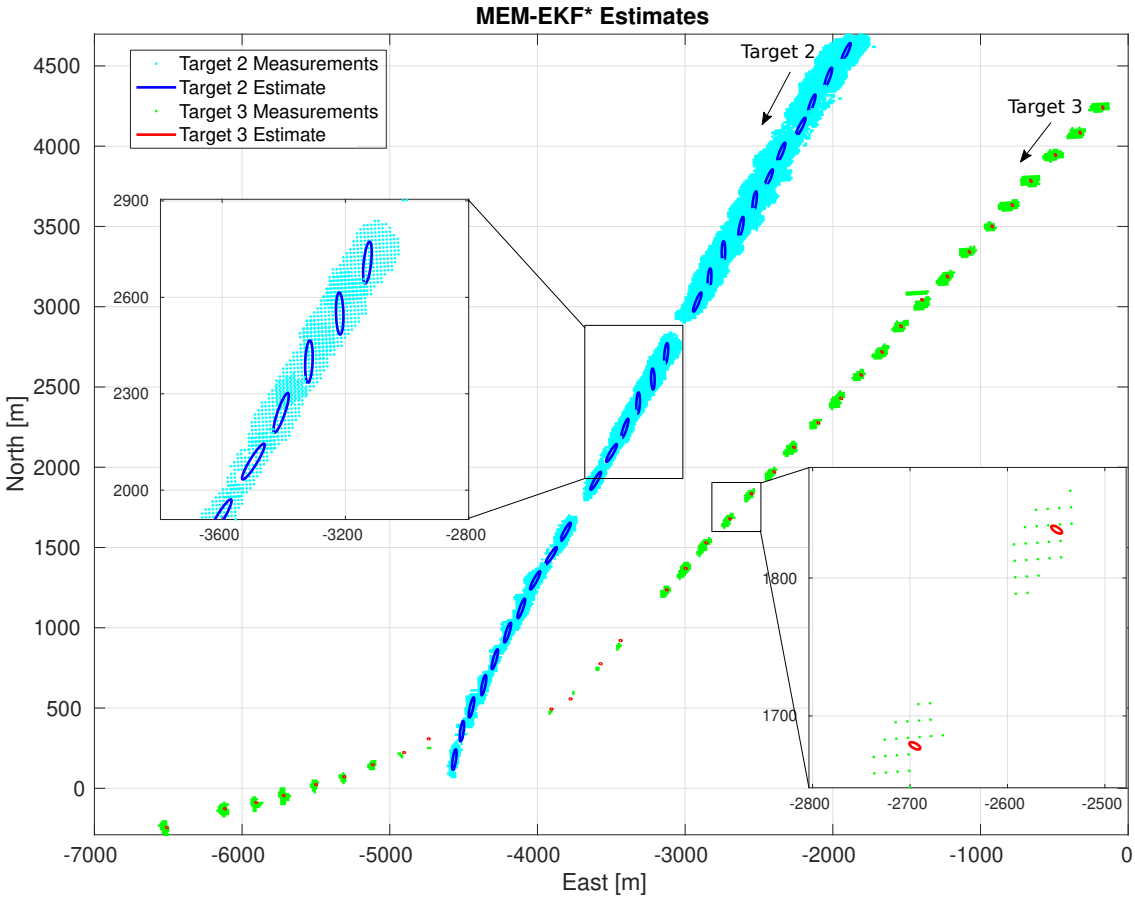

Figure 4.3: Illustration of the elliptical estimates over the trajectory at intervals of 20 observation steps. Each target was processed separately. Target 2 has dimensions 129m by 23m and Target 3 12m by 4m. Image adapted from [5]©2019IEEE

two methods, the orientation estimates show different mixed behaviours for the individual targets, presented in Figure 4.5.

4.1.5 Discussion

Based on the plots in Figure 4.4, we see that Target 2's orientation estimates diverged between $k = 100$s to $k = 300$ owing to occlusion from Target 3 to the own perspective. The length and width were more or less aligned with their respective ground truths. On the other hand, the dimension estimates for Target 3 are closer to the ground truth as compared to the orientation estimates. At around $k = 480$ to $k = 620$, the target suffered due to sparse measurements (for example, there were missed detections at consecutive steps). The other prime factor is due to the rather coarse sensor resolution, where for this dataset, 1 pixel of the image represented 11m. This means that the vessel's width has a tendency to being over-represented and is therefore deemed to

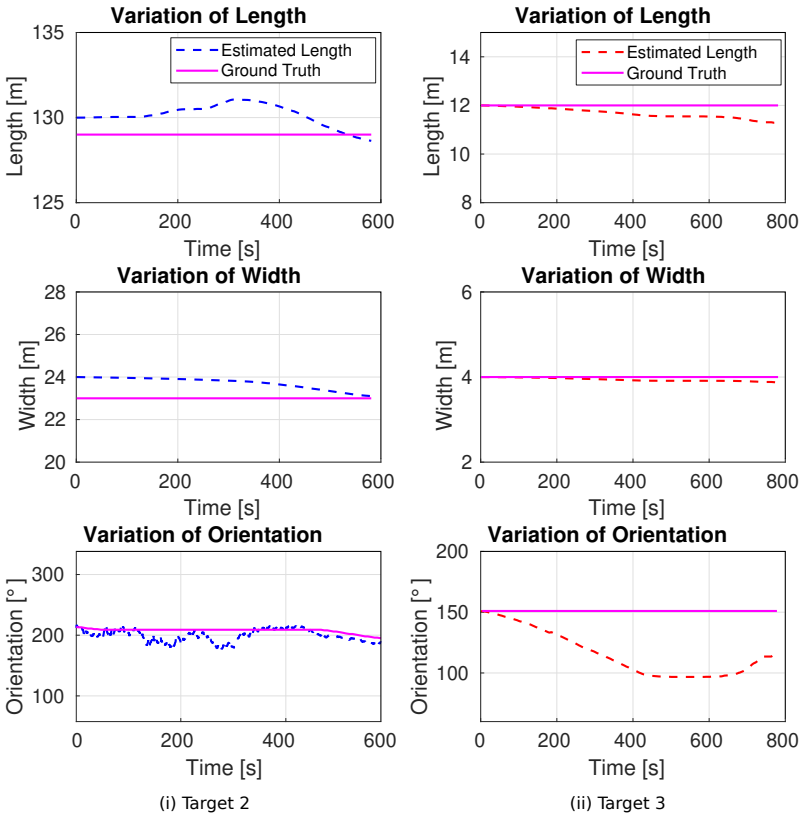

(a) The plots of how the estimates for length, width and orientation of the target vary over time for both targets. The AIS-based ground truth is represented by solid magenta line while the estimates in broken blue (Target 2) and red (Target 3) lines. Image adapted from [5]©2019IEEE

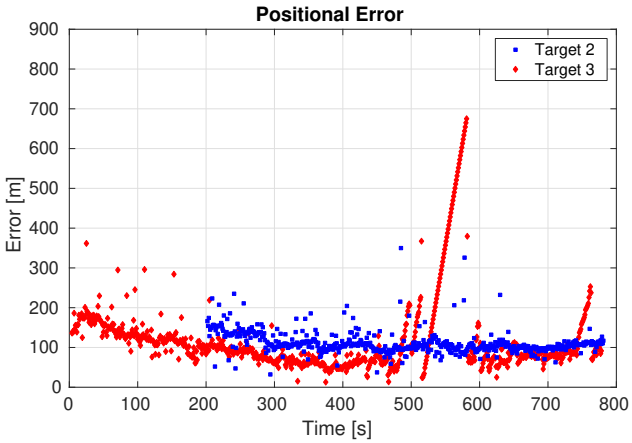

(b) The positional error calculated between the estimates and AIS-based ground truth. Image adapted from [5]©2019IEEE

Figure 4.4: Estimates of MEM-EKF* against AIS-based ground truth.

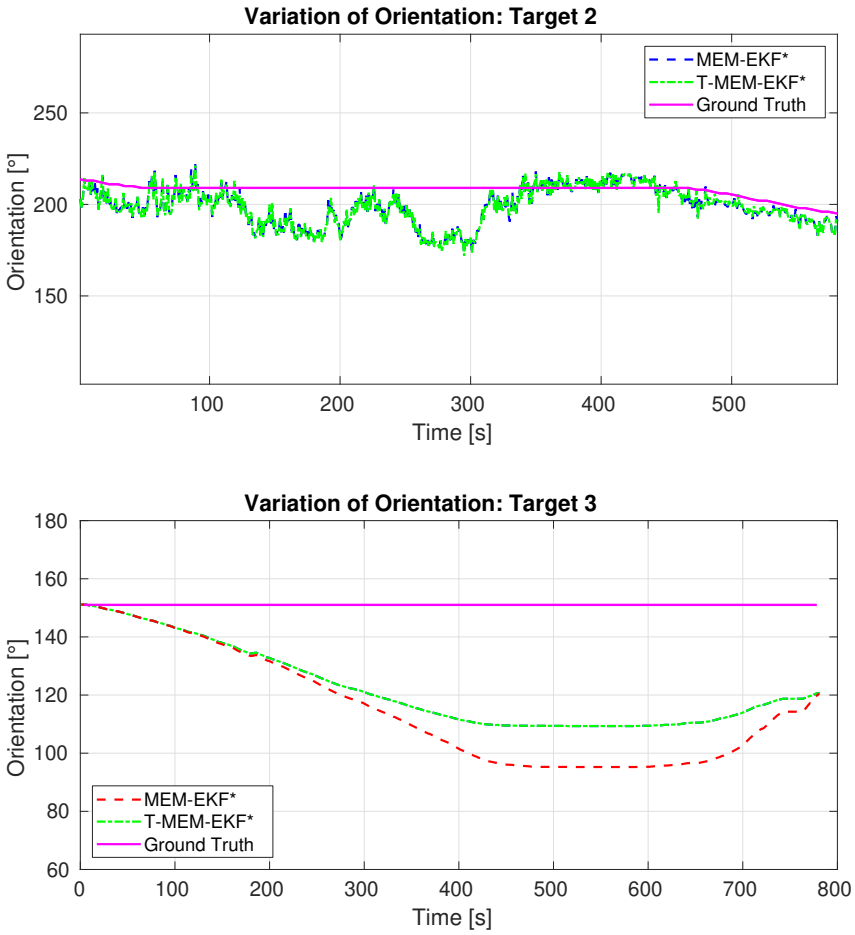

Figure 4.5: The orientations of MEM-EKF*, T-MEM-EKF* and the AIS-based ground truth over time. Image adapted from [5]©2019IEEE

Table 4.4: Filtering Execution Time [s]

Approach	MEM-EKF*	T-MEM-EKF*
Target 2	15.16	13.74
Target 3	2.73	2.33

contain insufficient data for an ETT consideration. Regarding the fact of how point clouds are seen as bigger and with more distortion from far ranges and get more accurate at closer ranges, this phenomenon has not been captured by the MEM-EKF* or T-MEM-EKF* due to the restriction in semi-axes imposed at the initialisation step.

The positional errors, obtained by comparing the kinematic position estimates against the AIS position on-board that is approximately taken as the vessel's centre. The errors are relatively high at first as the targets were far from the own. This is slightly improved as they get closer to the own vessel for up until $k = 450$. We also see higher estimation errors during the obscuration phase at $k = 480$ to $k = 620$ (poor detections due to outdoor conditions) and an occlusion phase from $k = 745$ to $k = 765$, where Target 3 was undetected as it was occluded by Target 2.

The estimates from the two filters for Target 2 in Figure 4.5 show a similar trend. When it comes to Target 3, however, the estimates deviated less for our approach despite still being sensitive to the missed detections and sensor resolution. This is taken as one of the limitations of the dataset. On the other hand, when we consider the filter execution times, we find that T-MEM-EKF* is again more computationally efficient (see Table 4.4).

The results, as a whole, show that within the context of tracking the orientation of a target with known spatial extent, T-MEM-EKF* is a better candidate as it can provide similar and accurate orientation estimates faster than its counterpart. Nonetheless, it was also observed that the number of measurements (intuitively and strongly correlated to the target's dimensions) affect both the processing time and the accuracy. The accuracy is also dependent on the perspective at which the target is visible from the own vessel which was also concluded in Appendix B.1, where targets of interest were manoeuvring around a static observing sensor platform [3]. We consider these two findings amongst others in order to formulate the next ETT approach.

4.2 Principal Axes Elliptical ETT

In the previous part, we have seen how the radar point clouds measurements affect the final estimates. We now attempt at optimising the elliptical approximation process by understanding their nature and quality with respect to the measurement model itself. More importantly, we ask ourselves the question of how well the model could represent the data in its entirety. To dive into this aspect, we consider the illustrations in Figure 4.6 attempting to emulate real-world data. The diagram contains some noisy radar point clouds measurements recorded from one sensor. Should there be an elliptical extent approximation in this case, the approximations would limit the accuracy in representing the true extent of the underlying target. This limitation is higher should we consider the radar backscattering impact [BPO02, JB06, SBNC+21]. For instance, if the surface of the vessel reflecting the radar is rough, the measurements have a tendency to be more distorted than if the surface would have been less smooth. When backscattering is considered on top of environmental factors, the measurements would be highly noisy, dense and all scattered much beyond the target's surface.

The number of measurements in each target-originated point cloud depends on the sensor resolution and the aforementioned factors, where one can expect larger vessels to yield a higher number of measurements that are often in the order of hundreds. These form part of our motivation to have a linear filter that can process all target-originated measurements through a batch update approach (all measurements processed in a single step) and at the same time, have a flexible explicit uncertainty representation for each of the extent parameters. In order to reach a proper trade-off between computational efficiency and accuracy, we particularly adopt the explicit parameterisation from (4.1.3) and utilise the concept of eigenvector decomposition (EVD) to obtain explicit measurements to update the extent parameters. The kinematic state is then updated based on the centroid of the target's point cloud directly.

Similar to the structure adopted for the first half, we shall next describe the relevant state-of-the-art, problem, our contributions and their results in the following parts within this second half of the chapter.

4.2.1 Related Work

Continuing upon the literature review for the first part of the chapter (See Chapter 4.1), we now consider the constructs of the elliptical models with respect to ease of parameterisation and computational effectiveness. While the RMM could offer a batch-like update per observation step, the standard ones [Koc08, FF08, FFK11] represent the uncertainty through a single scalar value. In the recent derivative, the axes' parameters have been explicitly modelled [TO21] based on inverse-gamma PDFs, and its orientation based on a Gaussian one. Both are then estimated using a variational Bayes method. This method, nonetheless, relies on a coupling between the target's velocity and orientation. In [LLL20], the orientation has been modelled by a vector and

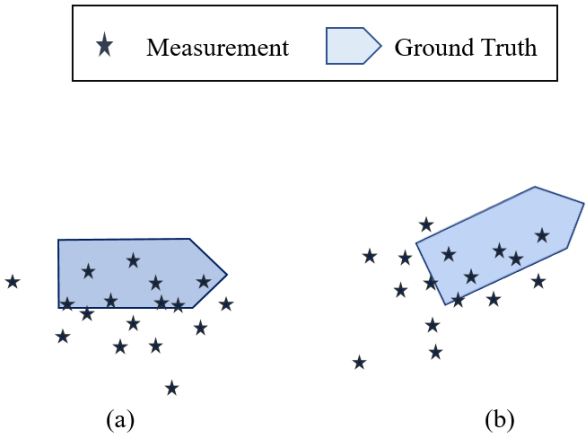

Figure 4.6: Sample illustration of noisy radar measurements being prominent over a specific visible side of the target limiting an accurate and complete representation of its true underlying extent.

the axes have been modelled as fixed non-random parameters and are estimated by a maximum likelihood method. The downside of this method is its high computational requirements. The MEM-EKF* [YB19] provides an explicit modelling, and requires measurements to be processed in a sequential manner, somehow making it more suitable for situations with sparse measurements. It relies as well on pseudo-measurements to update the extent, which adds to the computation. The orientation and velocity have a loose coupling.

In a similar direction, a method called the Independent Axes Estimation has been proposed, where the axes are estimated individually from an EVD of the dispersion matrix and the target is assumed to be velocity-aligned [Gov19]. The method by [DWS11] models the parameters explicitly as Gaussians and uses a two-stage filter with data-driven measurement noise which is restricted according to the minor-axis length. It is to be noted that due to the mentioned restrictions of these two methods, we do not consider them for the comparisons that follow.

4.2.2 Problem Description

At observation step k, a target's state is broken down into its kinematic state $\mathbf{r}_k$ defined by its ENU position $\mathbf{m}_k$ and velocity $\dot{\mathbf{m}}_k$ vectors as defined in (4.1.16). The extent parameter vector $\mathbf{p}_k$ contains the orientation α_k and semi-axes lengths $\ell_{1,k}$ and $\ell_{2,k}$, as defined in (4.1.3). The set of n_k measurements gathered at k is given by $\mathcal{Y}_k$. The measurements' sources are assumed to be spatially distributed over the target's surface.

Let $\bar{\mathcal{Y}}_k$ be the set that contains all the measurements up to k. The prior kinematic state and extent

parameter vector PDFs are Gaussian-approximated as follows,

$$p\left(\mathbf{r}_k|\bar{\boldsymbol{\mathcal{Y}}}_{k-1}\right) \approx \mathcal{N}\left(\mathbf{r}_k; \hat{\mathbf{r}}_{k|k-1}, \mathbf{C}^{\mathbf{r}}_{k|k-1}\right), \tag{4.2.1}$$

$$p\left(\mathbf{p}_k|\bar{\boldsymbol{\mathcal{Y}}}_{k-1}\right) \approx \mathcal{N}\left(\mathbf{p}_k; \hat{\mathbf{p}}_{k|k-1}, \mathbf{C}^{\mathbf{p}}_{k|k-1}\right). \tag{4.2.2}$$

Similarly, the posteriors are also assumed to be Gaussian distributed so that

$$p\left(\mathbf{r}_k|\bar{\boldsymbol{\mathcal{Y}}}_{k}\right) \approx \mathcal{N}\left(\mathbf{r}_k; \hat{\mathbf{r}}_{k|k}, \mathbf{C}^{\mathbf{r}}_{k|k}\right), \tag{4.2.3}$$

$$p\left(\mathbf{p}_k|\bar{\boldsymbol{\mathcal{Y}}}_{k}\right) \approx \mathcal{N}\left(\mathbf{p}_k; \hat{\mathbf{p}}_{k|k}, \mathbf{C}^{\mathbf{p}}_{k|k}\right). \tag{4.2.4}$$

The sensor models for both $\mathbf{r}_k$ and $\mathbf{p}_k$ are assumed linear with additive Gaussian measurement noise $\boldsymbol{\upsilon}_k^{(\bullet)}$ with specific measurement equations written as,

$$\boldsymbol{y}^{\mathbf{r}}_k = \mathbf{H}_{\mathbf{r}}\mathbf{r}_{k|k-1} + \boldsymbol{\upsilon}^{\mathbf{r}}_k, \tag{4.2.5}$$

$$\boldsymbol{y}^{\mathbf{p}}_k = \mathbf{H}_{\mathbf{p}}\mathbf{p}_{k|k-1} + \boldsymbol{\upsilon}^{\mathbf{p}}_k \tag{4.2.6}$$

with the measurement matrices $\mathbf{H}_{\mathbf{r}} = [\mathbf{I}_2, \mathbf{0}_2]$ and $\mathbf{H}_{\mathbf{p}} = \mathbf{I}_3$.

4.2.3 Principal Axes-based Kalman Filter

We propose the PAKF approach, that updates a target's extended state through a simple standard KF by using the centroid for the kinematic state and the decomposition of the dispersion matrix of a target-originated point cloud for the extent parameter vector update. This keeps both states decoupled from each other. The dispersion matrix is first *corrected* to account for the measurement noise prior to being subject to an EVD step.

Consider a two-dimensional ellipse that can be represented by dispersion matrix $\mathbf{C}^D$, which measures the spread of measurements (in East and North directions marked as e and n, respectively, in (4.2.8)) within the point cloud, given by

$$\mathbf{C}^D = \frac{1}{n_k - 1}\sum_{j=1}^{n_k}\left(\boldsymbol{y}^j_k - \bar{\boldsymbol{y}}_k\right)\left(\boldsymbol{y}^j_k - \bar{\boldsymbol{y}}_k\right)^T, \tag{4.2.7}$$

$$= \begin{bmatrix} \sigma_e^2 & \sigma_{en}^2 \\ \sigma_{en}^2 & \sigma_n^2 \end{bmatrix} \tag{4.2.8}$$

where $\bar{\boldsymbol{y}}_k$ is the mean of the measurements in $\boldsymbol{\mathcal{Y}}_k$. In the event that the measurement equation (4.2.5) is devoid of any noise, so that $\mathbf{C}^{\boldsymbol{\upsilon}}_{\mathbf{r}} = \operatorname{diag}[\mathbf{0}_2]$, $\mathbf{C}^D$ can be decomposed into its corresponding eigenvalues and eigenvectors thus relating to the lengths of the elliptical representation of the point cloud (see Figure 4.7). In the alternative case, when the system is corrupted with additive

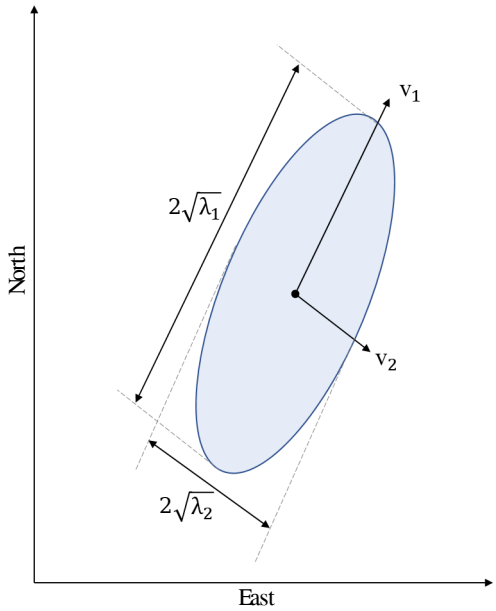

Figure 4.7: The relationship between the eigenvalues λ_1, λ_2 of a dispersion matrix and the lengths of the ellipse's axes. $\mathbf{v}_1$ and $\mathbf{v}_2$ are the eigenvectors. Image adapted from [6]©2021IEEE

noise, the dispersion matrix can be corrected by a subtraction operation yielding,

$$\mathbf{C}^{\hat{D}} = \mathbf{C}^{D} - \mathbf{C}_{\mathbf{r}}^{\boldsymbol{v}}. \tag{4.2.9}$$

The relationship between the corrected dispersion matrix of the target to the extent parameters could be established as follows,

$$\mathbf{C}^{\hat{D}} = \boldsymbol{\mathcal{R}}(\theta) \begin{pmatrix} a^2 & 0 \\ 0 & b^2 \end{pmatrix} \boldsymbol{\mathcal{R}}(\theta)^T, \tag{4.2.10}$$

with rotation matrix $\boldsymbol{\mathcal{R}}(\theta)$ and semi-axes a, b. The parameters could be reproduced based on the EVD of $\mathbf{C}^{\hat{D}}$, whose eigenvectors $\mathbf{V}$ and eigenvalues matrix $\boldsymbol{\lambda}$ can be related to (4.2.10) by,

$$\mathbf{C}^{\hat{D}} = \mathbf{V}\boldsymbol{\lambda}\mathbf{V}^T. \tag{4.2.11}$$

We denote the EVD operation by $\mathrm{eig}\,(\cdot)$ as follows,

$$[\mathbf{V}, \quad \boldsymbol{\lambda}] = \mathrm{eig}\left(\mathbf{C}^{\hat{D}}\right), \tag{4.2.12}$$

that returns the eigenvectors and eigenvalues.

It is to be noted that (4.2.9) could affect the positive definiteness requirement for EVD under certain

situations that could give rise to sparse measurements. We provide some workarounds for this constraint in Appendix B.2.

Post the EVD step, the largest diagonal obtained from $\boldsymbol{\lambda}$ which is also defined as the eigenvalue λ_1, corresponds to the major semi-axis a and the other diagonal λ_2 in turn corresponds to the minor semi-axis b based on the following relation,

$$a = \sqrt{\lambda_1}, \tag{4.2.13}$$

$$b = \sqrt{\lambda_2}. \tag{4.2.14}$$

The orientation θ is calculated from the elements of the eigenvector $\mathbf{v}_1$ that corresponds to λ_1

$$\theta = \text{atan2}\left(\frac{\mathbf{v}_{1,(n)}}{\mathbf{v}_{1,(e)}}\right) \tag{4.2.15}$$

where $\theta \in [-\pi, \pi]$. The intuition is to integrate the decomposition step within a KF to accomplish simultaneous estimation of the ellipse parameters. The measurement vector $\boldsymbol{y}_k^{\mathbf{p}} = [\theta_k, a_k, b_k]^T$ that is employed to update the extent in the KF is formed by the above operations (4.2.12-4.2.15). The values for $\mathbf{C}_{\mathbf{p}}^{\upsilon}$ are user-defined and can be tuned to reflect their uncertainties.

The algorithm for the both the kinematic state and extent parameter vector updates, with adjusted parameter notations from [6], can be found in Table 4.5.

We have also carried out some additional analyses on the impact of changing the number of measurements and noise levels on the algorithm, included in the Appendix B.2. They have been described and the results have been supported with appropriate plots.

4.2.4 Results

The PAKF was applied on a simulated trajectory and the results were evaluated and compared with two state-of-the-art methods (the MEM-EKF* by Yang [YB19] and the RMM by Feldmann $et\ al$ [FFK11]) based on the Gaussian Wasserstein (GW) distance. Following this, our algorithm was applied on the DAAN dataset.

Simulation

The standard trajectory that has been used multiple times for evaluating the performance of elliptical trackers in literature has been considered [FFK11, LL16, YB19, TO21]. It entails a target of dimensions 340m by 80m starting from the origin and moving at a constant speed of 50km/h. At every observation step, measurements were drawn from a Poisson PDF having a mean of 250.

An NCV model (Appendix A.1) was adopted for the kinematics state system model. The kinematic

Table 4.5: Updates based on Elliptical Principal Axes Model, adapted from [6].

Kinematic State Update
$\boldsymbol{y}_k^{\mathbf{r}} := \bar{\boldsymbol{y}}_k = \frac{1}{n_k} \sum_{j=1}^{n_k} \boldsymbol{y}_k^j$
$\hat{\boldsymbol{y}}_k^{\mathbf{r}} = \mathbf{H}_{\mathbf{r}} \hat{\mathbf{r}}_{k\|k-1}$
$\mathbf{C}_k^{\mathbf{ry}} = \mathbf{C}_{k\|k-1}^{\mathbf{r}} \mathbf{H}_{\mathbf{r}}^T$
$\mathbf{C}_k^{\boldsymbol{yy}} = \mathbf{H}_{\mathbf{r}} \mathbf{C}_{k\|k-1}^{\mathbf{r}} \mathbf{H}_{\mathbf{r}}^T + \mathbf{C}_{\mathbf{r}}^{\boldsymbol{v}}$
$\hat{\mathbf{r}}_{k\|k} = \hat{\mathbf{r}}_k + \mathbf{C}_k^{\mathbf{ry}} \left(\mathbf{C}_k^{\boldsymbol{yy}}\right)^{-1} \left(\boldsymbol{y}_k^{\mathbf{r}} - \hat{\boldsymbol{y}}_k^{\mathbf{r}}\right)$
$\mathbf{C}_{k\|k}^{\mathbf{r}} = \mathbf{C}_{k\|k-1}^{\mathbf{r}} - \mathbf{C}_k^{\mathbf{ry}} \left(\mathbf{C}_k^{\boldsymbol{yy}}\right)^{-1} \left(\mathbf{C}_k^{\mathbf{ry}}\right)^T$
Computing Extent Measurements through EVD
$\mathbf{C}^D = \frac{1}{n_k - 1} \sum_{j=1}^{n_k} \left(\boldsymbol{y}_k^j - \bar{\boldsymbol{y}}_k\right) \left(\boldsymbol{y}_k^j - \bar{\boldsymbol{y}}_k\right)^{\mathrm{T}}$
$\mathbf{C}^{\hat{D}} = \mathbf{C}^D - \mathbf{C}_{\mathbf{r}}^{\boldsymbol{v}}$
$[\mathbf{V}, \boldsymbol{\lambda}_k] = \mathrm{eig}\left(\mathbf{C}^{\hat{D}}\right)$
$[\lambda_1, \lambda_2]^{\mathrm{T}} = \mathrm{diag}\left(\boldsymbol{\lambda}_k\right)$
$[a_k, b_k]^{\mathrm{T}} = \sqrt{[\lambda_1, \lambda_2]^{\mathrm{T}}}$
$\theta_k = \mathrm{atan2}\left(\frac{\mathbf{v}_{1,(n)}}{\mathbf{v}_{1,(e)}}\right)$
Extent Update
$\boldsymbol{y}_k^{\mathbf{p}} := [\theta_k, a_k, b_k]$
$\hat{\boldsymbol{y}}_k^{\mathbf{p}} = \mathbf{H}_{\mathbf{p}} \hat{\mathbf{p}}_{k\|k-1}$
$\mathbf{C}_k^{\mathbf{py}} = \mathbf{C}_{k\|k-1}^{\mathbf{p}} \mathbf{H}_{\mathbf{p}}^T$
$\mathbf{C}_k^{\boldsymbol{yy}} = \mathbf{H}_{\mathbf{p}} \mathbf{C}_{k\|k-1}^{\mathbf{p}} \mathbf{H}_{\mathbf{p}}^T + \mathbf{C}_{\mathbf{p}}^{\boldsymbol{v}}$
$\hat{\mathbf{p}}_{k\|k} = \hat{\mathbf{p}}_k + \mathbf{C}_k^{\mathbf{py}} \left(\mathbf{C}_k^{\boldsymbol{yy}}\right)^{-1} \left(\boldsymbol{y}_k^{\mathbf{p}} - \hat{\boldsymbol{y}}_k^{\mathbf{p}}\right)$
$\mathbf{C}_{k\|k}^{\mathbf{p}} = \mathbf{C}_{k\|k-1}^{\mathbf{p}} - \mathbf{C}_k^{\mathbf{py}} \left(\mathbf{C}_k^{\boldsymbol{yy}}\right)^{-1} \left(\mathbf{C}_k^{\mathbf{py}}\right)^T$
Measurement matrices $\mathbf{H}_{\mathbf{r}} = \begin{bmatrix} 1 & 0 & 0 & 0 \\ 0 & 1 & 0 & 0 \end{bmatrix}$ and $\mathbf{H}_{\mathbf{p}} = \begin{bmatrix} 1 & 0 & 0 \\ 0 & 1 & 0 \\ 0 & 0 & 1 \end{bmatrix}$

Table 4.6: Filtering Execution Time

Approach	MEM-EKF*	RMM	PAKF
Time [s]	$1.50e^{-2}$	$2.50e^{-4}$	$1.70e^{-4}$

settings for all three approaches were kept similar: the process noise covariance of kinematic state was $\mathbf{C}_{\mathbf{r}}^{\boldsymbol{\omega}} = \mathrm{diag}(150^2, 150^2, 5^2, 5^2)$. The measurement noise covariance was set as $\mathbf{C}_{\mathbf{r}}^{\boldsymbol{\upsilon}} = \mathrm{diag}(30^2, 30^2)$.

The state equations for $\mathbf{p}$ are the same as in (4.1.17). The initialisations of PAKF and MEM-EKF* were realised with the same parameters for a fair comparison. The covariance of the process noise for the extent parameter vector was taken as $\mathbf{C}_{\mathbf{p}}^{\boldsymbol{\upsilon}} = \mathrm{diag}(0.1^2, 2^2, 1^2)$. Individual settings for $\tau = 50$ and $\upsilon = 56$ are used for RMM.

The measurements, ground truth, and estimates from all three approaches from a single run have been plotted at regular intervals over the trajectory in Figure 4.8. The filters were executed for 1000 Monte Carlo runs and have been evaluated using the GW distance metric. The GW distance, a scalar value, is a recommended metric measure for evaluating elliptical approximation performance of an estimated ellipse against its ground truth [GS84, YBG16]. Its definition is provided in Appendix A.3. The extension errors calculated as GW Mean Squared Error (MSE) distances at every step are shown in Figure 4.8b.

The PAKF has errors that are comparable to those of MEM-EKF*. The RMM errors are higher around the turns in particular, despite being on par with its counterparts on the straight parts of the trajectory. As we are looking for computational efficiency, we recorded the execution time taken by each method. For a single observation step with a target generating 250 measurements on average, the execution times are shown in Table 4.6, where PAKF outperforms the others.

In Appendix B.2, we provide additional error plots and insights by examining the effects of the mean number used for measurement generation.

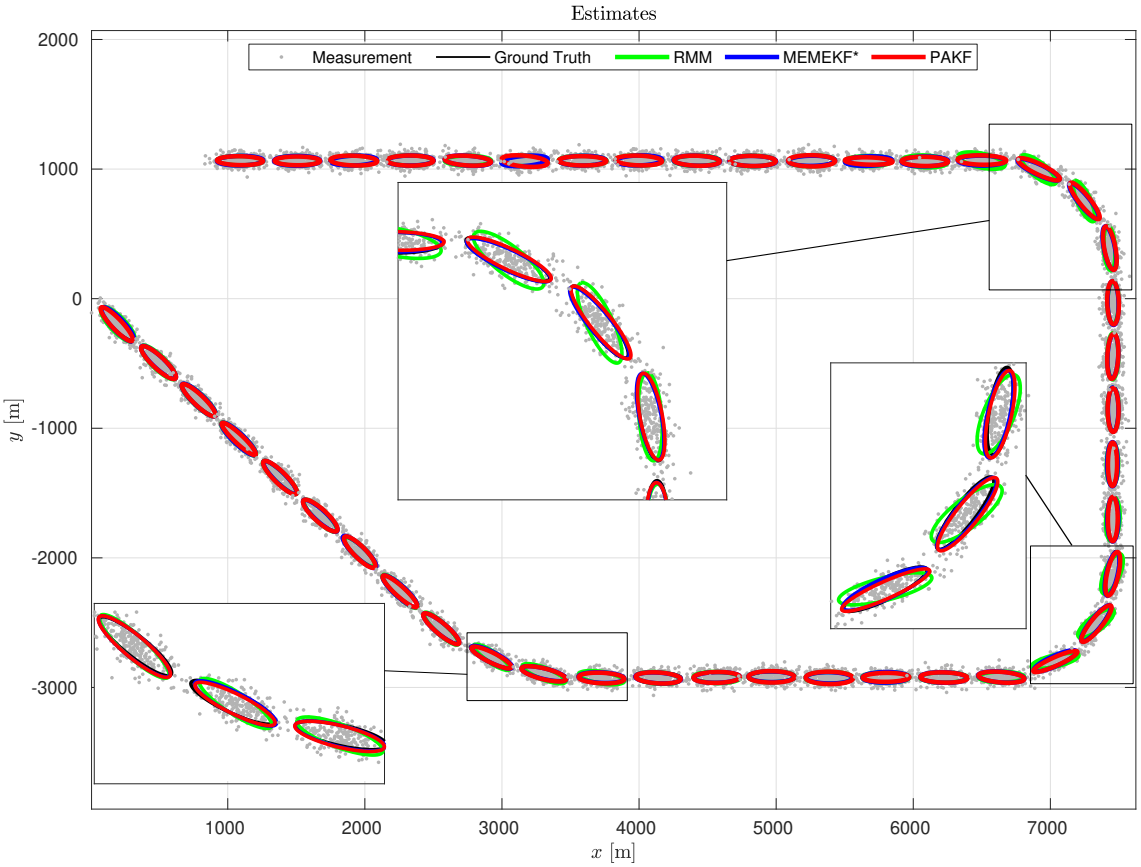

(a) Estimated elliptical approximations of the target from each method.

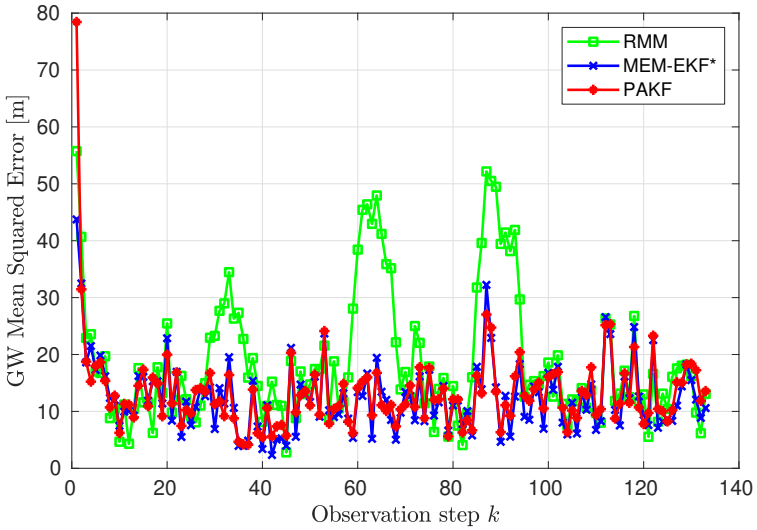

(b) GW distance over 1000 runs.

Figure 4.8: Images from [6]©2021IEEE

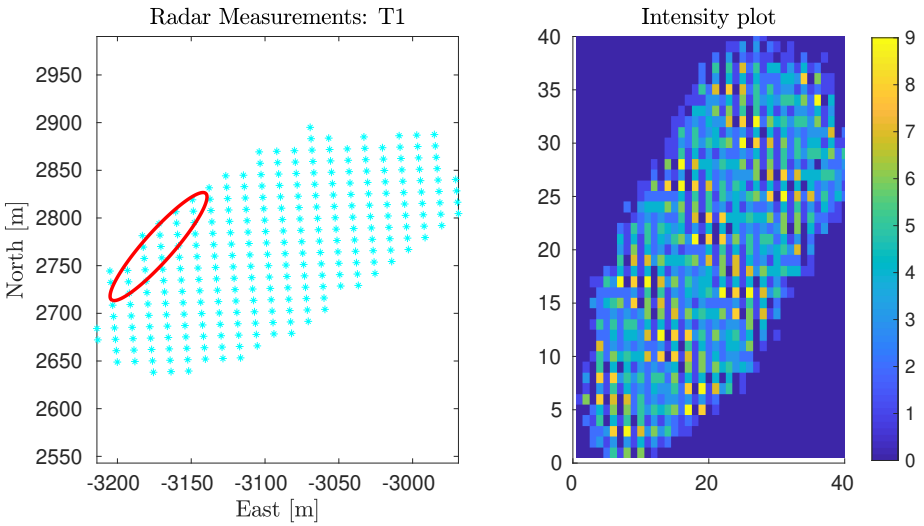

Figure 4.9: The left plot shows a vessel's elliptical extent that has been reconstructed from its AIS information. The cyan asterixes are the challenging radar measurements from frame $k = 450$. The sensor is in a South-Eastern direction. On the right is an intensity plot of cumulative radar measurements over 10 consecutive frames using 40 bins. Image from [6]©2021IEEE

Dataset

The performance of PAKF is now demonstrated on real-world data from the DAAN dataset which, as a recall, is affected by heavy distortion, smearing, occlusion and aids to navigation. A closer look to the noisy measurements from Target 2 (129m by 23m), our target of interest, can be found in Figure 4.9. With the intensity plot, it can also be seen that some regions are likely to produce a higher density of measurements when accumulated over time. Only the point cloud measurements that correspond to Target 2 were input to the filter. The point clouds are more widely spread from afar, with respect to the own, and improve as from $k = 450$. The target kinematic state was initialised from the exact AIS values (hence the initial bias seen in Figure 4.10, where the first elliptical estimates are more Eastwards than the point clouds).

The kinematic measurement noise covariance was taken as $\mathbf{C}_{\mathbf{r}}^{\boldsymbol{\upsilon}} = \text{diag}(30^2, 35^2)$ for this experiment. The extent parameter vector $\mathbf{p}_0 = [2.36, 175, 25]^T$ with covariance $\mathbf{C}_0^{\mathbf{p}} = \text{diag}(0.14^2, 200^2, 25^2)$ because of the initial distortion. To compensate for the fluctuations and high noise, the measurement noise covariance for $\mathbf{p}$ was set to $\mathbf{C}_{\boldsymbol{\upsilon}}^{\mathbf{p}} = \text{diag}(0.01^2, 20^2, 10^2)$ and the extent process noise covariance to $\mathbf{C}_{\mathbf{p}}^{\boldsymbol{\omega}} = \text{diag}(0.1, 350, 50)$.

The PAKF estimates and the extent parameters over time are depicted in Figure 4.10 and Figure 4.11. The elliptical estimates were plotted at every 35 steps.

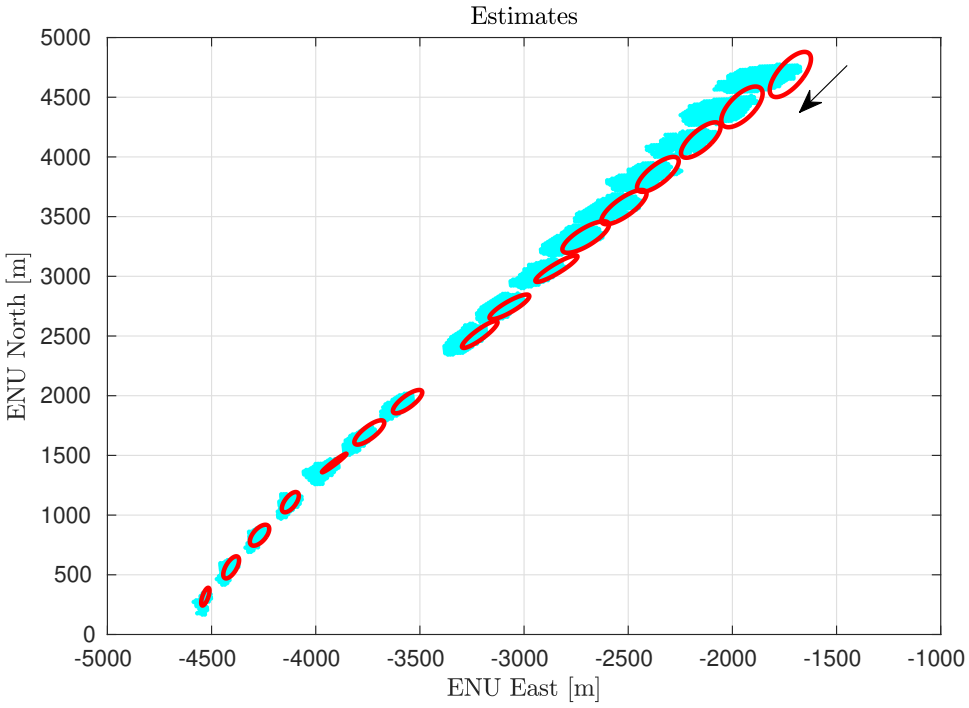

Figure 4.10: Elliptical PAKF estimates (red ellipses) plotted over the radar measurements (cyan dots) at regular 35 step-intervals. Image from [6]©2021IEEE

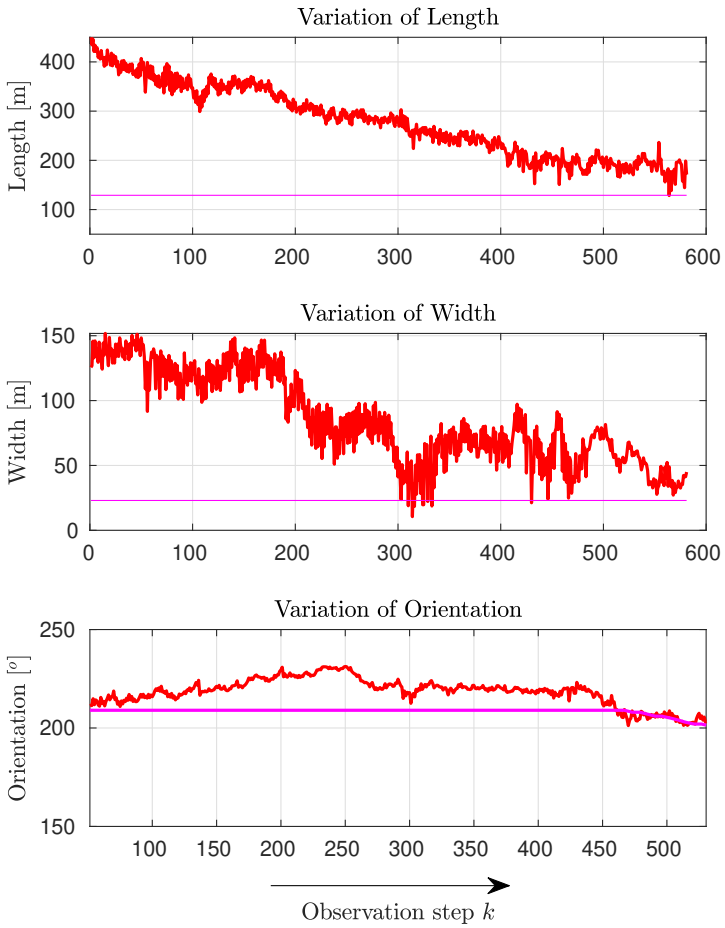

Figure 4.11: The estimated extent parameters throughout the trajectory. The red solid lines are the estimates and the magenta ones are the AIS values. Image from [6]©2021IEEE

4.2.5 Discussion

When looking at Figure 4.10, one can notice a correlation between the estimated length and width values and the spread of the point clouds. In Figure 4.11, the dimension estimates start nearing the reference values. The orientation estimates were affected around moments of occlusion but picked up eventually to detect the turn.

The current estimates reflect some contrast to the T-MEM-EKF* results in Section 4.1.5, specifically for the orientation. This is because in the latter approach, there exists a loose coupling between the orientation and velocity which influenced the results. The PAKF extent is completely decoupled from the kinematic state. Nonetheless, as a blind decoupled estimator (without any prior knowledge of dimensions) with the possibility of explicit extent noise parameters, the PAKF is a reliable and efficient tracker for elliptical ETT as the estimates converge closely to their references as the target gets within a clearer perspective and nearer range.

4.3 Chapter Summary

Two methods were proposed in this chapter, the T-MEM-EKF* approach and the PAKF approach for elliptical ETT. The T-MEM-EKF* is essentially a custom version of the MEM-EKF*, focussing on applications that require estimating the orientation of targets having known spatial distributions. The proposed approach was able to improve on its basis in terms of computational efficiency. However, its sequential updating approach would still affect the performance for dense point clouds per target, especially if we consider noisy and distorted measurements. The linear PAKF approach was then formulated with the aim of having explicit parameter representation for the extent and could process the measurements in a batch-like manner. The settings of the measurement noise covariance (of the kinematic state) with respect to the target dimension and application play an important role in ensuring positive definiteness along with workarounds when challenged. PAKF's performance was analysed compared to two state-of-the-art methods and also applied on real-world marine radar data. The results showed a comparable performance to the MEM-EKF* with dense point clouds for the accuracy, and it was fastest among the methods used.

The contributions presented in this chapter were published in conference proceedings [5] and [6].

Chapter 5

Elliptical Multiple Extended Target Tracking

This chapter broadly aims at proposing an approach for elliptical METT that builds up on our works from the earlier chapters for single targets to now multiple targets. We first focus on marine radar data from the on board sensors onto which we apply a multi-target tracker, before eventually proceeding to integrate the final METT algorithm in the framework from Chapter 2.1 for processing ASTERIX radar video streams.

Contents

Two approaches are proposed, the EC-JPDA and the PAKF-based EC-JPDA Filter (PAKF-JPDA). The EC-JPDA is our approach for MTT that uses the data association scheme by taking a target-originated point cloud's typically noisy spread into consideration. The second approach, PAKF-JPDA, is our proposed elliptical multiple target tracker that essentially combines features of the PAKF and the EC-JPDA. The results from both methods are presented with comparative metrics to other standard approaches, where applicable. Finally, we also illustrate the overall framework's feasibility supported by results captured from the demonstrator that feeds on radar

video streams. Continuing with our convention, the notations used from the initial chapters are retained.

5.1 Centroid-based Multiple Target Tracking

Most observation regions, for example, harbours or vessel range-based regions in our context, record detections from multiple targets of interest. The targets are likely to generate point clouds, as are clutter due to error sources or environment-based artifacts. Classical DA approaches for MTT consider tracking the kinematics of targets primarily under the $1-1$ association assumption that a point measurement could have originated from only one target and that one target could have produced only one measurement [BSWT11]. With multiple point cloud measurements, the assumptions would no longer hold. However, the measurement set could be partitioned by appropriate methods such as clustering, enabling a cluster-to-target association without the need to resort to complex $m-1$ association schemes.

In this section, we exploit this possibility and propose a custom JPDA filter that accounts for the extension of a target while estimating its kinematic properties as a whole. The radar image-extracted measurements described in Chapter 2.2 are clustered into potential target-originated point clouds. The centroids obtained from the clusters are then taken for updating the kinematic parameters. Furthermore, information about the target's extension is retained by the corresponding cluster's dispersion matrix that is later included in the gating and association processes, whose fundamentals are covered in Chapter 3.3 and shall be continued upon in this chapter. The proposed algorithm has been applied on our marine radar datasets, and we compare the results of our approach and a standard JPDA filter against the AIS positions.

5.1.1 Related Work

On top of the DA-based MTT algorithms mentioned in Chapter 2.1, the JPDA has commonly been used in maritime tracking applications in the works [BGV$^+$12, SBHH17, Sie17]. The basic standard JPDA algorithm as well as some of its approximations [RCBSW10] are however constrained to the point target assumption, which would not be suitable for dense point clouds of high cardinality as the combinational computation still ends up rendering the tracker inefficient.

Group Tracking (GT) is another form of target tracking approach that has been brought forward by Blackman in [Bla86], then as central and formation group tracking, respectively, which was further developed and applied in the works of [GWD17, GPRD20, ZLLW20]. These methods are basically concerned about tracking a number of closely-spaced targets that are moving in the same direction with respect to some metric such as distance or velocity over time. For an ETT perspective, the MEM-EKF* algorithm [YB19] derived an extent-based covariance to account for the target's shape as such.

5.1.2 Problem Description

Let $\boldsymbol{\mathcal{X}}_k$ represent the set of T_k individual target states (assumed to be known in the current context) existing at observation step k and be given by

$$\boldsymbol{\mathcal{X}}_k = \left\{\boldsymbol{x}_k^t\right\}_{t=1}^{T_k} \tag{5.1.1}$$

where each target state comprises its ENU-based position, COG and SOG:

$$\boldsymbol{x}_k^t = \left[m_{e,k}, m_{n,k}, \psi_k, \vartheta_k\right]^T. \tag{5.1.2}$$

We obtain a set of measurements $\boldsymbol{\mathcal{Y}}_k = \{\boldsymbol{y}\}_{j=1}^{r_k}$ of cardinality r_k that is assumed to have come from *all* targets within the observation region, including clutter which is assumed to be spatially and uniformly distributed over the observation region. It is further assumed that the specific track-originated measurements are likely to fall within its validation region.

As the JPDA assumes a $1-1$ association restriction between a measurement j and a target t, we define such an association by θ_{jt}. Let the set of c_k number of centroids obtained from clustering $\boldsymbol{\mathcal{Y}}_k$ be denoted by $\overline{\boldsymbol{\mathcal{Y}}}_k \equiv \{\bar{\boldsymbol{y}}\}_{j=1}^{c_k} \subseteq \boldsymbol{\mathcal{Y}}_k$. We would like to jointly estimate $\boldsymbol{\mathcal{X}}_k$ by determining the posterior PDF of the joint association event conditioned on the set $\overline{\boldsymbol{Y}}^k$ [VMBS+15],

$$p\left(\boldsymbol{\theta}_k|\overline{\boldsymbol{Y}}^k\right) = \frac{1}{a_1} p\left(\overline{\boldsymbol{\mathcal{Y}}}_k|\boldsymbol{\theta}_k, u_k, \overline{\boldsymbol{Y}}^{k-1}\right) p\left(\boldsymbol{\theta}_k|u_k\right) \tag{5.1.3}$$

where u_k is the number of validated measurements (centroids), and a_1 is a normalisation constant. The centroid measurements gathered up to observation steps k and $k-1$ are denoted by $\overline{\boldsymbol{Y}}^k := \overline{\boldsymbol{Y}}^{0:k}$ and $\overline{\boldsymbol{Y}}^{k-1} := \overline{\boldsymbol{Y}}^{0:k-1}$ respectively, and the joint association events by $\boldsymbol{\theta}_k$.

5.1.3 Extended Centroid-based JPDA Filter

GT and ETT are analogous concepts relying on similar constructs [SG99, MCS+14, GBR17]. In a quest to cater for ETT in an advanced step, we suggest using the idea from Blackman [Bla86] as an intermediary step towards integrating the extent parameters in a target's state being estimated within an MTT framework. In [Bla86], multiple targets that are navigating close to each other at almost similar velocities under the single point assumption (see Chapter 1) are tracked as a group instead of individually. The group position and velocity are based on the centre of gravity and group dynamics as a whole.

We therefore adopt the centroid-based concept for a target-originated point cloud, facilitated by clustering, and expand its use in the JPDA algorithm through an adaptive gating step and calculation of association probabilities.

At k, measurements in the set $\boldsymbol{\mathcal{Y}}_k$ are subject to a clustering approach from which a set of centroids

$\overline{\boldsymbol{\mathcal{Y}}}_k = \{\bar{\boldsymbol{y}}\}_{j=1}^{c_k}$ is obtained. Each centroid measurement is assumed to be corrupted with additive zero-mean Gaussian measurement noise $\boldsymbol{v}_k$,

$$\bar{\boldsymbol{y}}_k^j = \underbrace{\mathbf{H}\boldsymbol{x}_{k|k-1}^t}_{\widehat{\boldsymbol{y}}_k^t} + \quad \boldsymbol{v}_k \tag{5.1.4}$$

where measurement matrix $\mathbf{H} = [\mathbf{I}_2, \mathbf{0}_2]^T$. We also denote the predicted centroid-measurement of target t by $\widehat{\boldsymbol{y}}_{k|k-1}^t$.

Adaptive Gating

In the first step to establish the above relationship, the centroids are validated by track t's ellipsoidal gate (see Chapter 3.3.1) that we redefine as follows,

$$\boldsymbol{\mathcal{G}}^t := \{\bar{\boldsymbol{y}}_k : \left(\bar{\boldsymbol{y}}_k - \widehat{\boldsymbol{y}}_{k|k-1}^t\right)^T \left(\mathbf{C}_k^{\bar{\boldsymbol{y}},t}\right)^{-1} \left(\bar{\boldsymbol{y}}_k - \widehat{\boldsymbol{y}}_{k|k-1}^t\right) \leq \gamma\}, \tag{5.1.5}$$

with threshold γ and predicted measurement $\widehat{\boldsymbol{y}}_{k|k-1}^t$. The innovation covariance $\mathbf{C}_k^{\bar{\boldsymbol{y}},t}$, originally defined in (3.1.16) is now expressed as

$$\mathbf{C}_k^{\bar{\boldsymbol{y}},t} = \mathbf{H}\mathbf{C}_k^{\boldsymbol{x},t}\mathbf{H}^T + \mathbf{C}_k^{\boldsymbol{v}} + \mathbf{C}_{k-1}^{D,t}. \tag{5.1.6}$$

$\mathbf{C}_{k-1}^{D,t}$ is the dispersion matrix of the cluster corresponding to target t at $k-1$. When a centroid falls within the gate, all measurements that belong to the specific cluster are also checked for validity. Eventually, the most recent $\mathbf{C}_k^{D,t}$ is computed based on the validated cluster measurements and is used for gating in the next step recursively.

The dispersion matrix describes the spread of validated measurements belonging to the validated cluster in the East and North directions and it is given by,

$$\mathbf{C}_k^{D,t} = \begin{bmatrix} \sigma_e^2 & \sigma_{en}^2 \\ \sigma_{en}^2 & \sigma_n^2 \end{bmatrix}. \tag{5.1.7}$$

The value of $\mathbf{C}_k^{D,t}$ is adaptive in the gating process, based on the immediate previous observation step $k-1$, and based on the assumption that measurements arising from a target's surface fall within the validation region. This allows the filter to adapt to gradual changes in a specific target-originated point cloud, as a result of the sensor's varying perspective for instance, throughout its trajectory.

This process is illustrated in Figure 5.1. Hereupon, $\overline{\boldsymbol{\mathcal{Y}}}_k$ is regarded as the general measurement set to be processed by the tracker.

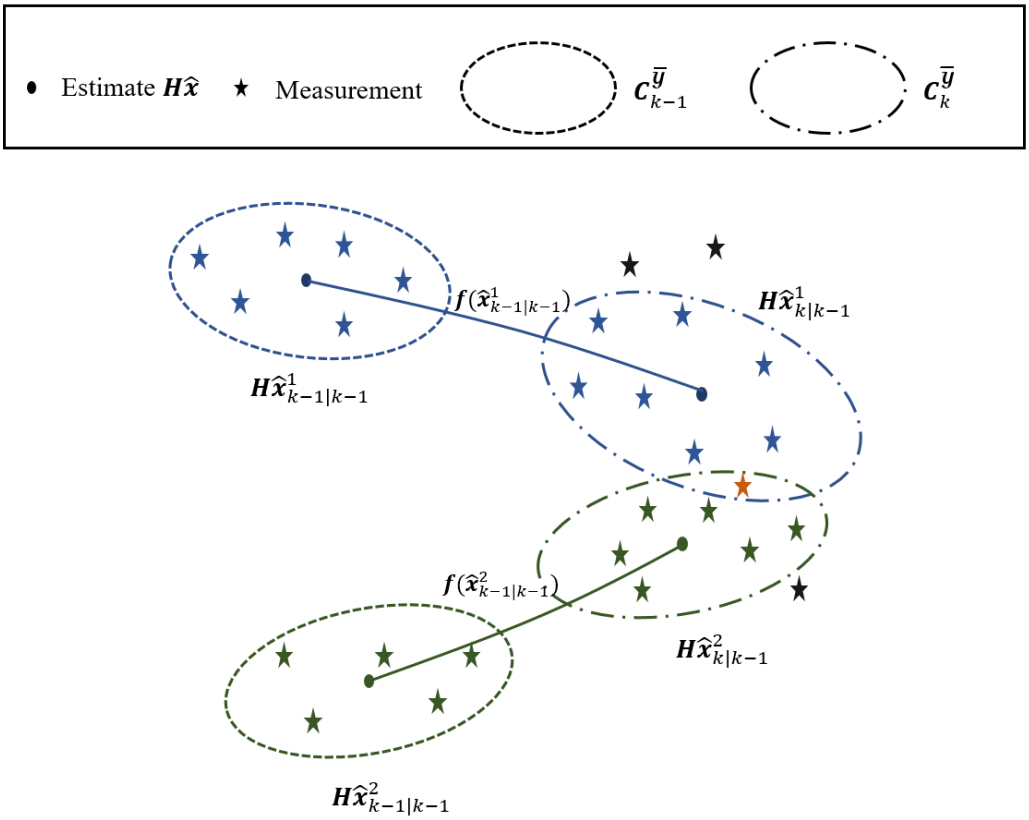

Figure 5.1: Validation and association of cluster measurements to obtain $\mathbf{C}_k^{D,t}$. Two tracks are displayed with their simplistic past and current measurements, as well as the tracks' predictions. In the first step, the centroids are validated. Then, the cluster measurements belonging to the respective cluster are further gated so that only those that lie in the gate of a track t, to which they shall be assigned later, are used to calculate $\mathbf{C}_k^{D,t}$ which is in turn integrated into the innovation covariance $\mathbf{C}_{k-1}^{\bar{y},t}$ for the adaptive gating at k. $\mathbf{C}_k^{\bar{y},t}$ will be used at $k+1$, and so forth.
For illustrative purposes, measurements are colour-coded with respect to the tracks. Common measurements from overlapping gates (orange) are shared and measurements falling out of the gates (black) are discarded.

Joint Association Probabilities

Let $\boldsymbol{\theta}$ represent joint association events and be defined (omitting k) as

$$\boldsymbol{\theta} = \bigcap_{j=1}^{c_k} \theta_{jt} \tag{5.1.8}$$

where θ_{jt} is the individual event that centroid $\bar{\boldsymbol{y}}_j$ has originated from target t.

A binary matrix $\boldsymbol{\Omega}$ of size $([T_k + 1] \times c_k)$ is constructed for representing the validated cluster-to-track (the additional row dimension accounts for cluster-to-clutter) pairings as,

$$\boldsymbol{\Omega} = [\zeta_{jt}], \tag{5.1.9}$$

where the binary variable ζ indicates the individual cluster-to-track validation and can be expressed as follows,

$$\zeta_{jt} = \begin{cases} 1 & \text{if centroid } \bar{\boldsymbol{y}}_j \in \boldsymbol{\mathcal{G}}^t \\ 0 & \text{otherwise.} \end{cases} \tag{5.1.10}$$

Let the number of validated centroids be denoted as u_k. An association matrix $\widehat{\boldsymbol{\Omega}}$ of feasible joint events is computed by applying the $1-1$ constraint to $\boldsymbol{\Omega}$, so that each cluster could have only arisen from a single target or clutter and that every target could have only produced one cluster:

$$\widehat{\boldsymbol{\Omega}} = \left[\widehat{\zeta_{jt}}\left(\boldsymbol{\theta}\right)\right], \tag{5.1.11}$$

where $\widehat{\zeta}_{jt}\left(\boldsymbol{\theta}\right) = 1$ for every cluster-track association event $\theta_{jt} \subset \boldsymbol{\theta}$ and $\widehat{\zeta}_{jt}\left(\boldsymbol{\theta}\right) = 0$ otherwise.

In order to enforce the constraint that a measurement could originate from only one target, $\sum_{t=0}^{T_k} \widehat{\zeta_{jt}}\left(\boldsymbol{\theta}\right) = 1$ should be satisfied for all j. In addition, we use a binary target detection indicator δ_t which takes care that the constraint of a target producing only one single measurement based on the joint associated events is satisfied. It is defined as $\delta_t := \sum_{j=1}^{u_k} \widehat{\zeta}_{jt}\left(\boldsymbol{\theta}\right)$ for all $t \in T_k$.

A measurement association indicator $\tau_j := \sum_{t=1}^{T_k} \widehat{\zeta}_{jt}\left(\boldsymbol{\theta}\right)$ is defined to denote that a cluster has originated from one of the T_k targets. By this definition, the unassociated clusters are thus expressed as $\Phi := \sum_{j=1}^{u_k}(1 - \tau_j)$.

From (5.1.3), the likelihood of a joint association event can be further expressed as a product of the probability of each individual centroid conditioned on association events over all past measurements individually [BSDH09][1],

$$p\left(\overline{\boldsymbol{\mathcal{Y}}}_k | \boldsymbol{\theta}_k, u_k, \overline{\boldsymbol{Y}}^{k-1}\right) = \prod_{j=1}^{u_k} p\left(\bar{\boldsymbol{y}}_j | \theta_{jt}, \overline{\boldsymbol{Y}}^{k-1}\right) \tag{5.1.12}$$

whose PDFs can be described using,

$$p\left(\overline{\boldsymbol{\mathcal{Y}}}_k|\boldsymbol{\theta}_k, u_k, \overline{\boldsymbol{Y}}^{k-1}\right) = \begin{cases} \left[\mathcal{N}\left(\bar{\boldsymbol{y}}_j; \widehat{\boldsymbol{y}}^t, \mathbf{C}_k^{\bar{\boldsymbol{y}},t}\right)\right] := f_{tj}\left(\bar{\boldsymbol{y}}_t\right) & \text{if } \tau_j = 1 \\ V^{-1} & \text{if } \tau_j = 0. \end{cases} \tag{5.1.13}$$

$\mathbf{C}_k^{\bar{\boldsymbol{y}},t}$ is obtained from (5.1.6), taking the target's extension in account. V defines the volume of the validation region and is given by [BSDH09]:

$$V = n_{\boldsymbol{y}}\left(\gamma^{n_{\boldsymbol{y}}/2}\right)\sqrt{|\mathbf{C}_k^{\bar{\boldsymbol{y}},t}|} \tag{5.1.14}$$

where $n_{\boldsymbol{y}}$ corresponds to the measurement dimension, here 2, and γ is the threshold.

The prior, as defined in (5.1.3), reflects the probability of $\boldsymbol{\Omega}$ conditioned on the validated centroids as follows,

$$p\left(\boldsymbol{\Omega}|u_k\right) = \frac{1}{a_2}\frac{\Phi!\,\mu\left(\Phi\right)}{u_k!}\prod_{t=1}^{T_k}\left(P_G P_D^t\right)^{\delta_t}\left(1 - P_G P_D^{\delta_t}\right)^{1-\delta_t} \tag{5.1.15}$$

with P_D^t being the target-specific detection probability, P_G the gating probability, and a_2 a normalisation constant. The unassociated clusters are regarded as clutter and are assumed to follow a uniform distribution defined by the Probability Mass Function (PMF) $\mu\left(\Phi\right)$. Assuming a Poisson PMF for the clutter spatial distribution with rate λ, such that

$$\mu\left(\Phi\right) = e^{-\lambda V}\frac{\left(\lambda V\right)^{\Phi}}{\Phi!}, \tag{5.1.16}$$

the posterior probability of the association event becomes [BSDH09],

$$p\left(\boldsymbol{\theta}_k|\overline{\boldsymbol{Y}}^k\right) = \frac{1}{a_3}\prod_{j=1}^{u_k}\left\{\frac{1}{\lambda}f_{t_j}\left(\bar{\boldsymbol{y}}_j\right)\right\}^{\tau_j}\prod_{t=1}^{T_k}\left(P_G P_D^t\right)^{\delta_t}\left(1 - P_G P_D^{\delta_t}\right)^{1-\delta_t}, \tag{5.1.17}$$

where a_3 is a normalisation constant.

Using relationship (3.3.15), the marginal association probabilities are used with KF equations in (3.3.10)-(3.3.13) for the target's state estimation.

5.1.4 Results

The proposed EC-JPDA approach has been applied on all the three marine radar datasets from the DLR repository. The regular JPDA has also been applied using the same initialisation values for the state (according to known AIS information or some rough estimate otherwise) and system model. The proposed method, in essence, can account for the extent of the target by considering its point cloud spread within the dispersion matrix. Normally, the JPDA-based algorithms allow target states to be modelled differently at the time of their initialisation, although for uniformity we

chose to use the same model for each one. The state equation was as in 4.1.6. The results obtained from both methods were compared based on the positional errors evaluated against AIS positions using the Euclidean distance and presented.

Clusters were determined via the simple k-means algorithm [Mac67, Boc08], where a strategy was adopted to estimate the number of clusters to be given as a parameter to the k-means algorithm at each observation step (See Chapter 2.2 as review). In the appendix B.3, we provide some examples of clustered point clouds over the trajectories of targets from the datasets.

Two gating approaches, rectangular and ellipsoidal gating were applied. The first gating broadly filtered out most of the far ranged centroids (as in some cases, the point cloud from a single target could yield more than one cluster). The refined ellipsoidal gating was then applied to those centroids that were within the rectangular gate. The centroids were then tracked by both aforementioned filters.

The overall tracking results as obtained by EC-JPDA are shown in Figure 5.2. We use the observation steps found in them as well as the ensemble error plots in Figures 5.3 and 5.4 to provide more insight in the upcoming discussion part. The same colour-code was maintained for each vessel for easy referencing.

5.1.5 Discussion

From the trajectory estimation plot, the tracks for both Targets 2 and 3 in DAAN show distinct associations and estimates for the most part. Around $k = 300$, the estimates of Target 3 are affected due to the presence of an aid-to-navigation, which is also supported by its error plot. The high error at the beginning corresponded to the measurements suffering beam spreading, smearing and poor visibility from far range with respect to the own. On the other hand, Target 2 shows high errors between approximately $k = 500$ to $k = 650$ due to the occlusion phase before picking up as soon as the target is detected again.

The estimates of Target 2 in DARC fluctuate for the first half of the trajectory, although they remain persistent over its trajectory. The fluctuations are owed to the RACON-originated measurement continuously interfering with the target-originated radar measurements that in turn affect the clustering results. Figure 5.3 again supports the observations. Around $k = 350$ onwards, we find an increase in the errors for the remaining trajectory. These could be a combined effect from two situations: the presence of an aid-to-navigation and the perspective of the vessel as seen from the dynamic own.

Additionally, the error can be expected to be higher due to the vessel size (Target 2 in DAAN is 129m $\times$ 23m and the one in DARC 180m $\times$ 29m) and the location at which the AIS transponder would be mounted on the vessel, as mentioned in the thesis already. As we expect that the position of the vessel is dominated by the vessel's centre, the mount location-to-centre discrepancy increases the larger a vessel is.

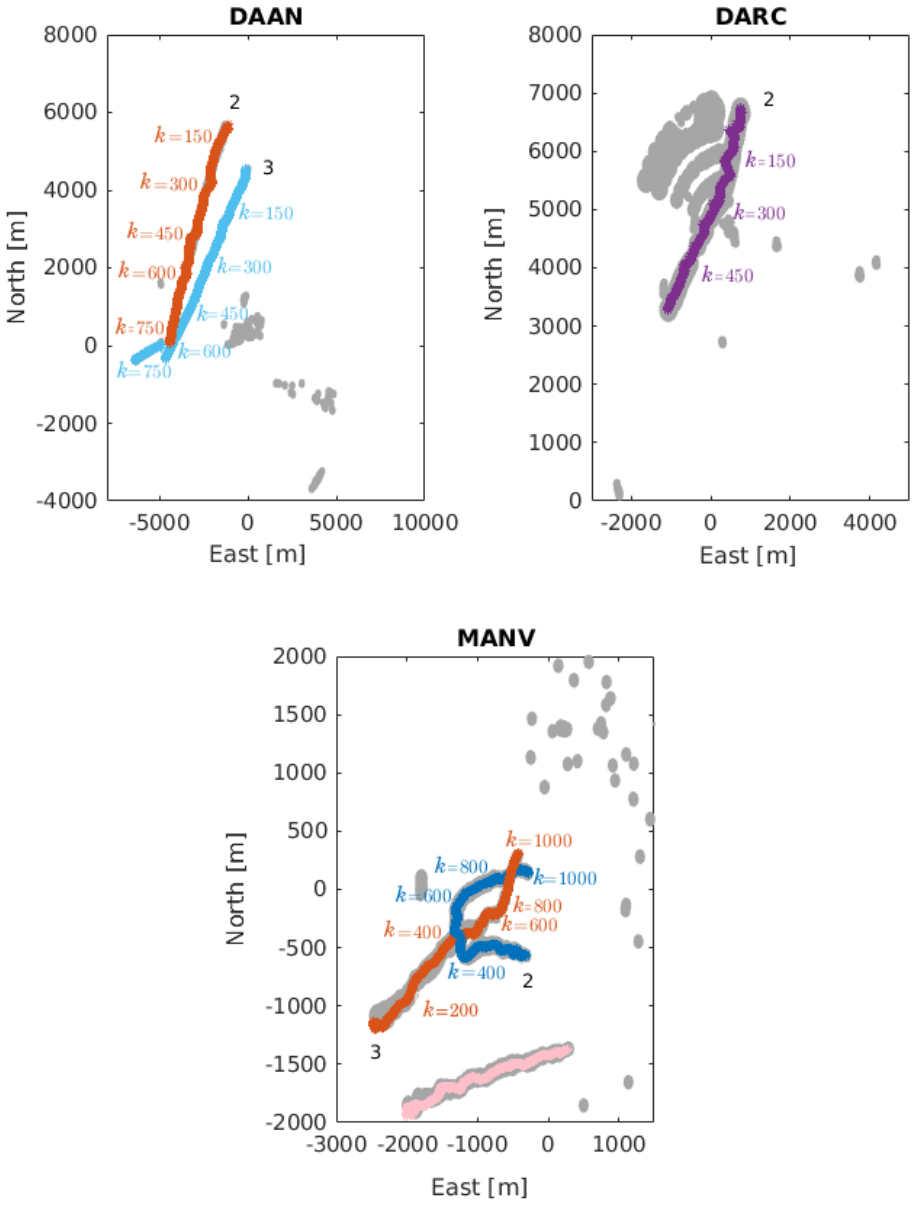

Figure 5.2: Estimates (non-grey coloured points) obtained from EC-JPDA plotted on top of radar measurements (grey point clouds) for each dataset. The tracks are numbered, and the observation steps k are included over their respective trajectories. Image adapted from [1] ©2021MDPI.

Figure 5.3: Positional errors for DAAN and DARC over time. Images adapted from [1] ©2021MDPI.

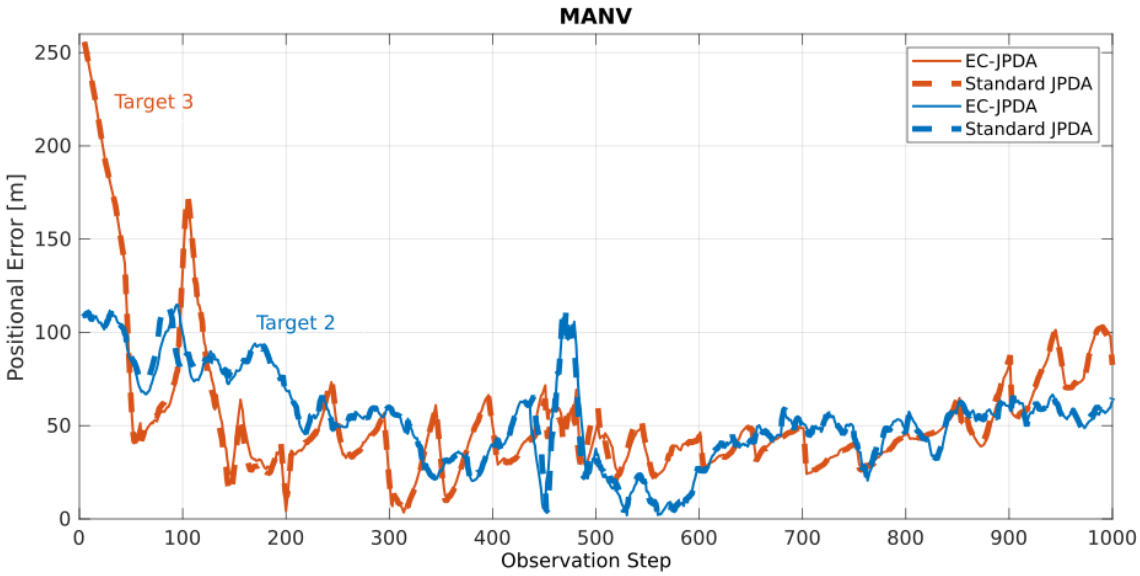

Figure 5.4: Positional errors for MANV. Image adapted from [1] ©2021MDPI.

In MANV, the estimated tracks are distinct and clear, including the track of the unknown vessel (which had also been initiated). Its overall positional errors are relatively lower than for the other two datasets due to its better resolution. Some fluctuations can still be observed due to the target's fast manoeuvres over time. From Figure 5.4, the higher peaks in the beginning correspond to the vessel's poor visibility from afar, similar to the previous case. Between $k = 450$ to $k = 500$, around their intersection/crossing, the associations for Target 2 were mixed up and then improved as the vessels navigated away from each other. Towards the end, Target 3 was partially occluded due to Target 2, hence the higher errors.

When relating the results of the proposed approach to the standard JPDA, one can observe comparable performances for MANV and Target 3 in DAAN from a wider perspective. For DARC, a clear improvement over most of its trajectory can be noticed, and an improvement for Target 2 in DAAN in the first half of its trajectory (in poor visibility and some occlusion situations). DARC is a very challenging dataset because of the constant RACON interferences. In this case, using the dispersion matrix in EC-JPDA to account for the vessel's measurement spread, and intuitively its extents, proves to provide more accurate results and robust performance in persistent interferences. The results also support our statement about a correlation between vessel size and gain of accuracy as the results for smaller vessels are comparable but are only different with large vessels.

Besides the resolution-related effect, some limitation lies in the basic k-means clustering approach: it tends to favour spherical clusters and ends up with at least 2 clusters for a single elongated point cloud. In addition, the cluster evaluation method does not guarantee that we have the right number of clusters (See Appendix B.3 for instance). In the next endeavour, our framework shall

be adapted based on other clustering approaches (e.g. the Density-based Spatial Clustering of Applications with Noise (DBSCAN)).

5.2 Multi-Sensor Multi Extended Target Tracking

This section is an amalgamation of the cumulative findings and the previous methods for achieving the final objective of having a multi-sensor (MS) tracking system for MTSAM. We integrate the elliptical model-based PAKF with the EC-JPDA filter to track the extended states of multiple vessels over a specific observation region from ASTERIX input. The detections and sensor resolution from the ASTERIX streams can be expected to be much finer in comparison to those from the standard on board radars, where a pixel could be almost 1.1m in the streams. This changes the spatial distribution of the point clouds, that would now be less noisy and would be more elongated instead of spherical. We can also expect the number of measurements to be even higher. Nonetheless, we could still expect to face perspective limitations. We demonstrate two examples in Figure 5.5 where a more detailed and complete view of the underlying target's extent within a real-world scenario captured from random instances of the stream is shown. If we were to estimate the extent parameters of the target using only the orange point clouds of one sensor, it would be unlikely that the estimates would reflect the vessel's surface itself as the reflections are more prominent on the visible side. When combined with the blue teal point clouds of the other sensor, however, we could expect to have a more unbiased view in this case, being our core motivation in this section.

Therefore, the prime idea is to apply the proposed PAKF-JPDA tracker in a sequential MS update scheme centrally within our demonstrator system. We note that testing out more complex MS architectures or topologies is out of scope of the thesis. Our basis is now the processing chain defined in Chapter 2 to process all measurements at discrete steps observed from ground radar stations strategically located at a harbour. A few changes have been made to boost the tracker with an automatic track management scheme that takes care of track initiations and deletions. In contrast to the previous section, we employ a different clustering approach, the DBSCAN [EKSX96], to account for the non-spherical, arbitrary nature of most point clouds. These are explained next and the final results are then included in this section with some discussion.

It is highlighted that, unlike the format from the previous sections bearing contributions, this one follows a slightly different style with more focus on individual interacting components from our proposed processing chain for the demonstrator.

5.2.1 Related Work

We consider the concepts and applications for elliptical METT based on DA. For an in-depth review, a thorough explanation on METT approaches is provided in the recent compilation from [GB22]. Several measurement-track schemes have been mentioned in literature, the $1-1$, $m-1$ (cluster set-track), or even $m-n$ [Bau15]. Based on the association scheme in use, several methods have been developed, each targeting some specific scheme. For instance, in an MEM-EKF* implementation [YTB18, YWB20][3], multiple individual measurements are associated to a single target and the work [YWB20] proposed a JPDA extension to aid track management via existence

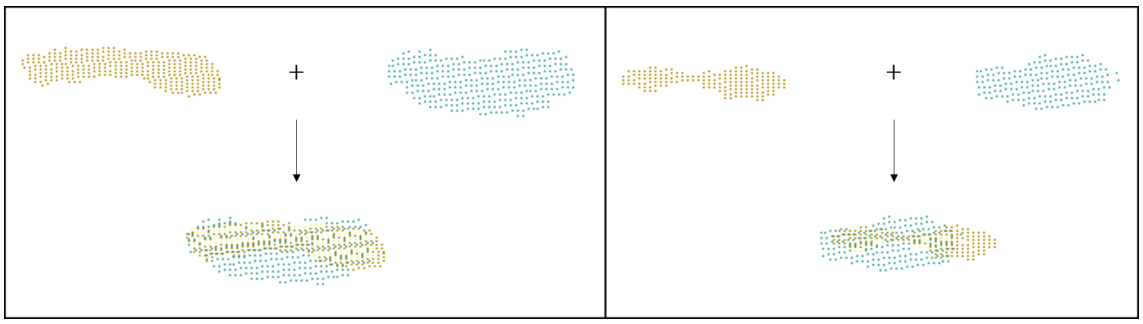

Figure 5.5: The left and right plots are of two different targets captured at different observation steps by two radar sensors. On the first row, the individual sensor point cloud measurements are provided in orange and teal blue. The orange yielding sensor is found in the North-East and the other around North-West directions. On the second row, point clouds from both sensors are plotted together. Overlapping measurements have a yellowish-green tone.

probabilities, also known as the Joint Integrated Probabilistic Data Association (JIPDA) [CMME11, ME04]. The JIPDA method has been exploited by the RMM [SRW15] for tracking targets from the marine radar. The RMM has also been integrated in the probabilistic multi-hypothesis tracker for addressing the elliptical METT problem [WK10]. A JPDA filter took in measurements from a maximum likelihood detector and clustering approach applied to marine radar data in the work of Vivone *et al.* [VB16]. Instead of using existence probabilities for track management, the M/N (measurements/observation steps) logic was also applied [BSWT11].

Under strategically located MS systems, one could ensure a more comprehensive traffic view as discussed above. Several approaches exist for fusing their data under the RMM framework that was developed for and applied in the maritime context [VGBW16, VGBW17]. Alternatively, a specialised elliptical fusion approach has been proposed to fuse explicitly parameterised ellipses based on the random ellipse density and a GW distance approximation [TB21a].

5.2.2 Problem Description

At observation step k, the multi(extended)-target state $\boldsymbol{\mathcal{X}}_k$ is defined as the set of T_k individual extended target (vessel) states given by

$$\boldsymbol{\mathcal{X}}_k = \left\{\boldsymbol{x}_k^t\right\}_{t=1}^{T_k}. \tag{5.2.1}$$

Each individual target state $\boldsymbol{x}_k$ is modelled by virtue of its kinematic properties $\mathbf{r}_k$ and elliptical-extent parameter vector $\mathbf{p}_k$ that are in turn modelled separately as in the following (omitting target superscript indices t for readability),

$$\boldsymbol{x}_k = \left[\mathbf{r}_k^T, \mathbf{p}_k^T\right]^T, \tag{5.2.2}$$

with the parameters of interest expressed as,

$$\begin{aligned} \mathbf{r}_k &= \left[\boldsymbol{m}_k^T, \dot{\boldsymbol{m}}_k^T\right]^T, \\ \mathbf{p}_k &= \left[\alpha_k, \ell_{1,k}, \ell_{2,k}\right]^T, \end{aligned} \tag{5.2.3}$$

where $\boldsymbol{m}_k$ is the position vector in ENU coordinates, and $\dot{\boldsymbol{m}}_k$ the velocity vector. The vessel is orientated at α_k with length and width related to semi-axes $\ell_{1,k}$ and $\ell_{2,k}$.

The observation region is covered by S sensors, where each sensor generates a set of point cloud measurements defined by c_k centroids, matching the description in the first part of the chapter, $\overline{\boldsymbol{\mathcal{Y}}}_k^s = \{\boldsymbol{y}_k^{s,1}, ..., \boldsymbol{y}_k^{s,c_k}\}_{s=1}^S$ that are assumed to have come from potential targets within the region. Let the set $\overline{\boldsymbol{\mathcal{Y}}}_{k-1}^S$ denotes the multi-sensor measurements sequentially combined and accumulated until the previous observation step $0:k-1$ over sensors $s=1:S$.

We would like to estimate the posterior of the multi-target state conditioned on our measurements, which can be expressed based on Bayes formula in a similar context as in (3.1.1) as follows,

$$p\left(\boldsymbol{\mathcal{X}}_k|\overline{\boldsymbol{\mathcal{Y}}}_k^S\right) \propto \prod_{s=1}^{S}\prod_{t=1}^{T_k} p\left(\overline{\boldsymbol{\mathcal{Y}}}_k^s|\boldsymbol{x}_k^t\right) p\left(\boldsymbol{x}_{k-1}^t|\overline{\boldsymbol{\mathcal{Y}}}_{k-1}^S\right), \tag{5.2.4}$$

where the likelihood PDF is given by $p\left(\overline{\boldsymbol{\mathcal{Y}}}_k^s|\boldsymbol{x}_k^t\right)$ and the prior state PDF by $p\left(\boldsymbol{x}_{k-1}^t|\overline{\boldsymbol{\mathcal{Y}}}_{k-1}^s\right)$.

The prediction of a target state can be expressed as an integral of the form,

$$p\left(\boldsymbol{x}_k^t|\overline{\boldsymbol{\mathcal{Y}}}_{k-1}^S\right) = \int p\left(\boldsymbol{x}_k^t|\boldsymbol{x}_{k-1}^t\right) p\left(\boldsymbol{x}_{k-1}^t|\overline{\boldsymbol{\mathcal{Y}}}_{k-1}^s\right) d\boldsymbol{x}_{k-1}, \tag{5.2.5}$$

with target state transition PDF $p\left(\boldsymbol{x}_k^t|\boldsymbol{x}_{k-1}^t\right)$.

The individual target state $p\left(\boldsymbol{x}_k^t\right)$ is the approximation of the posterior by the marginal association probabilities β_{jt}^s, that is the probability that cluster centroid j from sensor s, denoted by $\bar{\boldsymbol{y}}_k^{s,j}$, has been assigned to track t,

$$p\left(\boldsymbol{x}_k^t\right) \approx \sum_{j=1}^{c_k} \beta_{jt}^s\, p\left(\boldsymbol{x}_k^t|\bar{\boldsymbol{y}}_k^{s,j}\right). \tag{5.2.6}$$

Under a typical setting (e.g. see Figure 5.6), having knowledge of the number of vessels that are present and those that have been detected is challenging, given that all measurements are unassociated at first. We are also interested in an elliptical approximation of the individual targets, for which the integration of an elliptical model within an association scheme is vital. As the traffic in the observation region is dynamic, the number of vessels change over time and requires tracks to be initiated and terminated accordingly. For instance, the unassociated point cloud in Figure 5.6 could belong to either clutter or a target, and would generally require successive steps for that to be determined. Thus, an METT solution comprises solving the problems of track management,

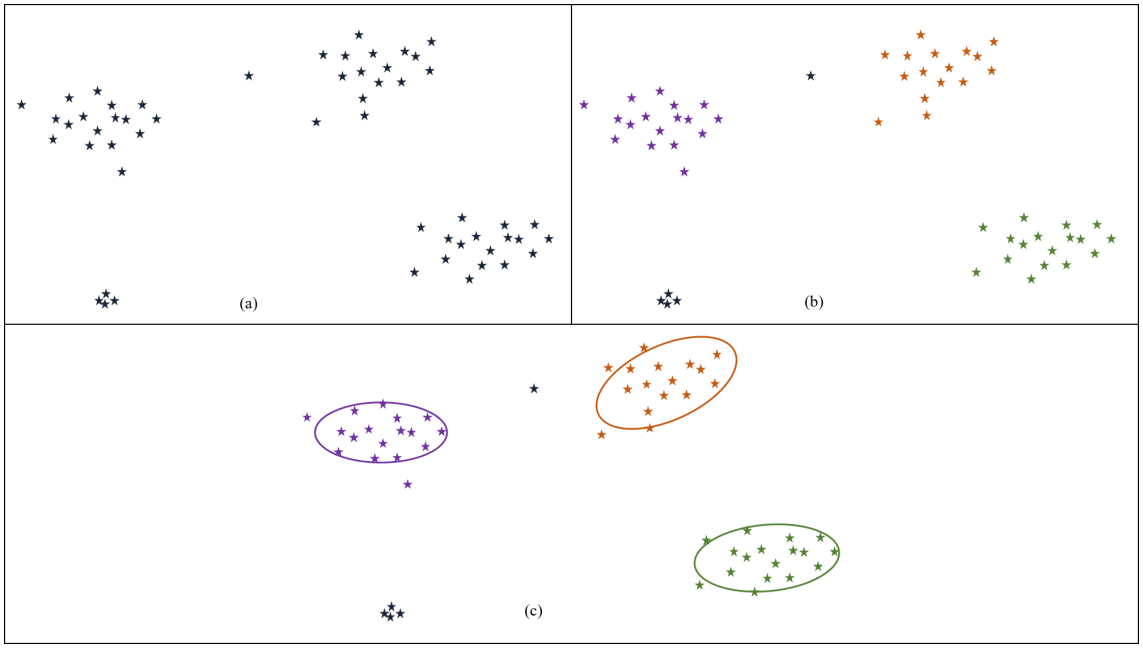

Figure 5.6: The METT problem simplified at a glance. (a) Unassociated set of point cloud measurements (black). (b) The potential associations are assigned different colours, and everything else that are considered as clutter stay black. (c) Elliptical extent estimates based on the association.

DA and elliptical extent estimation efficiently as a whole in a MS setting.

5.2.3 The PAKF-based EC-JPDA Approach

We refer to the processing chain described in Chapter 2.1. The *raw* measurements are the detections from the sensor that are first decoded, and registered onto a common Cartesian frame with a known reference location. The measurements are then processed sensor-wise, the initial step being clustering, followed by cluster-to-track assignment whereby marginal association probabilities are calculated and then state estimation is carried out by the filter. The kinematic state of a target is assumed to bear no correlation to the extent parameter vector, and the assumptions that applied for the PAKF and EC-JPDA are maintained. The flowchart in Figure 5.7 shows an overall flow of the filtering logic for PAKF-JPDA. Note that the value of T_k is updated by the track management function at every k.

Clustering

Clustering is an important step to ensure that measurement set $\boldsymbol{\mathcal{Y}}_k$ has been partitioned to improve the overall data processing. The clusters' centroids and their respective cluster members are taken as the input parameters to our proposed filter. DBSCAN has proven to be an effective method in terms of both computational efficiency and its ability at recognising arbitrarily-shaped clusters,

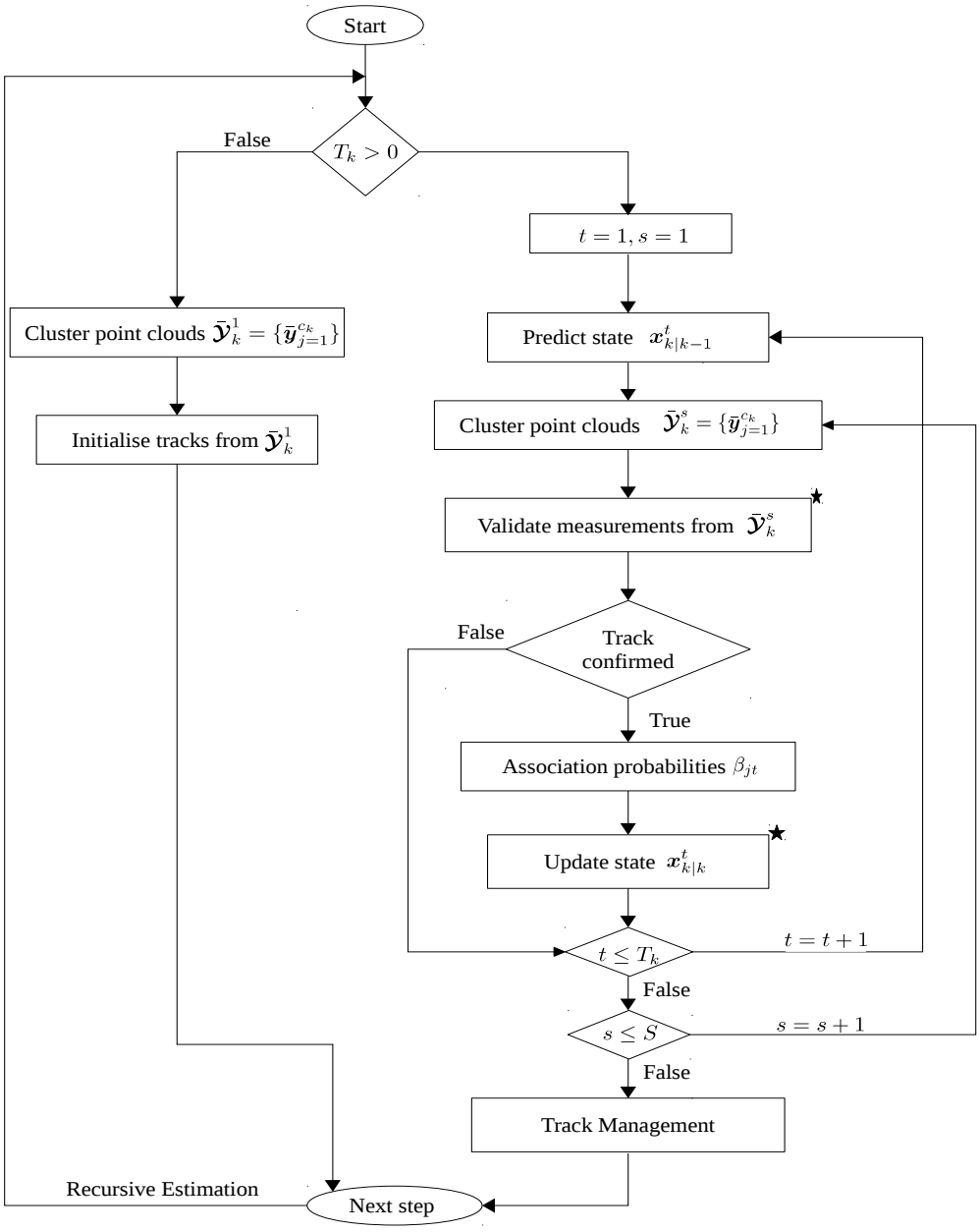

Figure 5.7: Flowchart for MS-METT.

justifying our choice. The DBSCAN relies on two parameters for its cluster search. The first one is used to define a specific neighbourhood, based on which a point can reach the next one belonging to the same cluster, and the second parameter defines the minimum of points that are needed to form a cluster [EKSX96].

As we consider a sequential sensor processing approach, we refer to the measurement set from sensor s as $\boldsymbol{\mathcal{Y}}_k^s$. After the measurement partitioning step, the dispersion matrix $\mathbf{C}_k^{D,j}$ corresponding to each centroid over $j = 1 : c_k$ in $\overline{\boldsymbol{\mathcal{Y}}}_k^s$ is calculated.

The spread of a cluster having centroid $\bar{\boldsymbol{y}}_k^{\mathbf{r},j}$ is derived based all its cluster members as follows (omitting index s),

$$\mathbf{C}_k^{D,j} = \frac{1}{d_k - 1} \sum_{i=1}^{d_k} \left(\boldsymbol{y}_k^{ji} - \bar{\boldsymbol{y}}_k^{\mathbf{r},j} \right) \left(\boldsymbol{y}_k^{ji} - \bar{\boldsymbol{y}}_k^{\mathbf{r},j} \right)^T \tag{5.2.7}$$

so that $\boldsymbol{y}_k^{ji}$ denotes index of i^{th} measurement belonging to cluster j and d_k is the number of measurements (members) within the cluster.

To distinguish between the measurements required for updating the kinematic state and extent parameter vector, we introduce superscripts $\mathbf{r}$ and $\mathbf{p}$. Thus, $\bar{\boldsymbol{y}}_k^{\mathbf{r}}$ is a two-dimensional Cartesian measurement vector employed for the kinematic update, while $\boldsymbol{y}_k^{\mathbf{p}}$ is a three-dimensional measurement vector employed for updating the extent parameters.

Gating

The gating scheme adopted is a marginally modified version from the adaptive gating in subsection 5.1.3. In the current one, once a centroid has been validated, its corresponding dispersion matrix calculated from (5.2.7) is taken directly to be used in the calculation of association probabilities and the adaptive gating in the next step.

State Estimation

Algorithm 1 outlines the DA and the updating procedures at a single observation step within the tracking framework. The specific equations that are employed have been referenced at every procedure for reviewing convenience. Note that in the first initialisation step, we use the sensor with the most extensive coverage for initialising targets. After that, any unassigned measurement, regardless of the sensor, will form the basis to initialise a new track to be considered for the next observation step. The target state is updated sequentially sensor-wise, and its prediction reflects a step-wise transition. As mentioned before, marginal association probabilities are computed based on the validated measurements $\bar{\boldsymbol{y}}_k^{\mathbf{r}}$ and are used for updating the kinematic state of the targets. The dispersion matrix of the cluster that has been associated to a specific target is used for obtaining the measurement vector $\boldsymbol{y}_k^{\mathbf{p}}$ for updating the extent parameters. The sensor-wise measurement noise uncertainty is denoted using $\mathbf{C}_{\mathbf{r}}^{\boldsymbol{v},s}$ and $\mathbf{C}_{\mathbf{p}}^{\boldsymbol{v},s}$.

Algorithm 1: Outline of PAKF-JPDA procedures at step k

Data:
- Measurement set $\mathcal{Y}_k^s$ from all $s \in S$
- Extended state ensemble $\hat{\mathbf{r}}_{k-1|k-1}^t$, $\hat{\mathbf{p}}_{k-1|k-1}^t$ for each track $t \in T_k$ ($T_k \neq \emptyset$)
- State covariances $\mathbf{C}_{k-1|k-1}^{\mathbf{r},t}$ and $\mathbf{C}_{k-1|k-1}^{\mathbf{p},t}$

Result: Estimates $\hat{\mathbf{r}}_k^t$, $\hat{\mathbf{p}}_k^t$, and their covariances $\mathbf{C}_k^{\mathbf{r},t}$ and $\mathbf{C}_k^{\mathbf{p},t}$

for *each track* t **do**

  Kinematic state prediction (from A.1)

  $\left[\hat{\mathbf{r}}_{k|k-1}^t, \mathbf{C}_{k|k-1}^{\mathbf{r},t}\right]$ = KF_kin_update$\left(\hat{\mathbf{r}}_{k-1|k-1}^t, \mathbf{C}_{k-1|k-1}^{\mathbf{r},t}, \mathbf{F}_{\mathbf{r}}, \mathbf{C}_{\mathbf{r}}^{\boldsymbol{\omega}}\right)$

  Extent parameter vector state prediction (from 4.1.17)

  $\left[\hat{\mathbf{p}}_{k|k-1}^t, \mathbf{C}_{k|k-1}^{\mathbf{p},t}\right]$ = KF_ext_update$\left(\hat{\mathbf{p}}_{k-1|k-1}^t, \mathbf{C}_{k-1|k-1}^{\mathbf{p},t}, \mathbf{F}_{\mathbf{p}}, \mathbf{C}_{\mathbf{p}}^{\boldsymbol{\omega}}\right)$

  for *each sensor* s **do**

    Cluster measurement set using DBSCAN

    $\left[\overline{\mathcal{Y}}_k^s, \{\mathbf{C}_k^{D,j}\}_{j=1}^{c_k}\right]$ = cluster_measurements$(\mathcal{Y}_k^s)$

    Measurement validation (from 5.1.5)

    $\left[\bar{\boldsymbol{y}}_j^{\mathbf{r}}\right]$ = validate_measurements $\left(\overline{\mathcal{Y}}_k^s, \hat{\mathbf{r}}_{k|k-1}^t, \mathbf{C}_{k|k-1}^{\mathbf{r},t}, \mathbf{H}_{\mathbf{r}}, \mathbf{C}_{\mathbf{r}}^{\boldsymbol{\upsilon},s}, \mathbf{C}_{k-1}^{D,j}\right)$

    Measurement likelihood over each measurement j (from 5.1.13)

    $\left[\{f_{tj}(\bar{\boldsymbol{y}}_j^{\mathbf{r}})\}_{j=1}^{c_k}\right]$ = pdf$\left(\{\bar{\boldsymbol{y}}_j^{\mathbf{r}}\}_{j=1}^{c_k}, \hat{\mathbf{r}}_{k|k-1}^t, \mathbf{C}_{k|k-1}^{\mathbf{r},t}, \mathbf{H}_{\mathbf{r}}, \mathbf{C}_k^{\bar{\boldsymbol{y}},t}\right)$

    if t *is confirmed* **then**

      Association probabilities (from 5.1.17)

      $\left[\{\beta_{jt}\}_{j=0}^{c_k}\right]$ = compute_marg_assoc_prob$\left(\{f_{tj}(\bar{\boldsymbol{y}}_j^{\mathbf{r}}\}_{j=1}^{c_k}, P_D^s, \lambda\right)$

      Kinematic State Update (3.3.10 to 3.3.13)

      $\left[\hat{\mathbf{r}}_{k|k}^t, \mathbf{C}_{k|k}^{\mathbf{r},t}\right]$ = state_update$\left(\hat{\mathbf{r}}_{k|k-1}^t, \mathbf{C}_{k|k-1}^{\mathbf{r},t}, \{\bar{\boldsymbol{y}}_j^{\mathbf{r}}\}_{j=1}^{c_k}, \{\beta_{jt}\}_{j=0}^{c_k}, \mathbf{C}_k^{\bar{\boldsymbol{y}},t}\right)$

      Extract elliptical measurements through EVD (from 4.5)

      $\boldsymbol{y}_j^{\mathbf{p}}$ = get_elliptical_measurements$\left(\mathbf{C}_k^{D,j}, \mathbf{C}_{\mathbf{r}}^{\boldsymbol{\upsilon},s}\right)$

      Extent parameter vector update (3.3.10 to 3.3.13 by adjusting parameters for $\mathbf{p}$)

      $\left[\hat{\mathbf{p}}_{k|k}^t, \mathbf{C}_{k|k}^{\mathbf{p},t}\right]$ = extent_update$\left(\hat{\mathbf{p}}_{k|k-1}^t, \mathbf{C}_{k|k-1}^{\mathbf{p},t}, \boldsymbol{y}_j^{\mathbf{p}}, \{\beta_{jt}\}_{j=0}^{c_k}, \mathbf{H}_{\mathbf{p}}, \mathbf{C}_{\mathbf{p}}^{\boldsymbol{\upsilon},s}\right)$

  Output estimates:
  - Estimates $\hat{\mathbf{r}}_k^t$ and $\hat{\mathbf{p}}_k^t$
  - Covariances $\mathbf{C}_k^{\mathbf{r},t}$ and $\mathbf{C}_k^{\mathbf{p},t}$

Track Management

One of the most important step to maintain a smooth filtering operation is by employing an automated track management function, included in Figure 5.7. In principle, it is responsible for track initiation (both when there are existing tracks and not) as well as track termination. Appropriate counters are implemented to account for the validation and update phases (marked by a star in the flowchart). The track management core processes are explained as follows:

1. Track Initialisation
   A potential track is initialised based on the first detection at the beginning of the observation altogether. For the demonstrator, we used the detection(s) from one sensor that is believed to be more likely to detect vessels on the expected and common routes within the region of interest due to its vantage location.

   Other than initialisation at $k = 1$, the measurements that have been left without any association are monitored at every step and used to initialise a potential track.

2. Track Confirmation
   The potential track is confirmed as soon as it has had one measurement continuously validated (M) times over some specific number of observation steps (N), otherwise the track is discarded. Confirmed tracks are updated according to our association and filtering schemes.

3. Track Merging
   At every k, the tracks are checked for correlation with other tracks. For some *acceptable* (based on the traffic and measurement quality over the region) track-to-track correlation threshold, the tracks are merged to eliminate any duplication. Two tracks can be compared by carrying out a track-to-track correlation test.

   Given the kinematic states of two tracks $\mathbf{r}_k^1$ and $\mathbf{r}_k^2$ and their covariances $\mathbf{C}_k^{\mathbf{r},1}$ and $\mathbf{C}_k^{\mathbf{r},2}$, a correlation quantity Λ is computed using the following,

$$\Lambda = \left(\hat{\mathbf{r}}_k^1 - \hat{\mathbf{r}}_k^2\right)^T \left(\mathbf{C}_k^{\mathbf{r},12}\right)^{-1} \left(\hat{\mathbf{r}}_k^1 - \hat{\mathbf{r}}_k^2\right) \tag{5.2.8}$$

   where the cross covariance matrix $\mathbf{C}_k^{\mathbf{r},12} = \mathbf{C}_k^{\mathbf{r},1} + \mathbf{C}_k^{\mathbf{r},2}$. Λ is then compared to a merging threshold γ_t so that the hypothesis that the two tracks are likely to have come from the same source is confirmed if $\Lambda < \gamma_t$. The threshold value has a $\chi^2_{n_\mathbf{r}}$ PDF where $n_\mathbf{r}$ is the dimension of the state vector.

   The correlated tracks can then be merged based on the basic fusion approach from [SK71],

$$\begin{aligned} \hat{\mathbf{r}}_k &= \mathbf{C}_k^{\mathbf{r},2}\left[\mathbf{C}_k^{\mathbf{r},1} + \mathbf{C}_k^{\mathbf{r},2}\right]^{-1} \hat{\mathbf{r}}_k^1 + \mathbf{C}_k^{\mathbf{r},1}\left[\mathbf{C}_k^{\mathbf{r},1} + \mathbf{C}_k^{\mathbf{r},2}\right]^{-1} \hat{\mathbf{r}}_k^2 \\ \mathbf{C}_k^{\mathbf{r}} &= \mathbf{C}_k^{\mathbf{r},1}\left[\mathbf{C}_k^{\mathbf{r},1} + \mathbf{C}_k^{\mathbf{r},2}\right]^{-1} + \mathbf{C}_k^{\mathbf{r},2}. \end{aligned} \tag{5.2.9}$$

The above computations are quite extensive and could slow down the processing especially if a high number of targets are present (for example, more than 10). In this situation, the demonstrator can switch to another approach which is programmed to terminate the more recent track and instead retain the older track.

4. Track Termination
   A confirmed track is terminated in case there were no validated measurements for some consecutive observation steps given by M^-/N^-.

The track management function also assigns an unique identification or label to the tracks at the moment of initialisation.

5.2.4 Results

In this subsection, we present the sensor set-up, details pertaining to specific parameters of the algorithms employed and the captured images of the final results at random observation steps to demonstrate the working framework. For security reasons, the date and time of the recording as well as the true coordinates of the reference system are not mentioned.

Sensor Set-Up

The observation region of interest is an area around the port of Hamburg. The sensors are cooperating ground-based radar stations in strategic locations providing data over the region. In all, there are three main sensors with dominant views in the North-East (Sensor 1), North-West (Sensor 2) and South-West (Sensor 3) directions that have been considered. They have all been registered with a common reference point in a local ENU coordinate system.

Based on our familiarity with the setting and data being streamed, it is believed that Sensor 1 and Sensor 2 have a comparatively larger coverage than Sensor 3 for the most part. Sensor 1 was assigned the highest target detection probability, and was thus used to initialise the targets at the beginning.

Parameters and State Initialisation

The parameters of DBSCAN were determined based on a trial and error basis to obtain the duo that works well without any over- or under-fitting. The eps value was set to 20 and minimum number of samples to form a cluster set to 50.

The NCV model was assumed as a standard system model for all targets, with sampling interval T set to 2.5s. The kinematic state was initialised using the centroid position. The extent parameter vector followed the linear time propagation model described in (4.1.17). The parameter settings and descriptions are provided in Table 5.1.

Table 5.1: Parameter Settings

Parameter	Value	Description
eps	20	DBSCAN eps value
$min\_samples$	50	DBSCAN minimum number of samples
$\mathbf{C}_0^{\mathbf{r}}$	$\mathrm{diag}(2^2, 2^2, 3^2, 3^2)$	Initial kinematic state covariance
$\mathbf{C}_0^{\mathbf{p}}$	$\mathrm{diag}(0.25^2, 1^2, 1^2)$	Initial extension vector covariance
$\mathbf{C}_{\mathbf{r}}^{\boldsymbol{\omega}}$	$\mathrm{diag}(20^2, 20^2, 0.2^2, 0.2^2)$	Kinematic state process noise
$\mathbf{C}_{\mathbf{p}}^{\boldsymbol{\omega}}$	$\mathrm{diag}(0.5^2, 0.2^2, 0.1^2)$	Extension vector process noise
$\mathbf{C}_{\mathbf{r}}^{\boldsymbol{\upsilon},1}$	$\mathrm{diag}(2^2, 2^2)$	Sensor 1 measurement noise
$\mathbf{C}_{\mathbf{r}}^{\boldsymbol{\upsilon},2}$	$\mathrm{diag}(3^2, 3^2)$	Sensor 2 measurement noise
$\mathbf{C}_{\mathbf{r}}^{\boldsymbol{\upsilon},3}$	$\mathrm{diag}(6^2, 6^2)$	Sensor 3 measurement noise
$\mathbf{C}_{\mathbf{p}}^{\boldsymbol{\upsilon}}$	$\mathrm{diag}(20^2, 20^2, 0.2^2, 0.2^2)$	Extension measurement noise
P_D	$0.95, 0.85, 0.85$	Detection probabilities for Sensors 1-3
P_G	0.99	Gating probability
λ	3.00	Clutter rate
c_g	4	Rectangular gate threshold
γ	9.21	Ellipsoidal gate threshold
M/N	$5/6$	Confirmation condition
M^-/N^-	$4/4$	Termination condition
γ_t	5	Threshold for track correlation

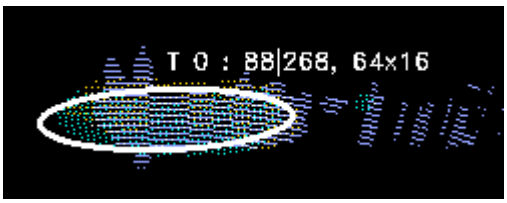

Figure 5.8: Magnified image of an exemplar elliptical estimate overlaid over the MS detections. The estimated parameters are printed in the format explained in (5.2.10).

Illustrations

Random images with the tracking results are shown in the following figures. The stream occurs in a dark background setting, with detections from Sensor 1 given in orange Sensor 2 in teal blue and Sensor 3 in magenta. A magnified version is shown in Figure 5.8. Overlapping detections often give a yellowish-green hue. The estimates are printed over the detections based on the format below:

$$T\# : \underbrace{\alpha_k^t | \tilde{\alpha}_k^t}_{\text{heading}}, \underbrace{2\ell_{1,k}^t \times 2\ell_{2,k}^t}_{\text{length}\times\text{width}}, \tag{5.2.10}$$

where

- the number in $T\#$ is the step at which the target got initialised,
- the headings given in $\alpha_k^t | \tilde{\alpha}_k^t$ are printed so that if the target follows a trajectory from West to East, its heading is given by α_k^t, and in the opposite case, the heading is given by $\tilde{\alpha}_k^t = \alpha_k^t + \pi$.
- $2\ell_{1,k}^t \times 2\ell_{2,k}^t$ represent the length and width, respectively.

We next provide the tracking results of all three sensors and then of two sensors, Sensor 1 and Sensor 2 as Sensor 3 would give rise to much clutter and radar backscattering effects. The discussion is carried out in the next subsection.

5.2.5 Discussion

For the record, while we target live monitoring for MTSAM, we have used a live-recorded stream from the three sensors with permission of the Hamburg Port Authority in this thesis. This helped us to present results by varying the number of sensors over the same situation. Due to the lack of any reference, we are unable to provide exact evaluations but we focus on the tracking results with respect to the situations.

In the first case, we consider all three sensors. The plots in Figures 5.9 and 5.10 show the estimates at some random observation steps. Specific outlines of the harbour from each sensor are visible, together with some docked vessels (e.g. the horizontal dominant orange detections to the right). The aids to navigation in the observation region have been masked, and are thus not estimated as

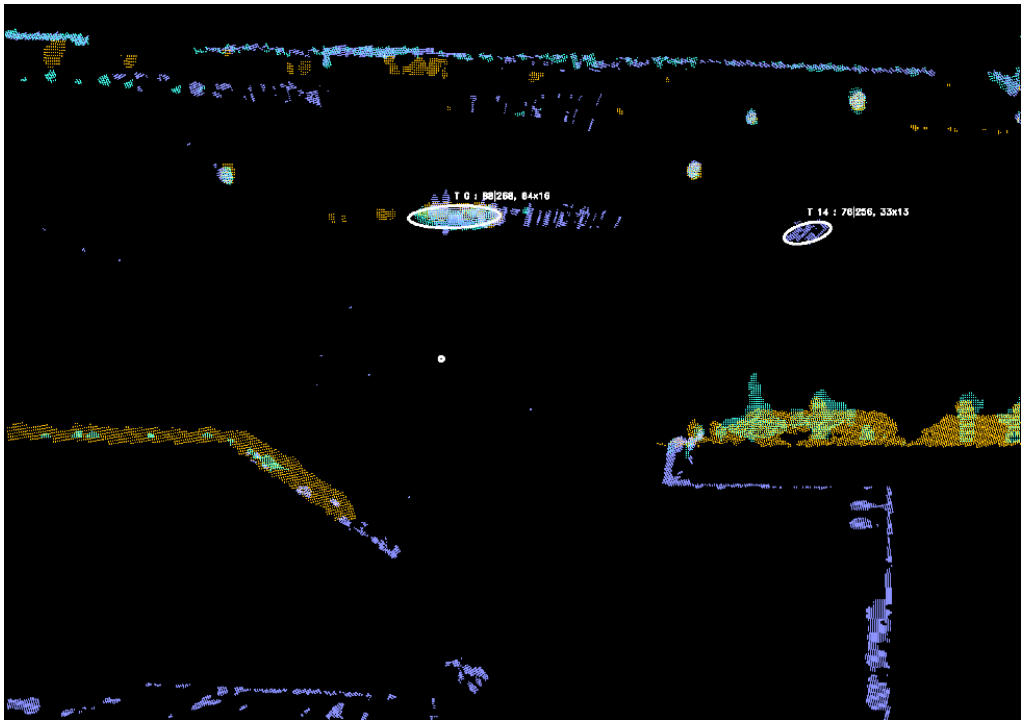

(a) Estimates from one vessel and a ghost vessel in the East (result of radar reflections).

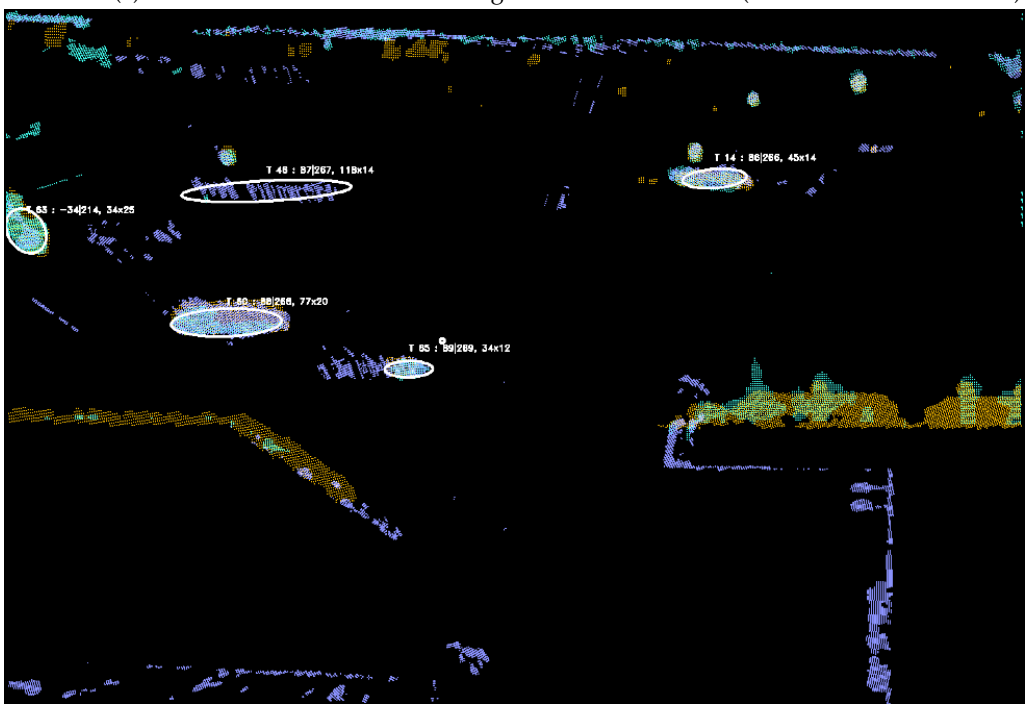

(b) Estimates from four vessels and another ghost vessel (inner North West from centre).

Figure 5.9: Estimates of PAKF-JPDA with three sensors. [Sensor 1: Orange, Sensor 2: Teal, Sensor 3: Magenta]

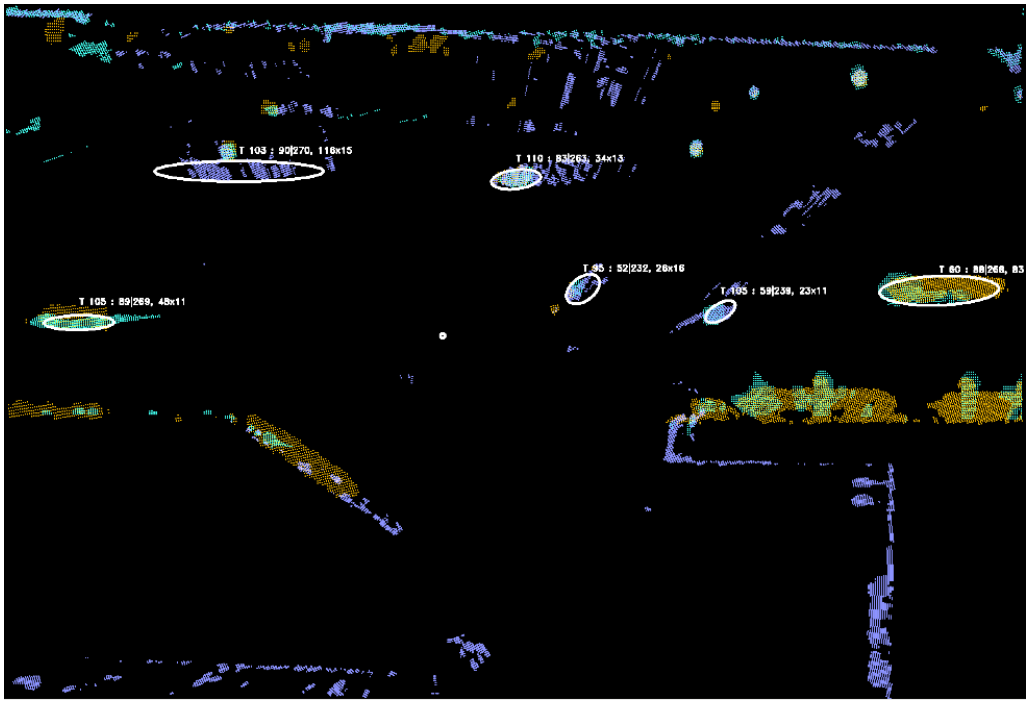

(a) Estimates from four vessels and a ghost vessel (inner North West from centre).

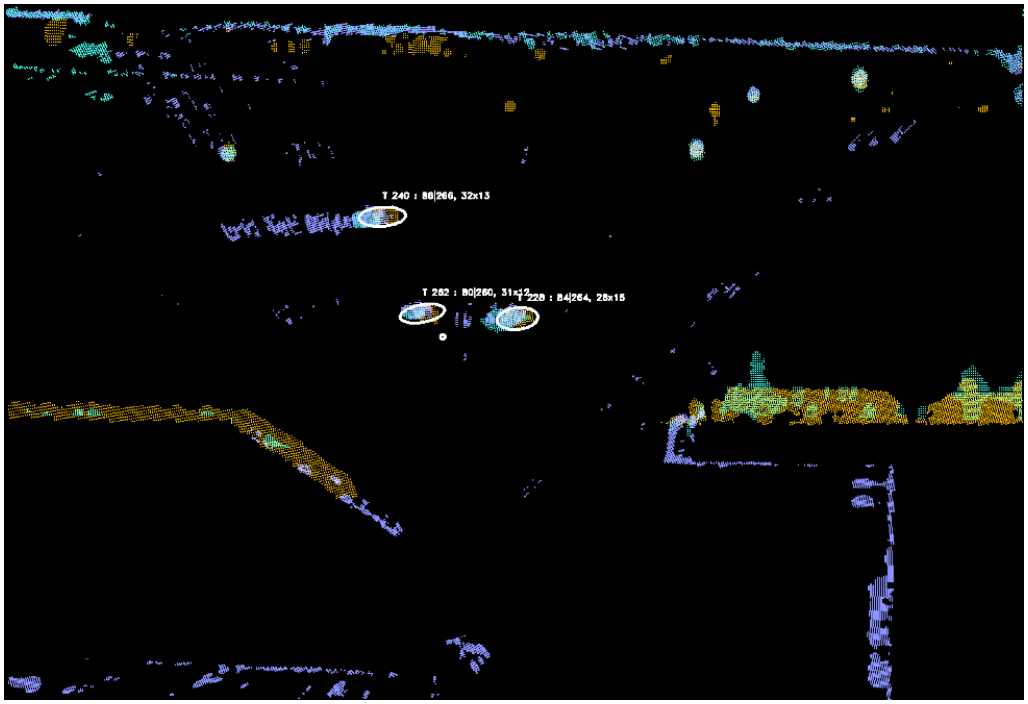

(b) Estimates from three vessels. Notice the radar reflections the water trail of the upper target.

Figure 5.10: Estimates of PAKF-JPDA with three sensors. [Sensor 1: Orange, Sensor 2: Teal, Sensor 3: Magenta]

targets. The extended states so far seem to be able to represent the full underlying vessels covered from the different perspectives.

We can also observe clutter and radar scattering occasionally occurring within the region, where Sensor 3 suffers comparatively more from those compared to the other sensors. Consequently, the radar detections falsely resulted into targets, which we call ghost vessels, that are quite challenging to eliminate. However, as they are temporary, single-sourced, and exist for much shorter periods, it becomes clear that those occurrences are mere clutter. The track management function will eliminate the track eventually. In addition to this, reflections due to water trails can also be seen and they do not interfere with the estimated extent parameters as much as the reflections yielding ghost vessels.

Completely to the left in Figure 5.9b, there was a large vessel turning around, under limited visibility. This caused the detections and clustering results to be processed in an uncanny way, jumping between ellipses and circles on and off. An important observation is also a synchronisation issue with the sensors, for instance in Figure 5.10b, where the detections are not entirely aligned. We would like to note that investigating the synchronisation is not within the scope of the thesis and shall rather be looked at in the future works.

In the second case, Figures 5.11 and 5.12 depict results from Sensor 1 and 2. Overall, the estimates seem to be representing the underlying vessels, where the different perspectives from both sensors are complemented in a less cluttered representation of the same environment as before. This is especially true for the large vessel in Figure 5.11 where the benefits of having MS can be clearly seen. Unlike the results from the three sensors, the reflections from Sensor 1 have not been detected as a potential target. There could be two possible reasons for this. Firstly, based on the clustering parameters, the minimum number of points for a cluster to be detected might not have been reached. Secondly, the reflections had a tendency to fluctuate a lot from one step to the other, so that even if a track would be initialised, the chance of it getting confirmed was low.

In Figure 5.12, the first single vessel has been included to illustrate that the elliptical estimate represents mostly the overlapping detections, thereby complementing each sensor quite well. The same can be seen in Figure 5.12b for the most part. One of the targets (the left one) at the centre is moving towards the South and the other towards the East. Still, the perspective-difference from the sensors is vivid, making it hard to figure how accurate the estimate is, without any reference.

We have recorded the computation times for the different steps to assess the overall performance, as we processed the streaming using PyCharm 2019 (Python 3.6 version) platform on a 2.60 GHz Intel Quad Core processor. Considering all the three sensors, the average computation time taken over 50 steps of streaming, for a single observation step is 1.98s. We broke down the whole operation into three different stages comprising the MS measurement registration and loading, clustering and tracking. The first two stages dominated the total computation time by accounting for almost 70% of the execution, where measurement loading and clustering were balanced at 35% and 34%

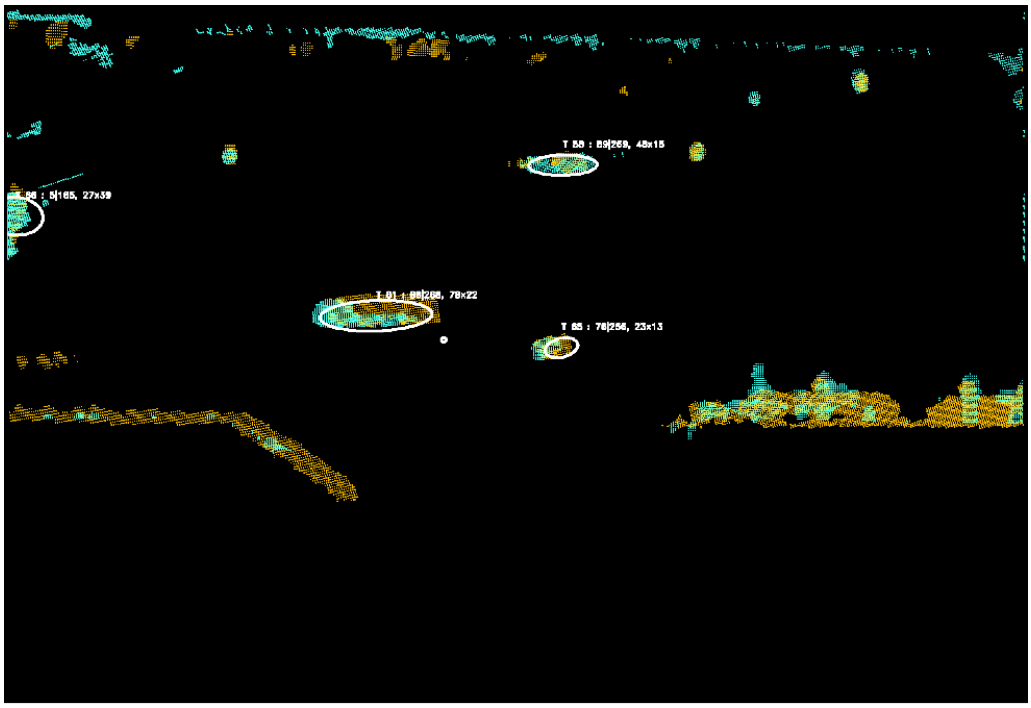

(a) Estimates of four vessels. Notice the reflections West from Sensor 1 (orange) due to the large vessel.

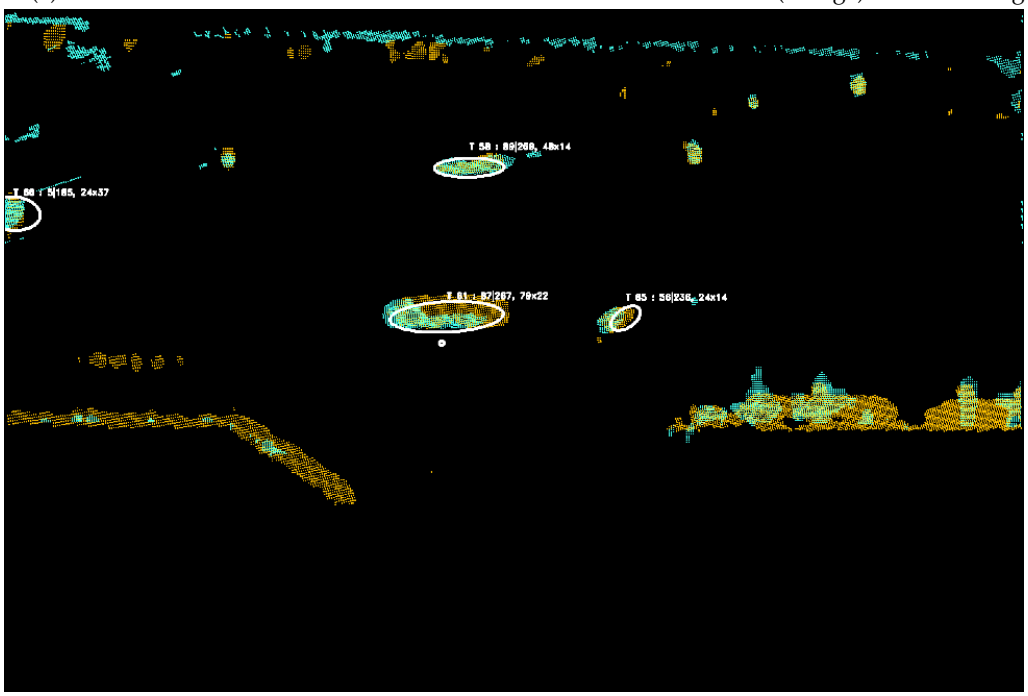

(b) Estimates of the same four vessels after approximately 15s.

Figure 5.11: Estimates of PAKF-JPDA with two sensors. [Sensor 1: Orange, Sensor 2: Teal]

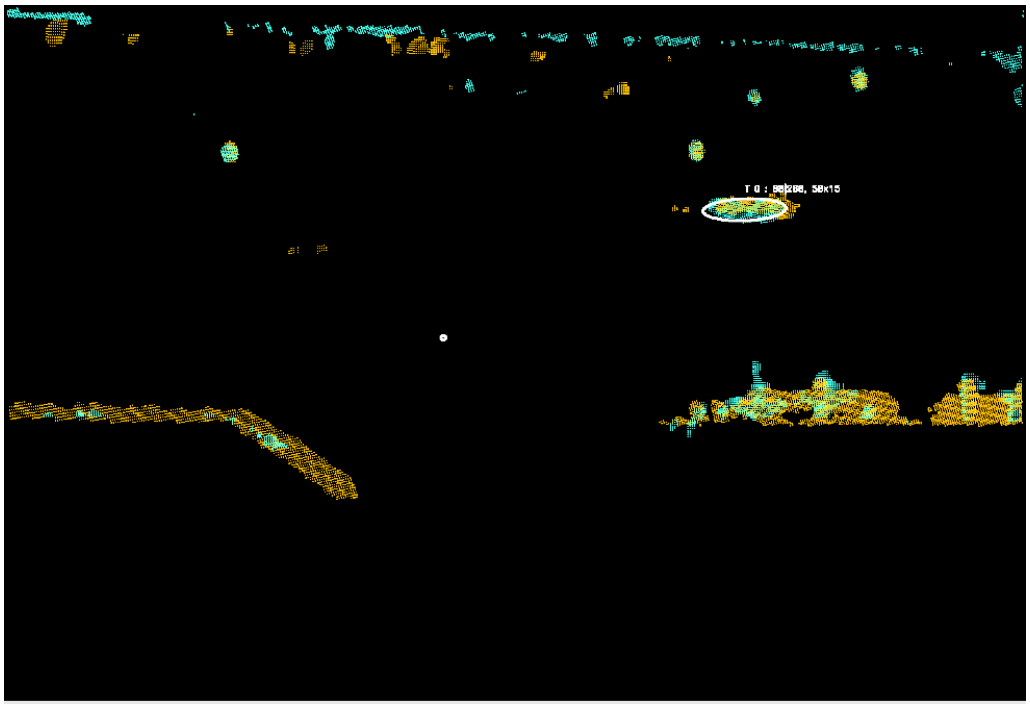

(a) Estimate of a single vessel.

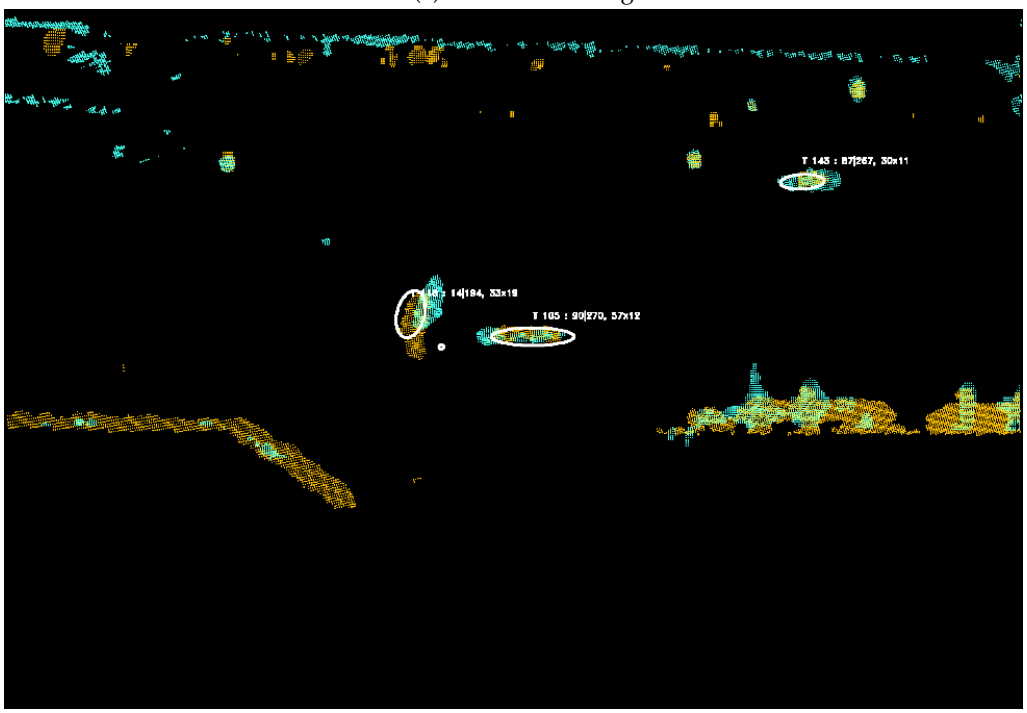

(b) Estimates of three vessels, with a target turning.

Figure 5.12: Estimates of PAKF-JPDA with two sensors. [Sensor 1: Orange, Sensor 2: Teal]

respectively. Our proposed tracker accounted for the remaining 31%. This applies to a situation where a step had at least two medium vessels (between 70m to 100m in length). A higher number of vessels is more prone to influence the clustering and tracking computation times, while the measurement loading remains more or less constant.

5.3 Chapter Summary

In the first part of the chapter, an EC-JPDA filter taking the target's extent into consideration was proposed for MTT, whose association was carried out between clusters and target tracks, upholding the $1-1$ cluster to track constraint. The clusters were obtained from the k-means clustering method on the detections. The algorithm was applied to the datasets of the DLR-repository and improvements in the positional estimates of larger vessels were observed when compared to the standard JPDA filter against the AIS positions. Around closer ranges, and with the smaller vessels, similar performances were observed from both filters.

The second part of the chapter introduced the MS-METT problem and proposed a processing chain with the PAKF-JPDA algorithm to tackle the problem. The essential feature of this algorithm is it being a combination of the PAKF for elliptical ETT and the EC-JPDA for multiple targets DA and state estimation. A MS-based flowchart and an outline of the algorithm were provided, which were experimented on an ASTERIX-based data stream. Results from multiple ground-based radar sensors were shown and discussed. The benefits of using multiple sensors in providing a more complete picture over the observation region were clearly visible. We also deduced that having more sensors may not necessarily improve the results –depending on the sensor's placement and for instance, its quality (which was a challenge in our stream) –where perhaps using a specific sensor combination could be more reliable.

The contributions presented in this chapter were partially published in journal article [1]. The proposed algorithm MS-PAKF-JPDA is planned to be published as a journal article in the near future.

Chapter 6

Conclusion

The advantages of a proper MTSAM are bountiful especially when it comes to increasing the awareness over a certain observation region of interest. The support system that helps achieving the same relies on the early stage processing, such as gathering measurements that are in the form of point clouds, detecting potential targets and eventually estimating their (extended) states over time. This is what we have considered in this thesis.

We have proposed frameworks to process marine radar data, from both dynamic sensors (on board vessels) and static sensors (anchored vessels and ground radar stations) with the objective of having an efficient and accurate elliptical METT tracker. Our research was therefore centred on obtaining an elliptical model with explicit parameterisation, and on its integration in an MTT DA-based tracker. The contributions are thereafter summarised.

A real-world marine radar-based repository with three different trajectories, available to the research community, has been proposed for the evaluation of target tracking methods. Some typical and day-to-day situations were considered, such as having a target navigating amidst aids to navigation or trajectories affected by occlusion. The algorithms that we have developed in the next phases shall be evaluated against these datasets.

The first elliptical model at which we look for ETT is the MEM-EKF* one. We proposed a tailored approach, T-MEM-EKF* based on the MEM-EKF* model that allows us to estimate the orientation of a vessel while keeping the semi-axes fixed. Compared to the original formulation, the T-MEM-EKF* has proven to be more computationally efficient as well as accurate when applied to simulations and trajectories from our dataset. The two methods, however, use a sequential approach to process measurements and could cause substantial reduction in efficiency should there be higher numbers of measurements in a target's point cloud. This led to a search for a batch approach to the problem retaining an explicit parameterisation of the elliptical extent.

The PAKF has then been proposed, particularly suited for problems with noisy and high number of measurements. It uses a custom EVD operation by which measurements for updating the extent

parameters are obtained. This is in addition a contrast to the previous approach that constructs pseudo-measurements for updating the extent parameters. PAKF turned out to be the trade-off between efficiency and accuracy, as shown by our simulations and comparisons against state-of-the-art methods. The results obtained from our dataset were overall satisfactory, given the challenges with the data itself.

The next focus would be MTT, where EC-JPDA was proposed to estimate the multi-target kinematic state of a known number of targets from our datasets. In essence, the algorithm processes target-originated point clouds' centroids and accounts for the spread of a target's point cloud by including the dispersion matrix in the gating step adaptively and in the calculation of innovation covariance in general. When applied to our datasets and compared against the standard JPDA version, the results of EC-JPDA were more accurate the larger a vessel was. This approach is used as a basis for the next contribution.

We have proposed a framework for MS elliptical METT with a track management function with the PAKF-JPDA approach. As the name suggests, it is a combination of our two aforementioned contributions that is implemented for processing data from three ground radar stations in a real-world harbour setting. The measurement quality of the latter is higher as compared to the on board marine radar in terms of resolution and noise. We have used a sequential supdate to account for the different sensors, and our track management function was responsible for track initiation, confirmation, and deletion. The results from our demonstrator were illustrated, accompanied by appropriate discussions. The robustness of the system as a whole lies in our tuning parameters for clustering, extension process noise covariance and track management.

Future Research

Some open questions remain when it comes to advancement and improvement of our work. In the thesis, much focus was put on target tracking. Some of the related and dependent concepts are therefore yet to be explored.

The target detection and clustering processes could be further improved by investigating the performance of the tracker based on more specific clustering approaches. When we presented the framework and tracking implementations, the average time to process multiple target-originated measurements from a single observation step included the time taken for measurement detection, extraction and clustering summed up. Optimising the early-stage pre-filtering processes is thus a relevant consideration. We shall study performance with respect to more complex clustering approaches, for instance, the hierarchical-based agglomerative clustering.

Regarding MS processing, a central-level setting was considered for our tracker, where a main module processes measurements from each sensor sequentially. Nonetheless, with distributed sensor systems (both dynamic and static), several topologies could be used and instead of the sequential update, an MS-based batch update could be implemented by using composite measure-

ments. The opportunity to integrate the sophisticated ellipse fusion approach from [TB21a] could also be taken advantage of. Additionally, we shall look into ways to make the system compensate for synchronisation problems, that we currently have little provision for.

The DA method could be reinforced by exploiting more complex inter-dependencies, for instance, the system could take the vessel's velocity into account. Finally, our next task would be to collect data and build appropriate neural networks-based models for vessel classification based on its extent estimates. Not only would it improve MTSAM, it would even be the basis to use awareness strategies for anomaly detection.

Appendix A

Supplementary Methodology Definitions

A.1 Nearly Constant Velocity Model

Consider the kinematic state of a target $\boldsymbol{x}_k$ that contains the target position $[m_1, m_2,]^T$ and velocity $[\dot{m}_1, \dot{m}_2,]^T$ at observation step $k-1$,

$$\boldsymbol{x}_{k-1} = [m_1, m_2, \dot{m}_1, \dot{m}_2]^T . \tag{A.1.1}$$

The state equation relies on the assumption that the target moves in a straight line with a *nearly* constant velocity in a two-dimensional coordinate system. By representing the sampling interval with T, the discretised system model (also known as discrete white noise acceleration model) can be expressed as [BSKL02],

$$\boldsymbol{x}_k = \mathbf{F}\boldsymbol{x}_{k-1} + \underbrace{\boldsymbol{\Gamma}\mathbf{v}_{k-1}}_{\boldsymbol{\omega}_{k-1}} \tag{A.1.2}$$

where

- transition matrix $\mathbf{F} = \begin{bmatrix} 1 & 0 & T & 0 \\ 0 & 1 & 0 & T \\ 0 & 0 & 1 & 0 \\ 0 & 0 & 0 & 1 \end{bmatrix}$
- process noise distribution matrix $\boldsymbol{\Gamma} = \begin{bmatrix} \frac{1}{2}T^2 & 0 \\ 0 & \frac{1}{2}T^2 \\ T & 0 \\ 0 & T \end{bmatrix}$,
- and the process noise $\mathbf{v}_{k-1} = [\mathrm{v}_1, \mathrm{v}_2]^T$.

Overall additive noise term $\boldsymbol{\omega}_{k-1}$ follows a Gaussian PDF defined by $\boldsymbol{\omega}_{k-1} \sim \mathcal{N}\left(0, \boldsymbol{\Gamma}\mathbf{C}_{\mathbf{v}}\boldsymbol{\Gamma}^T\right)$.

A.2 Coordinates Transformation

Expressing target positions in Cartesian coordinates provides the possibility to use the simple standard KF for tracking. The point clouds measurements that are obtained in our case are normally in polar coordinates that are each then transformed into their ENU-based Cartesian equivalents. For readability, we omit the measurement and observation step indices j and k.

Let each measurement vector $\boldsymbol{\Omega}$ from the set of measurements received be expressed in the terms of its range r and bearing (azimuth) φ with respect to the observing sensor platform as $\boldsymbol{\Omega} = [r, \varphi]^T$. The measurement is modelled as some source with additive zero-mean Gaussian noise of variances σ_r^2 and σ_φ^2. The first step is to apply the classical standard coordinate conversion equation [LBS93],

$$\underbrace{\begin{bmatrix} \tilde{y}_e \\ \tilde{y}_n \end{bmatrix}}_{:=\tilde{\boldsymbol{y}}} = \begin{bmatrix} r\sin(\varphi) \\ r\cos(\varphi) \end{bmatrix} \tag{A.2.1}$$

where φ defines the angle between the North-axis and the vector pointing towards the respective target in a clockwise direction.

In order to obtain the covariance matrix of the measurement noise $\boldsymbol{v}$ and account for the conversion errors, assumed zero-mean, (A.2.1) is linearised by computing its second order error statistics based on the following equations derived in [Fra07]:

$$\mathbf{C}^{\boldsymbol{v}} = \boldsymbol{\mathcal{T}}_\varphi \begin{bmatrix} \mu\left(c\sigma_{\boldsymbol{y}}^2 + \sigma_r^2\right) + 2cr^2 & 0 \\ 0 & \mu s\left(\sigma_y\right)^2 \end{bmatrix} \boldsymbol{\mathcal{T}}_\varphi^T \tag{A.2.2}$$

where the abbreviations

- $\mu = e^{\sigma_\varphi^2}$,
- $\sigma_{\boldsymbol{y}}^2 = r^2 + \sigma_r^2$,
- $c = \cosh\left(\sigma_\varphi^2\right) - 1$, and,
- $s = \sinh\left(\sigma_\varphi^2\right)$.

The transformation matrix $\boldsymbol{\mathcal{T}}_\varphi$ is calculated as [Fra07],

$$\boldsymbol{\mathcal{T}}_\varphi = \begin{bmatrix} \sin(\varphi) & \cos(\varphi) \\ \cos(\varphi) & -\sin(\varphi) \end{bmatrix}. \tag{A.2.3}$$

The final (unbiased) converted measurements are then obtained by the following equation [Fra07]

$$\boldsymbol{y} = \frac{1}{\sqrt{\mu}}\tilde{\boldsymbol{y}} \tag{A.2.4}$$

A.3 Gaussian Wasserstein Distance Metric

The GW distance is a common and accepted metric for evaluating elliptical trackers [YBG16]. It computes the distance between two ellipses by taking both their centres and covariances into account.

Let the extended state of a target $\boldsymbol{x}$ at a distinct observation step be represented by $\boldsymbol{x} = [\mathbf{m}, \alpha, \ell_1, \ell_2]^T$ defined by its position $\mathbf{m}$ and its elliptical extent parameters. $\boldsymbol{x}$ is assumed to follow a Gaussian PDF $\boldsymbol{x} \sim \mathcal{N}(\mathbf{m}, \mathbf{C}^{\boldsymbol{x}})$, where its covariance is obtained based on the following relation,

$$\mathbf{C}^{\boldsymbol{x}} = \boldsymbol{\mathcal{R}}(\alpha)\mathbf{D}\boldsymbol{\mathcal{R}}(\alpha)^T \tag{A.3.1}$$

where $\boldsymbol{\mathcal{R}}(\alpha) = \begin{bmatrix} \cos\alpha & -\sin\alpha \\ \sin\alpha & \cos\alpha \end{bmatrix}$ is the rotation matrix and $\mathbf{D} = \begin{bmatrix} \ell_1^2 & 0 \\ 0 & \ell_2^2 \end{bmatrix}$ represents the covariance of the semi-axes.

If a similarly defined extended state $\boldsymbol{y}$ is also Gaussian distributed so that $\boldsymbol{y} \sim \mathcal{N}(\hat{\mathbf{m}}, \mathbf{C}^{\boldsymbol{y}})$, then the GW distance d between $\boldsymbol{x}$ and $\boldsymbol{y}$ is given by [GS84]

$$d := \sqrt{||\mathbf{m} - \hat{\mathbf{m}}||_2^2 + \mathrm{Tr}\left(\mathbf{C}^{\boldsymbol{x}} + \mathbf{C}^{\boldsymbol{y}} - 2\sqrt{\left(\sqrt{\mathbf{C}^{\boldsymbol{y}}}\mathbf{C}^{\boldsymbol{x}}\sqrt{\mathbf{C}^{\boldsymbol{y}}}\right)}\right)}. \tag{A.3.2}$$

When used for evaluating the estimates against a particular ground truth, the d is calculated for every observation step k.

Appendix B

Additional Results

B.1 T-MEM-EKF* Results for METT

In this appendix chapter, we present the results of applying the T-MEM-EKF* written in Table 4.1 on a second dataset, MANV, from the DLR repositories (See Chapter 2) [3]. The elliptical tracker was integrated into a linear JPDA framework [YTB18] for tracking the kinematic states and extent parameters of multiple targets simultaneously.

B.1.1 Setting and Evaluation

The same state definition and system model as defined from (4.1.5)-(4.1.8) were used for this dataset. The MANV dataset involves two main vessels of interest, Target 2 (29.0m $\times 6.7$m) and Target 3 (23.0m $\times 6.0$m), in very dynamic random manoeuvres recorded from a static own vessel over $k = 1000$ observation steps. There are three static targets, that are tracked as well. The targets were initialised based on the AIS information where available for their positions, COG, SOG and length and width. The estimates were plotted at every 25 steps, and are found in Figure B.1. The orientation estimates for the two targets and the overall positional errors as evaluated against the AIS (where available) ones using the Optimal Subpattern Assignment (OSPA) metric are shown in Figure B.2.

OSPA is an MTT evaluation metric that accounts for the positional and cardinality errors of every target combined. Let the set of estimated tracks be represented by $\hat{\boldsymbol{X}}$ of dimension n and that of the ground truth tracks by $\boldsymbol{G}$ of dimension m. For $m \leq n$, the OSPA distance between the two sets, considering a so-called cut-off value c and an order value p, is given by [SVV08, BVV17]:

$$d_{p,c}\left(\hat{\boldsymbol{X}}, \boldsymbol{G}\right) = \left[\frac{1}{n}\left(\sum_{i=1}^{m} d_c\left(\hat{\boldsymbol{x}}^i, \boldsymbol{g}^i\right)^p + c^p\left(n-m\right)\right)\right]^{1/p} \tag{B.1.1}$$

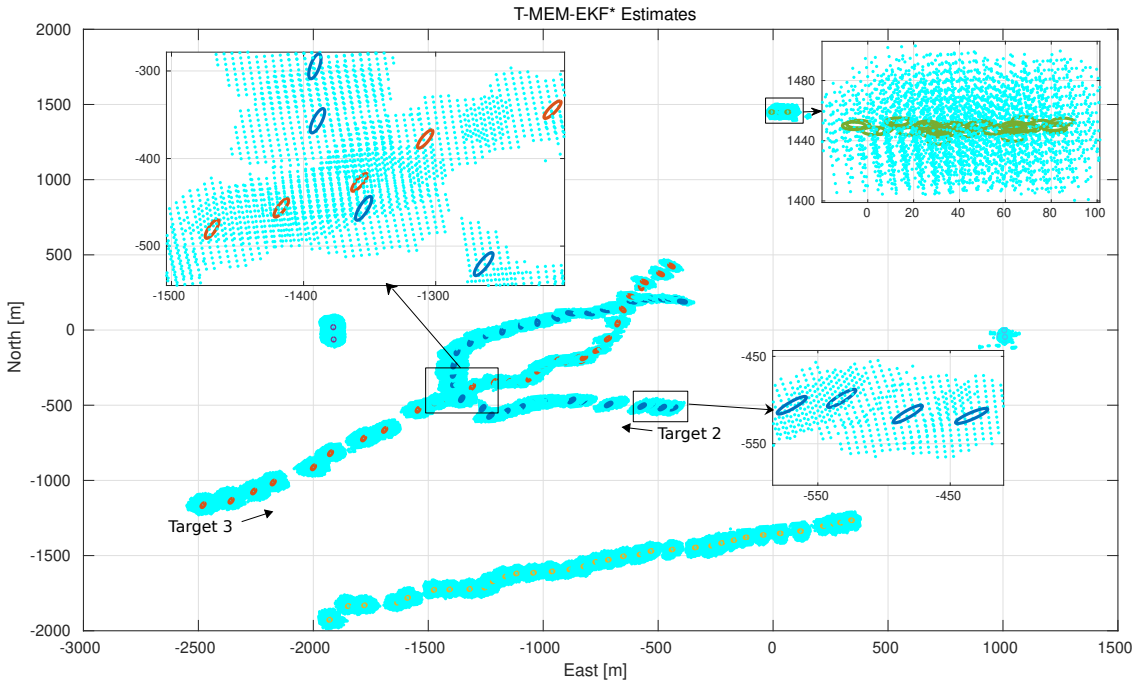

Figure B.1: Illustration of the elliptical estimates over the trajectory at intervals of 25 observation steps. The target ellipses are colour-coded, and the radar measurements are represented by the cyan dots. An unknown target was detected as from $[-2000, -2000]^T$. Image adapted from [3]©2019CMRE

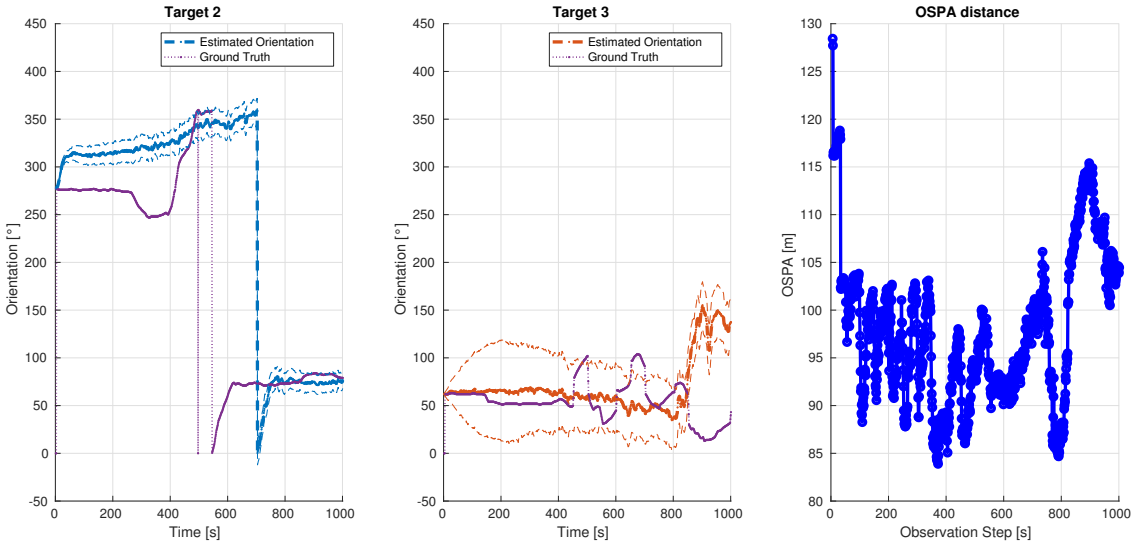

Figure B.2: The plots illustrate the orientation estimates of Target 2 (left) and Target 3 (middle) with their standard deviations over time and overall positional errors (right) as obtained by OSPA metric. Image from [3]©2019CMRE

where $d_c\left(\hat{\boldsymbol{x}}^i, \boldsymbol{g}^i\right) = \min\left(c, d\left(\hat{\boldsymbol{x}}^i, \boldsymbol{g}^i\right)\right)$ is a function for computing the Euclidean distance d between the estimated position and its corresponding ground truth values as long as the difference is less than c. The second term in the right hand side accounts for the cardinality error, weighted by $c > 0$. The value of p could be any number between 1 and ∞. Higher values signify harsher penalty to estimates that are far from their ground truth.

In our case, all the tracks, except for the unknown one (detected at around $[-2000, -2000]^T$ in FigureB.1) were used in the evaluation, where the $c = 150$m and $p = 2$. It is noted that the right estimate-to-ground truth mapping was ensured prior to and at the time of initialisation, hence the permutations described in [SVV08] could be skipped.

B.1.2 Discussion

A common feature of the radar measurements that can be observed in our datasets is the spread or scattering of targets-originated measurements the further away they are from the own vessel, anchored at the origin in Figure B.1. The arrows indicate their course at the beginning of their specific trajectories. The magnified rectangular bounding boxes, particularly for Target 2, show a rather strong correlation between the measurements spread and the estimated ellipses. This can also be confirmed in Figure B.2's orientation plot for most of its trajectory before 700s. However, the estimates improve upon approaching the own vessel. Target 3's orientation estimates were comparatively better throughout its trajectory, until the vessel was partly occluded by Target 2 from the own as of $k = 800$. The higher error around the same time in OSPA plot also corresponds with the occlusion of Target 3.

As a summary, besides being noisy, the point cloud measurements were more prominent on the visible side of the target from the own vessel's perspective. When far, the estimates would tend to be sensitive to the point-clouds' spreads although they improve as the targets get closer. In addition, the situation could be improved by having multiple strategically located sensors offering wider perspectives.

The contributions presented in this chapter were partly published in workshop proceedings [3].

B.2 PAKF Analyses and Discussions

In this section, we first present some analyses from our EVD sub-algorithm based on equations (4.2.9) to (4.2.15) by varying the measurement noise over a couple of simulations. We also consider using different mean (denoted n in this section) for generating the number of measurements to investigate any influence. Finally, we repeat our trajectory simulations with the three different trackers used for comparisons in Chapter 4.2 with varying number of measurements and present the findings.

Influence of $\mathbf{C}_{\mathbf{r}}^{\boldsymbol{v}}$ values

Different noise levels are assigned to $\mathbf{C}_{\mathbf{r}}^{\boldsymbol{v}}$ and their effects on obtaining the extent measurements, denoted by $\boldsymbol{y}^{\mathbf{p}} := [\theta, a, b]$, from simulated point cloud measurements are analysed at single-step runs. Measurements from a uniform distribution on a target's body, of size 80m by 20m and orientation of 135^{o} were generated. The number of measurements to be generated was intentionally chosen high to replicate sensors that yield dense point clouds and was drawn from a Poisson distribution of mean 250. Four noise settings are considered:

$$\begin{aligned} &\text{(i)} \quad \mathbf{C}_1^{\boldsymbol{v}} = \mathbf{0}_2 \\ &\text{(ii)} \quad \mathbf{C}_2^{\boldsymbol{v}} = \text{diag}(5^2, 5^2) \\ &\text{(iii)} \quad \mathbf{C}_3^{\boldsymbol{v}} = \text{diag}(15^2, 15^2) \\ &\text{(iv)} \quad \mathbf{C}_4^{\boldsymbol{v}} = \text{diag}(30^2, 30^2). \end{aligned} \tag{B.2.1}$$

Given the point clouds, we applied our EVD to obtain the elliptical measurement vector $\boldsymbol{y}^{\mathbf{p}}$ that would next be used for updating the extent parameters within the PAKF. The decomposed elliptical values are given in Table B.1 and their reconstructed ellipses in Figure B.3a. It is clear from the table that the values for $\boldsymbol{y}^{\mathbf{p}}$ are approximately within $\pm 5^{\text{o}}$ and ± 5m of the orientation's and the semi-axes ground truth values.

One should also note the appropriate noise value varies subjectively application-wise, as well as target dimension-wise. The high noise was simply chosen as a demonstration, although it wouldn't be sensible for a smaller target. Cars that are detected from close ranges would require ideally lower noises or another modelling strategy. It is also true that when we assess the standard marine radar measurements, they are not uniformly distributed and depend on the sensor perspective strongly amongst other factors. Under the real-world settings, we could expect the EVD values to be noisier and account for their uncertainties in $\mathbf{C}_{\mathbf{p}}^{\boldsymbol{v}}$.

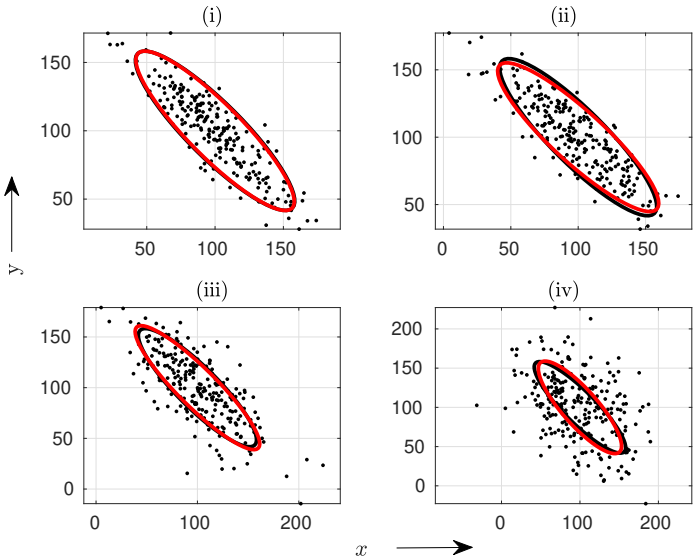

(a) Each plot represents noise levels from (B.2.1). The black points are the generated measurements over the target's surface (black ellipses) and the red ellipses have been reconstructed from the decomposed values.

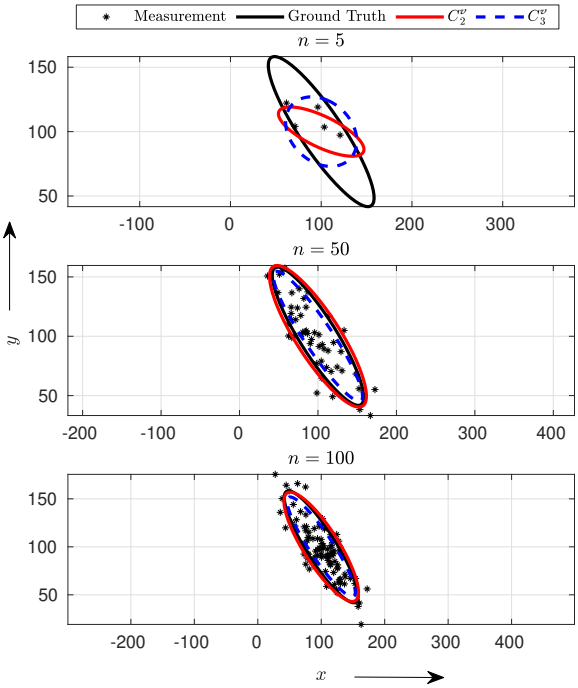

(b) Solid black ellipses are the ground truth, solid red and dotted blue ones are reconstructed ellipses for the different means using $\mathbf{C}_2^v$ and $\mathbf{C}_3^v$, respectively.

Figure B.3: Images adapted from [6]©2021IEEE

Table B.1: Values obtained from EVD [6]. [Ground truth: $\theta = 135^{\text{o}}$, $a = 80$m, $b = 20$m]

Measurement Noise Covariance	Orientation, θ [°]	Major Semi-axis, a $[m]$	Minor Semi-axis, b $[m]$
$\mathbf{C}_1^{\boldsymbol{v}}$	136.2	79.9	19.5
$\mathbf{C}_2^{\boldsymbol{v}}$	132.4	79.1	19.2
$\mathbf{C}_3^{\boldsymbol{v}}$	134.8	84.6	18.9
$\mathbf{C}_4^{\boldsymbol{v}}$	138.6	76.1	22.5

Table B.2: EVD parameters under different settings [6]. [Ground truth: $\theta = 135^{\text{o}}$, $a = 80$m, $b = 20$m]

Mean	Measurement Noise Covariance	θ $[^o]$	a $[m]$	b $[m]$
5	$\mathbf{C}_2^{\boldsymbol{v}}$	162.5	49.3	12.6
	$\mathbf{C}_3^{\boldsymbol{v}}$	162.5	40.4	25.3
50	$\mathbf{C}_2^{\boldsymbol{v}}$	136.2	82.5	23.8
	$\mathbf{C}_3^{\boldsymbol{v}}$	136.2	75.0	15.2
100	$\mathbf{C}_2^{\boldsymbol{v}}$	136.0	78.4	23.5
	$\mathbf{C}_3^{\boldsymbol{v}}$	136.0	75.9	17.7

Influence of Number of Measurements

We now investigate whether the number of measurements (in a point cloud) could affect the EVD and consequently the decomposed values. The same setting as above is used for our simulations, and we retain the two noise settings, $\mathbf{C}_2^{\boldsymbol{v}}$ and $\mathbf{C}_3^{\boldsymbol{v}}$ from (B.2.1). Different mean values are used for generating measurements from the target's surface under the two noise settings: 5, 50, and 100. The results from EVD are presented in Figure B.3b and Table B.2.

The first row of Figure B.3b captures a sparse-measurement situation, where corrected dispersion matrix $\boldsymbol{\Sigma}_{\hat{D}}$ had negative entries. This led to inaccurate representation of the underlying target. As n increases however, the values obtained from EVD improve and get more representative of the true dimensions. A workaround that we propose for ensuring the positive definiteness is assigning the negative entries, if at all, to very small non-zero values before processing them further.

Overall Impact of Number of Measurements

Finally, we include the overall impact of varying measurement means on the three filters, PAKF, RMM and MEM-EKF*, over the full simulated trajectory in Chapter 4.2. The simulations were

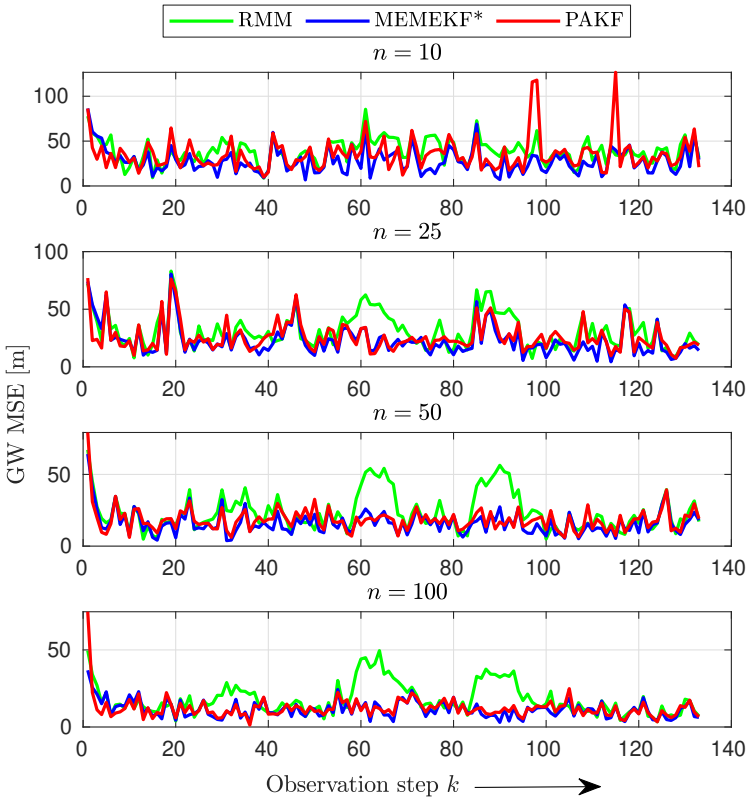

Figure B.4: GW-based extension errors for different mean values n. Images from [6] ©2021IEEE

carried out over 10,000 runs and the GW distance was used to evaluate the extension errors, plotted in Figure B.4. For $n = 10$, the errors are comparable except at $k \approx 95$ and $k \approx 115$, where the error was due to fluctuations in orientation estimates. For $n > 10$, RMM produces higher errors around the turns while PAKF and MEM-EKF* show more or less similar results.

The contributions presented in this chapter were published in conference proceedings [6].

B.3 EC-JPDA Filter: Clustering Visualisations

In this section, we share some k-means clustering visuals from the datasets, that were obtained after briefly description of how the number of clusters (here denoted as k) is determined. k-means clustering partitions data iteratively by minimising the distance of measurements belonging to some cluster to the cluster's centre (centroid), based on a predefined k and a stopping criterion. The cluster evaluation method used calculates the optimal number of clusters that can be obtained within a dataset of N observed measurements based on the variance ratio criterion, also known as Calinsky-Harabasz, which is given by [CJ74],

$$VRC_k = \frac{SS_B}{SS_W}\left(\frac{N_k - 1}{k - 1}\right). \tag{B.3.1}$$

SS_B is defined as the between-cluster variance and is obtained by

$$SS_B = \sum_{i=1}^{k} n_i ||\mathbf{m}_i - \mathbf{m}||^2 \tag{B.3.2}$$

where n_i is the number of cluster members or measurements in cluster i with mean $\mathbf{m}_i$, and $\mathbf{m}$ is the overall mean of the dataset measurements.

SS_W is defined as the within-cluster variance and is computed by

$$SS_W = \sum_{i=1}^{k} \sum_{\boldsymbol{x} \in c_i} ||\boldsymbol{x} - \mathbf{m}_i||^2 \tag{B.3.3}$$

where $\boldsymbol{x}$ is a measurement and c_i is the i^{th} cluster.

A clear and distinct partitioning would expect the ratio to be high, this is thus maximised with respect to k. It is this value of k which is then used to cluster the measurements at every observation step.

In our case, clustering is an intermediary step between target detection and tracking, so all the clusters are currently non-associated. The clusters from MANV were distinct and there were no multi-clusters resulting from a single target-originated point cloud. They are shown in Figure B.5.

For DAAN and DARC, the clusters were sometimes faulty and caused some disruptions with DA in the filtering step. Such examples were captured and have been added in this section for reference. The full trajectory-based are given in Figure B.6 for DAAN and Figure B.7 for DARC, with a magnified view in each to emphasise the possible limitations encountered with the approach.

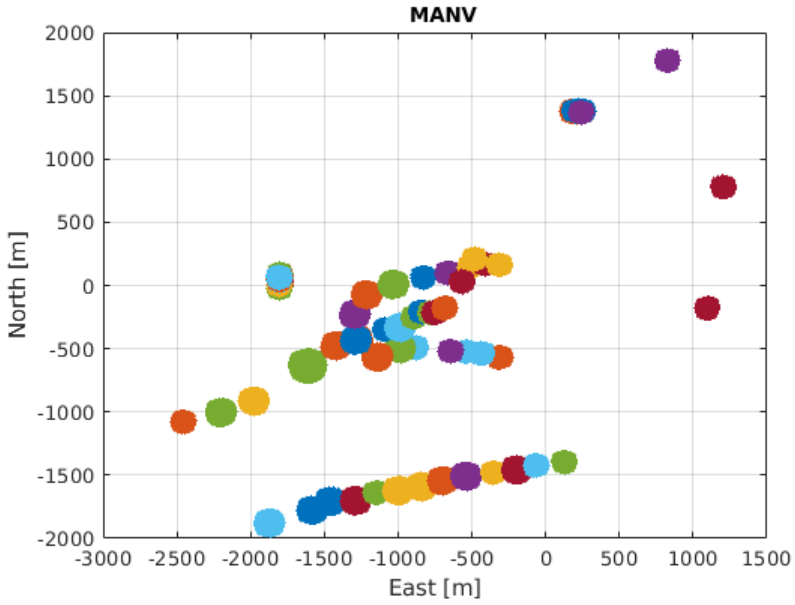

Figure B.5: Clear randomly coloured clusters from MANV plotted at regular intervals.

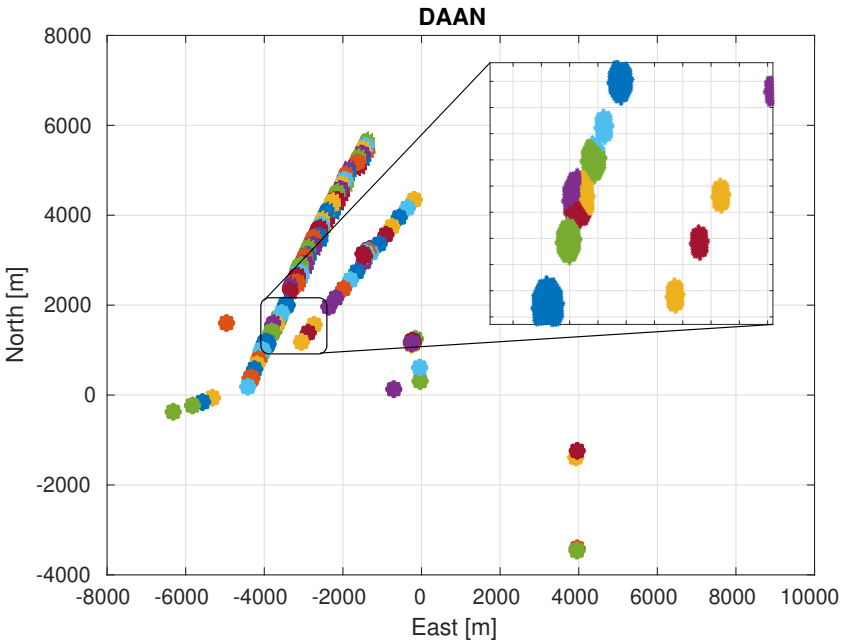

Figure B.6: Randomly coloured clusters from DAAN plotted at regular intervals. The magnified window contains a single target-originated point clouds that resulted in multiple clusters.

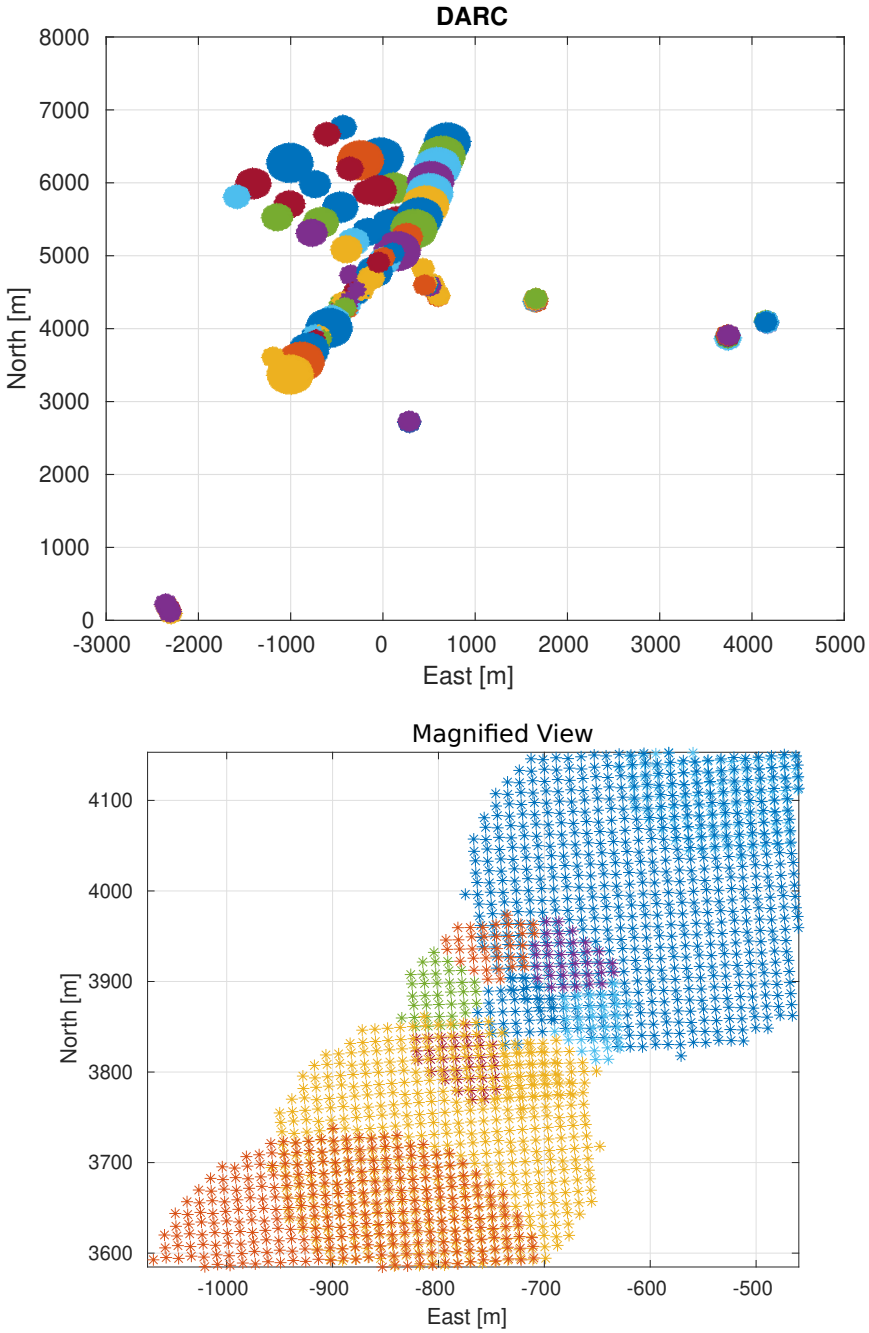

Figure B.7: Randomly coloured clusters from DARC plotted at regular intervals. The second plot is a magnified window with a single target-originated point clouds that resulted in multiple clusters.

Own Publications

[1] J. S. Fowdur, M. Baum, and F. Heymann, "Real-World Marine Radar Datasets for Evaluating Target Tracking Methods," *Sensors*, vol. 21, p. 4641, 07 2021. [Online]. Available: https://doi.org/10.3390/s21144641

[2] A. Kumar and J. S. Fowdur, "A Framework for Multisensor Multiple Extended Target Tracking with Vessel Size Categorisation," in *European Workshop on Maritime Systems Resilience and Security (MARESEC 2021)*, 10 2021. [Online]. Available: https://doi.org/10.5281/zenodo.5603349

[3] J. S. Fowdur, M. Baum, and F. Heymann, "A Marine Radar Dataset for Multiple Extended Target Tracking," in *1st Maritime Situational Awareness Workshop (MSAW 2019)*, La Spezia, Italy, 09 2019. [Online]. Available: https://elib.dlr.de/129565/

[4] S. Singh, J. S. Fowdur, J. Gawlikowski, and D. Medina, "Leveraging Graph and Deep Learning Uncertainties to Detect Anomalous Maritime Trajectories," *IEEE Transactions on Intelligent Transportation Systems*, pp. 1–15, 07 2022. [Online]. Available: https://doi.org/10.1109/TITS.2022.3190834

[5] J. S. Fowdur, M. Baum, and F. Heymann, "Tracking Targets with Known Spatial Extent Using Experimental Marine Radar Data," in *22nd International Conference on Information Fusion (FUSION 2019)*, Ottawa, Canada, 07 2019. [Online]. Available: https://ieeexplore.ieee.org/document/9011244

[6] ——, "An Elliptical Principal Axes-based Model for Extended Target Tracking with Marine Radar Data," in *24th International Conference on Information Fusion (FUSION 2021)*, 11 2021.

Bibliography

[ACE+16] H. Andersen, Z. J. Chong, Y. H. Eng, S. Pendleton, and M. H. Ang. Geometric Path Tracking Algorithm for Autonomous Driving in Pedestrian Environment. In *2016 IEEE International Conference on Advanced Intelligent Mechatronics (AIM)*, pages 1669–1674, 07 2016.

[AIS18] Automatic Identification System Overview. *The Navigation Center of Excellence*, 2018.

[AUT22] AUTOSHIP. Autonomous Shipping Initiative for European Waters. *Transport Research and Innovation Monitoring and Information System (TRIMIS)*, 2019-2022. (Accessed on 11/15/2021).

[Bar19] Barfoot, Timothy D. *State Estimation for Robotics*. Cambridge University Press, 2019.

[Bau15] M. Baum. Linear-time JPDAF based on Many-2-Many Approximation of Marginal Association Probabilities. *Electronics Letters*, 51:1526–1528(2), 09 2015.

[BE18] Edmund Brekke and Jo Eidsvik. LIDAR Extended Object Tracking of a Maritime Vessel Using an Ellipsoidal Contour Model. In *Proceedings of Symposium Data Fusion, Bonn, Germany*, 2018.

[BETV08] Herbert Bay, Andreas Ess, Tinne Tuytelaars, and Luc Van Gool. Speeded-Up Robust Features (SURF). *Computer Vision and Image Understanding*, 110(3):346–359, 2008. Similarity Matching in Computer Vision and Multimedia.

[BFH12] M. Baum, F. Faion, and U. D. Hanebeck. Modeling the Target Extent with Multiplicative Noise. In *2012 15th International Conference on Information Fusion*, pages 2406–2412, 07 2012.

[BGM+20] Dan Barnes, Matthew Gadd, Paul Murcutt, Paul Newman, and Ingmar Posner. The Oxford Radar RobotCar Dataset: A Radar Extension to the Oxford RobotCar Dataset. In *2020 IEEE International Conference on Robotics and Automation (ICRA)*, pages 6433–6438, 2020.

[BGV+12] Paolo Braca, Raffaele Grasso, Michele Vespe, Salvatore Maresca, and Jochen Horstmann. Application of the JPDA-UKF to HFSW Radars for Maritime Situational Awareness. In *15th International Conference on Information Fusion, FUSION 2012*, pages 2585–2592, 01 2012.

[BH09] M. Baum and U. D. Hanebeck. Random Hypersurface Models for Extended Object Tracking. In *2009 IEEE International Symposium on Signal Processing and Information Technology (ISSPIT)*, pages 178–183, 12 2009.

[BH11] M. Baum and U. D. Hanebeck. Shape Tracking of Extended Objects and Group Targets with Star-Convex RHMs. In *14th International Conference on Information Fusion*, pages 1–8, 07 2011.

[BH14] M. Baum and U. D. Hanebeck. Extended Object Tracking with Random Hypersurface Models. *IEEE Transactions on Aerospace and Electronic Systems*, 50(1):149–159, 01 2014.

[BHG20] Pawel Banys, Frank Heymann, and Maciej Gucma. Occurrence of Unknown Sensor Data within AIS Dynamic Messages. *NAŠE MORE, International Journal of Maritime Science and Technology*, 67(2):126–137, 2020.

[BKH10] Marcus Baum, Vesa Klumpp, and Uwe D. Hanebeck. A Novel Bayesian Method for Fitting a Circle to Noisy Points. In *2010 13th International Conference on Information Fusion*, pages 1–6, 2010.

[Bla86] S. S. Blackman. *Multiple-Target Tracking with Radar Applications*. Artech House Publishers, 1986.

[Bla04] Sam Blackman. Multiple Hypothesis Tracking for Multiple Target Tracking. *Aerospace and Electronic Systems Magazine, IEEE*, 19:5 – 18, 02 2004.

[Bla16] Sam Blackman. Abstracts of Previous Tutorials in this Series: Multiple Hypothesis Tracking for Multiple Target Tracking. *IEEE Aerospace and Electronic Systems Magazine*, 31:90–96, 03 2016.

[BNH10] Marcus Baum, Benjamin Noack, and Uwe Hanebeck. Extended Object and Group Tracking with Elliptic Random Hypersurface Models. In *2010 13th International Conference on Information Fusion*, pages 1 – 8, 08 2010.

[Boc08] Hans-Hermann Bock. Origins and Extensions of the k-means Algorithm in Cluster Analysis. *Journal Électronique d'Histoire des Probabilités et de la Statistique [electronic only]*, 4, 01 2008.

[BP99] S. Blackman and R. Popoli. *Design and Analysis of Modern Tracking Systems*. Artech House Publishers, 1999.

[BPO02] Robert Burkholder, Marcos Pino, and Fernando Obelleiro. Low Angle Scattering from 2-D Targets on a Time-Evolving Sea Surface. *IEEE Transactions on Geoscience and Remote Sensing*, 40:1185 – 1190, 06 2002.

[BRG+16] M. Beard, S. Reuter, K. Granström, B. Vo, B. Vo, and A. Scheel. Multiple Extended Target Tracking With Labeled Random Finite Sets. *IEEE Transactions on Signal Processing*, 64(7):1638–1653, 04 2016.

[BSDH09] Yaakov Bar-Shalom, Fred Daum, and Jim Huang. The Probabilistic Data Association Filter. *IEEE Control Systems Magazine*, 29(6):82–100, 12 2009.

[BSF88] Yaakov Bar-Shalom and T. E. Fortmann. *Tracking and Data Association*. Academic Press, 1988.

[BSH16] Paweł Banys, Gregor Siegert, and Frank Heymann. Rapid Variations of the Static Data Transmitted within AIS Message 5. In *International Symposium on Integrated Ship's Information Systems and Marine Traffic Engineering Conference (ISIS-MTE) 2016*, 09 2016.

[BSKL02] Yaakov Bar-Shalom, Thiagalingam Kirubarajan, and X.-Rong Li. *Estimation with Applications to Tracking and Navigation*. John Wiley & Sons, Inc., New York, NY, USA, 2002.

[BSWT11] Yaakov Bar-Shalom, Peter K. Willett, and Xin Tian. *Tracking and Data Fusion: A Handbook of Algorithms*. YBS Publishing, 2011.

[BVV17] Michael Beard, Ba Tuong Vo, and Ba-Ngu Vo. OSPA(2): Using the OSPA Metric to Evaluate Multi-Target Tracking Performance. In *2017 International Conference on Control, Automation and Information Sciences (ICCAIS)*, pages 86–91, 2017.

[BWE+19] Edmund Førland Brekke, Erik Falmar Wilthil, Bjørn-Olav H. Eriksen, D. Kwame Minde Kufoalor, Øystein Kaarstad Helgesen, I. B. Hagen, Morten Breivik, and Tor Arne Johansen. The Autosea Project: Developing Closed-Loop Target Tracking and Collision Avoidance Systems. *Journal of Physics: Conference Series*, 2019.

[CBL+20] Holger Caesar, Varun Bankiti, Alex H. Lang, Sourabh Vora, Venice Erin Liong, Qiang Xu, Anush Krishnan, Yu Pan, Giancarlo Baldan, and Oscar Beijbom. nuScenes: A Multimodal Dataset for Autonomous Driving. In *2020 IEEE/CVF Conference on Computer Vision and Pattern Recognition (CVPR)*, pages 11618–11628, 2020.

[CGT06] Stefano Coraluppi, Doug Grimmett, and Pascal Theije. Benchmark Evaluation of Multistatic Trackers. In *2006 9th International Conference on Information Fusion (FUSION 2006)*, pages 1 – 7, 08 2006.

[CJ74] Tadeusz Calinski and Harabasz JA. A Dendrite Method for Cluster Analysis. *Communications in Statistics - Theory and Methods*, 3:1–27, 01 1974.

[CMME11] Subhash Challa, Mark R. Morelande, Darko Mušicki, and Robin J. Evans. *Fundamentals of Object Tracking*. Cambridge University Press, 2011.

[DBMW18] Enrica D'Afflisio, Paolo Braca, Leonardo M. Millefiori, and Peter Willett. Detecting Anomalous Deviations from Standard Maritime Routes Using the Ornstein-Uhlenbeck Process. *IEEE Trans. Signal Processing*, 66(24):6474–6487, 2018.

[DWS11] Johan Degerman, Johannes Wintenby, and Daniel Svensson. Extended Target Tracking using Principal Components. In *14th International Conference on Information Fusion*, pages 1–8, 2011.

[EAFBV15] Borja Errasti-Alcala, Walter Fuscaldo, Paolo Braca, and Gemine Vivone. Realistic Ship Model for Extended Target Tracking Algorithms. In *Proc. of the IEEE International Geoscience and Remote Sensing Symposium (IGARSS 2015)*, 07 2015.

[EKSX96] Martin Ester, Hans-Peter Kriegel, Jörg Sander, and Xiaowei Xu. A Density-Based Algorithm for Discovering Clusters in Large Spatial Databases with Noise. In *Proceedings of the Second International Conference on Knowledge Discovery and Data Mining*, KDD'96, page 226–231. AAAI Press, 1996.

[EUR] EUROCONTROL. ASTERIX Protocol. [Online]. Available: `https://www.eurocontrol.int/asterix`. [Accessed: 2021-11-20].

[Eur20] European Maritime Safety Agency (EMSA). Analysis of Marine Casualties and Incidents Involving Container Vessels. *Safety Analysis of EMCIP Data—Container Vessels*, pages 8–9, 2020.

[Eur21] European Maritime Safety Agency (EMSA). EMSA Outlook 2021, 2021.

[EWF+18] Bjørn-Olav H. Eriksen, Erik Falmar Wilthil, Andreas Lindahl Flåten, Edmund Førland Brekke, and Morten Breivik. Radar-based Maritime Collision Avoidance Using Dynamic Window. *2018 IEEE Aerospace Conference*, pages 1–9, 2018.

[FBSS81] Thomas Fortmann, Yaakov Bar-Shalom, and Molly Scheffe. Multi-Target Tracking using Joint Probabilistic Data Association. In *Proceedings of the IEEE Conference on Decision and Control*, volume 2, pages 807 – 812, 01 1981.

[FBSS83] T. Fortmann, Y. Bar-Shalom, and M. Scheffe. Sonar Tracking of Multiple Targets using Joint Probabilistic Data Association. *IEEE Journal of Oceanic Engineering*, 8(3):173–184, 1983.

[FF08] M. Feldmann and D. Franken. Tracking of Extended Objects and Group Targets Using Random Matrices — A New Approach. In *2008 11th International Conference on Information Fusion*, pages 1–8, 06 2008.

[FFK11] M. Feldmann, D. Franken, and W. Koch. Tracking of Extended Objects and Group Targets Using Random Matrices. *IEEE Transactions on Signal Processing*, 59(4):1409–1420, 04 2011.

[Fra07] D. Franken. Consistent Unbiased Linear Filtering with Polar Measurements. In *Proceedings of the 10th International Conference on Information Fusion*, pages 1–8, 07 2007.

[FS85] A. Farina and F. A. Studer. *Radar Data Processing: Volume 1-Introduction and Tracking*. Research Studies Press, 1985.

[FZ20] Andrzej Felski and Karolina Zwolak. The Ocean-Going Autonomous Ship—Challenges and Threats. *Journal of Marine Science and Engineering*, 8(1), 2020.

[GB22] Karl Granström and Marcus Baum. A Tutorial on Multiple Extended Object Tracking. *10.36227/techrxiv.19115858.v1*, 02 2022.

[GBR17] Karl Granström, Marcus Baum, and Stephan Reuter. Extended Object Tracking: Introduction, Overview, and Applications. *Journal of Advances in Information Fusion*, 12:139–174, 12 2017.

[GCCG06] Odile Gerard, Stefano Coraluppi, Craig Carthel, and Doug Grimmett. Benchmark Analysis of NURC Multistatic Tracking Capability. In *2006 9th International Conference on Information Fusion (FUSION 2006)*, pages 1 – 8, 08 2006.

[Ger] German Aerospace Center (DLR). Real-World Marine Radar Datasets for Target Tracking. Available: `https://doi.org/10.26090/rwmr`.

[GFS16] K. Granström, M. Fatemi, and L. Svensson. Gamma Gaussian Inverse-Wishart Poisson Multi-Bernoulli Filter for Extended Target Tracking. In *2016 19th International Conference on Information Fusion (FUSION)*, pages 893–900, 07 2016.

[GFS19] Karl Granström, Maryam Fatemi, and Lennart Svensson. Poisson Multi-Bernoulli Mixture Conjugate Prior for Multiple Extended Target Filtering. *IEEE Transactions on Aerospace and Electronic Systems*, PP:1–1, 06 2019.

[GGMS05] Kevin Gilholm, S.J. Godsill, Simon Maskell, and David Salmond. Poisson Models for Extended Target and Group Tracking. *Proceedings of SPIE - The International Society for Optical Engineering*, 5913, 08 2005.

[GLO11] Karl Granström, Christian Lundquist, and Umut Orguner. Tracking Rectangular and Elliptical Extended Targets using Laser Measurements. In *14th International Conference on Information Fusion*, pages 1–8, 2011.

[GLO12] Karl Granström, Christian Lundquist, and Omut Orguner. Extended Target Tracking using a Gaussian-Mixture PHD Filter. *IEEE Transactions on Aerospace and Electronic Systems*, 48(4):3268–3286, 2012.

[GLSU13] A Geiger, P Lenz, C Stiller, and R Urtasun. Vision Meets Robotics: The KITTI Dataset. *International Journal of Robotics Research*, 32(11):1231–1237, 09 2013.

[GLZZ16] Lie Guo, Linhui Li, Yibing Zhao, and Zongyan Zhao. Pedestrian Tracking Based on Camshift with Kalman Prediction for Autonomous Vehicles. *International Journal of Advanced Robotic Systems*, 13(3), 2016.

[GO12] Karl Granström and Umut Orguner. A PHD Filter for Tracking Multiple Extended Targets Using Random Matrices. *IEEE Transactions on Signal Processing*, 60:5657–5671, 11 2012.

[Gov19] Felix Govaers. On Independent Axes Estimation for Extended Target Tracking. In *2019 Sensor Data Fusion: Trends, Solutions, Applications (SDF)*, pages 1–6, 2019.

[GPRD20] Louis Guerlin, Benjamin Pannetier, Michèle Rombaut, and Maxime Derome. Study on Group Target Tracking to Counter Swarms of Drones. In Ivan Kadar, Erik P. Blasch, and Lynne L. Grewe, editors, *Signal Processing, Sensor/Information Fusion, and Target Recognition XXIX*, volume 11423, pages 8 – 27. International Society for Optics and Photonics, SPIE, 2020.

[Gra18] Granström, Karl and Svensson, Lennart and Reuter, Stephan and Xia, Yuxuan and Fatemi, Maryam. Likelihood-Based Data Association for Extended Object Tracking Using Sampling Methods. *IEEE Transactions on Intelligent Vehicles*, 3:30–45, 2018.

[GRG+21] Lars Grundhöfer, Filippo Giacomo Rizzi, Stefan Gewies, Michael Hoppe, Jesper Bäckstedt, Marek Dziewicki, and Giovanni Del Galdo. Positioning with Medium Frequency R-Mode. *Navigation, Journal of the Institute of Navigation*, 2021.

[GRMS14] Karl Granström, Stephan Reuter, Daniel Meissner, and Alexander Scheel. A Multiple Model PHD Approach to Tracking of Cars under an Assumed Rectangular Shape. In *17th International Conference on Information Fusion (FUSION)*, pages 1–8, 2014.

[GS84] Clark R. Givens and Rae Michael Shortt. A Class of Wasserstein Metrics for Probability Distributions. *Michigan Math. J.*, 31(2):231–240, 1984.

[GS05] K. Gilholm and D. Salmond. Spatial Distribution Model for Tracking Extended Objects. *IEEE Proceedings - Radar, Sonar and Navigation*, 152(5):364–371, 10 2005.

[GWB15] K. Granström, P. Willett, and Y. Bar-Shalom. An Extended Target Tracking Model with Multiple Random Matrices and Unified Kinematics. In *2015 18th International Conference on Information Fusion (Fusion)*, pages 1007–1014, 07 2015.

[GWD17] Wen-dong Geng, Yuan-qin Wang, and Zheng-hong Dong. *Group-target Tracking*. Springer, Singapore, 2017.

[HBHE19] Øystein Kaarstad Helgesen, Edmund Brekke, Håkon Hagen Helgesen, and Øystein Engelhardtsen. Sensor Combinations in Heterogeneous Multi-sensor Fusion for Maritime Target Tracking. *2019 22th International Conference on Information Fusion (FUSION)*, pages 1–9, 2019.

[HBS15] Frank Heymann, P. Banys, and Cristina Saez. Radar Image Processing and AIS Target Fusion. *TransNav, the International Journal on Marine Navigation and Safety of Sea Transportation*, 9:443–448, 09 2015.

[HBSH17] Julian Hoth, Pawel Banys, Gregor Siegert, and Frank Heymann. Performance Analysis of a Simulated Distributed Multi-Radar System for Target Detection. In *18th International Radar Symposium (IRS) 2017*, pages 1–10, 06 2017.

[HHBS17] Frank Heymann, Julian Hoth, Pawel Banys, and Gregor Siegert. Validation of Radar Image Tracking Algorithms with Simulated Data. *TransNav, the International Journal on Marine Navigation and Safety of Sea Transportation*, 11:511–518, 09 2017.

[HK20] Jens Honer and Hauke Kaulbersch. Bayesian Extended Target Tracking with Automotive Radar using Learned Spatial Distribution Models. In *2020 IEEE International Conference on Multisensor Fusion and Integration for Intelligent Systems (MFI)*, pages 316–322, 2020.

[HKK21] Jungwook Han, Sun Young Kim, and Jinwhan Kim. Enhanced Target Ship Tracking With Geometric Parameter Estimation for Unmanned Surface Vehicles. *IEEE Access*, 9:39864–39872, 2021.

[HL97] David Hall and James Llinas. An Introduction to Multisensor Data Fusion. *Proceedings of the IEEE*, 85:6 – 23, 02 1997.

[HSRD16] T. Hirscher, A. Scheel, S. Reuter, and K. Dietmayer. Multiple Extended Object Tracking Using Gaussian Processes. In *Proceedings of the 19th International Conference on Information Fusion (Fusion 2016)*, pages 868–875, 07 2016.

[HTT+13] Biruk Habtemariam, Ratnasingham Tharmarasa, Thiviya Thayaparan, Mahendra Mallick, and Thia Kirubarajan. A Multiple-Detection Joint Probabilistic Data Association Filter. *IEEE Journal of Selected Topics in Signal Processing*, 7:461–471, 06 2013.

[JB06] Khalid Jamil and Robert Burkholder. Radar Scattering From a Rolling Target Floating on a Time-Evolving Rough Sea Surface. *IEEE Transactions on Geoscience and Remote Sensing*, 44:3330 – 3337, 12 2006.

[JBK21] Sushil Joshi, Stefan Baumgartner, and Gerhard Krieger. Tracking and Track Management of Extended Targets in Range-Doppler Using Range-Compressed Airborne Radar Data. *IEEE Transactions on Geoscience and Remote Sensing*, PP, 05 2021.

[Kal60] R. E. Kalman. A New Approach to Linear Filtering and Prediction Problems. *Journal of Basic Engineering*, 82(1):35–45, 03 1960.

[KBW16] H. Kaulbersch, M. Baum, and P. Willett. An EM approach for Contour Tracking based on Point Clouds. In *2016 IEEE International Conference on Multisensor Fusion and Integration for Intelligent Systems (MFI)*, pages 529–533, 09 2016.

[KBW17] H. Kaulbersch, M. Baum, and P. Willett. EM approach for Tracking Star-Convex Extended Objects. In *2017 20th International Conference on Information Fusion (Fusion)*, pages 1–7, 07 2017.

[KG20] Paul Koch and Stefan Gewies. Worldwide Availability of Maritime Medium-Frequency Radio Infrastructure for R-Mode-Supported Navigation. *Journal of Marine Science and Engineering*, 8(3), 2020.

[KHB18] Hauke Kaulbersch, Jens Honer, and Marcus Baum. A Cartesian B-Spline Vehicle Model for Extended Object Tracking. In *2018 21st International Conference on Information Fusion (FUSION)*, pages 1–5, 07 2018.

[KHB19] Hauke Kaulbersch, Jens Honer, and Marcus Baum. EM-based Extended Target Tracking with Automotive Radar using Learned Spatial Distribution Models. In *22nd International Conference on Information Fusion (FUSION 2019)*, Ottawa, Canada, 07 2019.

[Kir04] Kirubarajan, Thia and Bar-Shalom, Yaakov. Probabilistic Data Association Techniques for Target Tracking in Clutter. *Proceedings of the IEEE*, 92:536 – 557, 04 2004.

[KNW+15] Felix Kunz, Dominik Nuss, Jürgen Wiest, Hendrik Deusch, Stephan Reuter, Franz Gritschneder, Alexander Scheel, Manuel Stübler, Martin Bach, Patrick Hatzelmann, Cornelius Wild, and Klaus Dietmayer. Autonomous Driving at Ulm University: A Modular, Robust, and Sensor-Independent Fusion Approach. In *2015 IEEE Intelligent Vehicles Symposium (IV)*, pages 666–673, 2015.

[Koc08] Johann Wolfgang Koch. Bayesian Approach to Extended Object and Cluster Tracking using Random Matrices. *IEEE Transactions on Aerospace Electronic Systems*, 44(3):1042–1059, 07 2008.

[LBS93] D. Lerro and Y. Bar-Shalom. Tracking with Debiased Consistent Converted Measurements versus EKF. *IEEE Transactions on Aerospace and Electronic Systems*, 29(3):1015–1022, 07 1993.

[LL12] Jian Lan and X. Rong Li. Tracking of Extended Object or Target Group using Random Matrix — Part II: Irregular Object. In *2012 15th International Conference on Information Fusion*, pages 2185–2192, 2012.

[LL15] J. Lan and X. R. Li. Nonlinear Estimation by LMMSE-Based Estimation With Optimized Uncorrelated Augmentation. *IEEE Transactions on Signal Processing*, 63(16):4270–4283, 2015.

[LL16] Jian Lan and X. Rong Li. Tracking of Extended Object or Target Group Using Random Matrix: New Model and Approach. *IEEE Transactions on Aerospace and Electrical Systems*, 52(6):2973–2988, 12 2016.

[LL19] Jian Lan and X. Rong Li. Extended-Object or Group-Target Tracking Using Random Matrix With Nonlinear Measurements. In *IEEE Transactions on Signal Processing*, volume 67, pages 5130–5142, 2019.

[LLL20] Mingkai Li, Jian Lan, and X. Rong Li. Tracking of Elliptical Extended Object with Unknown but Fixed Lengths of Axes. In *2020 IEEE 23rd International Conference on Information Fusion (FUSION)*, pages 1–8, 2020.

[LNG06] Jack Li, William Ng, and S.J. Godsill. Online Multiple Target Tracking and Sensor Registration Using Sequential Monte Carlo Methods. In *2006 IEEE Nonlinear Statistical Signal Processing Workshop*, pages 55 – 58, 10 2006.

[Mac67] J. Macqueen. Some Methods for Classification and Analysis of Multivariate Observations. In *In 5th Berkeley Symposium on Mathematical Statistics and Probability*, pages 281–297, 1967.

[Mah00] R.P.S Mahler. An Introduction to Multisource-Multitarget Statistics and its Applications. *Lockheed Martin Technical Monograph*, 01 2000.

[Mah07] Ronald Mahler. PHD filters of Higher Order in Target Number. *IEEE Transactions on Aerospace and Electronic Systems*, 43(4):1523–1543, 2007.

[Mah19] Ronald Mahler. A GLMB filter for Unified Multitarget Multisensor Management. In Ivan Kadar, Erik P. Blasch, and Lynne L. Grewe, editors, *Signal Processing, Sensor/Information Fusion, and Target Recognition XXVIII*, volume 11018, pages 123 – 134. International Society for Optics and Photonics, SPIE, 2019.

[Mar] Marine Insight. Automatic Identification System (AIS) Integrating and Identifying Marine Communication Channels. `https://www.marineinsight.com/category/marine-navigation`. (Accessed on 02/15/2021).

[Mar21a] Marine Insight. The Ultimate Guide to Ship Sizes. [Online]. Available: `https://www.marineinsight.com/types-of-ships/the-ultimate-guide-to-ship-sizes/`, 10 2021. (Accessed on 11/15/2021).

[Mar21b] Maritime Manual. Marine Guide Column, Ship Sizes: Classification of Ships By Sizes. [Online]. Available: https://www.maritimemanual.com/ship-sizes-classification-of-ships-by-sizes/, 07 2021. (Accessed on 11/15/2021).

[MBMW17] Martin Michaelis, Philipp Berthold, Daniel Meissner, and Hans-Joachim Wuensche. Heterogeneous Multi-Sensor Fusion for Extended Objects in Automotive Scenarios Using Gaussian Processes and a GMPHD-Filter. In *2017 Sensor Data Fusion: Trends, Solutions, Applications (SDF)*, 10 2017.

[MCS+14] L. Mihaylova, A. Carmi, F. Septier, A. Gning, S. Pang, and S. Godsill. Overview of Bayesian Sequential Monte Carlo Methods for Group and Extended Object Tracking. *Digital Signal Processing*, 25:1–16, 02 2014.

[ME04] Darko Musicki and Rob Evans. Joint Integrated Probabilistic Data Association: JIPDA. *Aerospace and Electronic Systems, IEEE Transactions on*, 40:1093 – 1099, 08 2004.

[MZ01] Ronald Mahler and Tim Zajic. Multitarget Filtering using a Multitarget First-Order Moment Statistic. *Proceedings of SPIE - The International Society for Optical Engineering*, 4380:184–195, 01 2001.

[NLR+18] Lisa Nyman, Björn Lund, Roland Romeiser, Hans Graber, and Jochen Horstmann. A New Approach to Detect Surface Currents of Complex Flows Using Doppler Marine Radar. In *IGARSS 2018 - 2018 IEEE International Geoscience and Remote Sensing*, pages 1493–1496, 07 2018.

[NOK+19] Shinya Nakamura, Naoki Okada, Satoru Kuwahara, Koji Kutsuna, Takuya Nakashima, and Hideyuki Ando. Study on Automatic Collision Avoidance System and Method for Evaluating Collision Avoidance Manoeuvring Results. *Journal of Physics: Conference Series*, 1357:012033, 10 2019.

[PGMA12] Nikolay Petrov, A. Gning, Lyudmila Mihaylova, and Donka Angelova. Box Particle Filtering for Extended Object Tracking. In *IEEE 15th International Conference on Information Fusion, FUSION 2012*, pages 82–89, 01 2012.

[Pyt] Python Skimage. Determinant of Hessians (DoH) Algorithm. [Online]. Available: https://scikit-image.org/docs/dev/auto_examples/features_detection/plot_blob.html. [Accessed: 2021-12-15].

[RCBSW10] Kevin Romeo, David F. Crouse, Yaakov Bar-Shalom, and Peter Willett. The JPDAF in Practical Systems: Approximations. In *Proc. SPIE 7698, Signal and Data Processing of Small Targets*, volume 7698, pages 76981I–76981I–10, 2010.

[SBH16] Gregor Siegert, Pawel Banys, and Frank Heymann. Improving the Maritime Traffic Situation Assessment for a Single Target in a Multisensor Environment. In *Maritime Knowledge Discovery and Anomaly Detection Workshop*, 07 2016.

[SBHH17] Gregor Siegert, Pawel Banys, Julian Hoth, and Frank Heymann. Counteracting the Effects of GNSS Jamming in a Maritime Multi-Target Scenario by Fusing AIS with Radar Data. In *The Institute Of Navigation (ION) Annual Technical Meeting (ITM) 2017*, 02 2017.

[SBNC+21] Shahrzad Minooee Sabery, Aleksandr Bystrov, Miguel Navarro-Cía, Peter Gardner, and Marina Gashinova. Study of Low Terahertz Radar Signal Backscattering for Surface Identification. *Sensors*, 21(9):2954, 04 2021.

[SBZ+15] J. Steinbring, M. Baum, A. Zea, F. Faion, and U. D. Hanebeck. A Closed-Form Likelihood for Particle Filters to Track Extended Objects with Star-Convex RHMs. In *2015 IEEE International Conference on Multisensor Fusion and Integration for Intelligent Systems (MFI)*, pages 25–30, 09 2015.

[Sch18] Schubert Erich. Knowledge Discovery in Databases - Part III - Clustering. [Online]. Available: `https://dbs.ifi.uni-heidelberg.de/files/Team/eschubert/lectures/KDDClusterAnalysis17-screen.pdf`, 2018. [Accessed: 2022-01-12].

[SG99] D.J. Salmond and N.J. Gordon. Group and Extended Object Tracking. In *Proc SPIE - The International Society for Optical Engineering*, volume 3809, pages 16/1 – 16/4, 02 1999.

[SHBH18] Gregor Siegert, Julian Hoth, Paweł Banyś, and Frank Heymann. Generic Framework for Vessel Detection and Tracking based on Distributed Marine Radar Image Data. *CEAS Space Journal*, 11, 04 2018.

[Sie17] Gregor Siegert. Multi-Radar Multi-Target Tracking in the Context of Cooperative Maritime Traffic Situation Assessment. In *Young Researchers Seminar 2017*, 05 2017.

[SJHP13] Subirana J. Sanz, Zornoza J.M. Juan, and M. Hernandez-Pajares. *GNSS Data Processing: Volume I: Fundamentals and Algorithms*. European Space Agency, 2013.

[SK71] R.A. Singer and A.J. Kanyuck. Computer Control of Multiple Site Track Correlation. *Automatica*, 7(4):455–463, 1971.

[SL06] Taek Lyul Song and Dong Lee. A Probabilistic Nearest Neighbor Filter Algorithm for m Validated Measurements. *Signal Processing, IEEE Transactions on*, 54:2797 – 2802, 08 2006.

[SOL03] SOLAS. International Convention for the Safety of Life at Sea. *International Maritime Organization*, 2003.

[SRW15] M. Schuster, J. Reuter, and G. Wanielik. Probabilistic Data Association for Tracking Extended Targets under Clutter using Random Matrices. In *2015 18th International Conference on Information Fusion (Fusion)*, pages 961–968, 07 2015.

[SSGW11] Lennart Svensson, Daniel Svensson, Marco Guerriero, and P. Willett. Set JPDA Filter for Multitarget Tracking. *Signal Processing, IEEE Transactions on*, 59:4677 – 4691, 11 2011.

[STGS14] Pedro Silveira, A.P. Teixeira, and Carlos Guedes Soares. Assessment of Ship Collision Estimation Methods using AIS Data. In *Maritime Technology and Engineering*, 10 2014.

[SVV08] Dominic Schuhmacher, Ba-Tuong Vo, and Ba-Ngu Vo. A Consistent Metric for Performance Evaluation of Multi-Object Filters. *Signal Processing, IEEE Transactions on*, 56:3447 – 3457, 09 2008.

[Tai05] Peter Tait. *Introduction to Radar Target Recognition*. IEE Radar, Sonar, Navigation and Avionics Series 18. The Institution of Electrical Engineers (IEE), 2005.

[TB21a] Kolja Thormann and Marcus Baum. Fusion of Elliptical Extended Object Estimates Parameterized With Orientation and Axes Lengths. *IEEE Transactions on Aerospace and Electronic Systems*, PP:1–1, 02 2021.

[TB21b] Kolja Thormann and Marcus Baum. Incorporating Range-Rate Measurements in EKF-based Elliptical Extended Object Tracking. In *IEEE International Conference on Multisensor Fusion and Integration (MFI)*, pages 1–1, 2021.

[The20] The European GNSS Agency (GSA). Editor's Special on Space Data for Europe. *GNSS User Technology Report*, page 23, 2020.

[TKOA18] Barkin Tuncer, Murat Kumru, Emre Ozkan, and A. Aydin Alatan. Extended Object Tracking and Shape Classification. In *2018 21st International Conference on Information Fusion (FUSION)*, pages 1–5, 2018.

[TO21] Barkın Tuncer and Emre Özkan. Random Matrix Based Extended Target Tracking With Orientation: A New Model and Inference. *IEEE Transactions on Signal Processing*, 69:1910–1923, 2021.

[TYB20] Kolja Thormann, Shishan Yang, and Marcus Baum. A Comparison of Kalman Filter-based Approaches for Elliptic Extended Object Tracking. In *IEEE 23rd International Conference on Information Fusion, FUSION 2020*, pages 1–8, 2020.

[TYB21] Kolja Thormann, Shishan Yang, and Marcus Baum. Kalman Filter Based Extended Object Tracking with a Gaussian Mixture Spatial Distribution Model. In *2021 IEEE Intelligent Vehicles Symposium Workshops (IV Workshops)*, pages 293–298, 2021.

[VB16] Gemine Vivone and Paolo Braca. Joint Probabilistic Data Association Tracker for Extended Target Tracking Applied to X-Band Marine Radar Data. *IEEE Journal of Oceanic Engineering*, pages 1007–1019, 10 2016.

[VBG+15] G. Vivone, P. Braca, K. Granström, A. Natale, and J. Chanussot. Converted Measurements Random Matrix Approach to Extended Target Tracking Using X-band Marine Radar Data. In *2015 18th International Conference on Information Fusion (Fusion)*, pages 976–983, 07 2015.

[VBGW16] Gemine Vivone, Paolo Braca, Karl Granström, and Peter Willett. Multistatic Bayesian Extended Target Tracking. *IEEE Transactions on Aerospace and Electronic Systems*, 52(6):2626–2643, 2016.

[VGBW16] G. Vivone, K. Granström, P. Braca, and P. Willett. Multiple Sensor Bayesian Extended Target Tracking Fusion Approaches Using Random Matrices. In *2016 19th International Conference on Information Fusion (FUSION)*, pages 886–892, 2016.

[VGBW17] G. Vivone, K. Granström, P. Braca, and P. Willett. Multiple Sensor Measurement Updates for the Extended Target Tracking Random Matrix Model. *IEEE Transactions on Aerospace and Electronic Systems*, 53(5):2544–2558, 2017.

[VMBS+15] Ba-Ngu Vo, Mahendra Mallick, Yaakov Bar-Shalom, Stefano Coraluppi, Richard III, Ronald Mahler, and Ba-Tuong Vo. Multitarget Tracking. *Wiley Encyclopedia*, pages 1–25, 09 2015.

[VVH17] Ba-Ngu Vo, Ba Vo, and H.G. Hoang. An Efficient Implementation of the Generalized Labeled Multi-Bernoulli Filter. *IEEE Transactions on Signal Processing*, 65:1975–1987, 04 2017.

[VVP14] B. Vo, B. Vo, and D. Phung. Labeled Random Finite Sets and the Bayes Multi-Target Tracking Filter. *IEEE Transactions on Signal Processing*, 62(24):6554–6567, 12 2014.

[WBSWB19] Erik Falmar Wilthil, Yaakov Bar-Shalom, Peter K. Willett, and Edmund Førland Brekke. Estimation of Target Detectability for Maritime Target Tracking in the PDA Framework. *2019 22th International Conference on Information Fusion (FUSION)*, pages 1–8, 2019.

[WCM+16] Zheng Wan, Jihong Chen, Abdel El Makhloufi, Daniel Sperling, and Yang Chen. Four Routes to Better Maritime Governance. *Nature*, 540:27–29, 2016.

[WK10] Monika Wieneke and Wolfgang Koch. Probabilistic Tracking of Multiple Extended Targets using Random Matrices. In *Proceedings of SPIE - The International Society for Optical Engineering*, volume 7698, 04 2010.

[WO15] N. Wahlström and E. Özkan. Extended Target Tracking Using Gaussian Processes. *IEEE Transactions on Signal Processing*, 63(16):4165–4178, 08 2015.

[XGS+21] Yuxuan Xia, Karl Granström, Lennart Svensson, Maryam Fatemi, Ángel García-Fernández, and Jason Williams. Poisson Multi-Bernoulli Approximations for Multiple Extended Object Filtering. *IEEE Transactions on Aerospace and Electronic Systems*, PP:1–1, 09 2021.

[XT15] Dongkuan Xu and Yingjie Tian. A Comprehensive Study of Clustering Algorithms. *Annals of Data Science*, 2:165–193, 2015. Similarity Matching in Computer Vision and Multimedia.

[XWB+21] Yuxuan Xia, Pu Wang, Karl Berntorp, Lennart Svensson, Karl Granström, Hassan Mansour, Petros Boufounos, and Philip V. Orlik. Learning-Based Extended Object Tracking Using Hierarchical Truncation Measurement Model With Automotive Radar. *IEEE Journal of Selected Topics in Signal Processing*, 15(4):1013–1029, 2021.

[YAZ19] Haoyang Yu, Wei An, and Ran Zhu. Extended Target Tracking and Feature Estimation for Optical Sensors Based on the Gaussian Process. *Sensors*, 19:1704, 04 2019.

[YB16] S. Yang and M. Baum. Second-Order Extended Kalman Filter for Extended Object and Group Tracking. In *2016 19th International Conference on Information Fusion (FUSION)*, pages 1178–1184, 07 2016.

[YB17] S. Yang and M. Baum. Extended Kalman Filter for Extended Object Tracking. In *2017 IEEE International Conference on Acoustics, Speech and Signal Processing (ICASSP)*, pages 4386–4390, 03 2017.

[YB19] Shishan Yang and Marcus Baum. Tracking the Orientation and Axes Lengths of an Elliptical Extended Object. *IEEE Transactions on Signal Processing*, 67(18):4720–4729, 2019.

[YBG16] Shishan Yang, Marcus Baum, and Karl Granström. Metrics for Performance Evaluation of Elliptic Extended Object Tracking Methods. In *Proceedings of the 2016 IEEE International Conference on Multisensor Fusion and Integration for Intelligent Systems (MFI 2016)*, Baden-Baden, Germany, 09 2016.

[YTB18] Shishan Yang, Kolja Thormann, and Marcus Baum. Linear-Time Joint Probabilistic Data Association for Multiple Extended Object Tracking. In *2018 IEEE Sensor Array and Multichannel Signal Processing Workshop (SAM 2018)*, pages 6–10, Sheffield, United Kingdom, 07 2018.

[YWB20] Shishan Yang, Laura Wolf, and Marcus Baum. Marginal Association Probabilities for Multiple Extended Objects without Enumeration of Measurement Partitions. In *Proceedings of the 23rd International Conference on Information Fusion*, 07 2020.

[YWB+21] G. Yao, P. Wang, K. Berntorp, H. Mansour, P. Boufounos, and P. V. Orlik. Extended Object Tracking With Automotive Radar Using B-Spline Chained Ellipses Model.

In *ICASSP 2021 - 2021 IEEE International Conference on Acoustics, Speech and Signal Processing (ICASSP)*, pages 8408–8412, 2021.

[ZL20] Le Zhang and Jian Lan. Extended Object Tracking Using Random Matrix With Skewness. *IEEE Transactions on Signal Processing*, 68:5107–5121, 01 2020.

[ZL21] Le Zhang and Jian Lan. Tracking of Extended Object Using Random Matrix With Non-Uniformly Distributed Measurements. *IEEE Transactions on Signal Processing*, 69:3812–3825, 2021.

[ZLLW20] Yingjing Zhang, Mingyang Liu, Xin Liu, and Tianhao Wu. A Group Target Tracking Algorithm based on Topology. *Journal of Physics: Conference Series*, 1544:012025, 05 2020.

[ZWH+19] Yi Zhou, Tian Wang, Ronghua Hu, Hang Su, Yi Liu, Xiaoming Liu, Jidong Suo, and Hichem Snoussi. Multiple Kernelized Correlation Filters (MKCF) for Extended Object Tracking Using X-Band Marine Radar Data. *IEEE Transactions on Signal Processing*, 67(14):3676–3688, 2019.